ANALYSIS OF THE THERMAL DECOMPOSITION OF UNTEMPERED PEROXIDE SYSTEMS

A Dissertation

by

OLGA JULIANA REYES VALDES

Submitted to the Office of Graduate and Professional Studies of
Texas A&M University
in partial fulfillment of the requirements for the degree of

DOCTOR OF PHILOSOPHY

Chair of Committee,	M. Sam Mannan
Co-Chair of Committee,	Luc Véchot
Committee Members,	Perla Balbuena
	Tahir Cagin
	Chad Mashuga
	Valeria Casson Moreno
Head of Department,	Ibrahim Karaman

May 2016

Major Subject: Materials Science and Engineering

ABSTRACT

Several of the most catastrophic process safety incidents, such as Bhopal and most recently Texas West Fertilizer explosion, were initiated by runaway reactions. Consequences of such incidents include, fatalities, environmental damage, and in some instances corporate bankruptcy. To prevent conditions leading to a runaway, it is necessary to understand the kinetics, and physical and thermodynamic properties of the chemical system.

In the present research, calorimetric experiments were coupled with computational chemistry calculations to characterize the runaway behavior of two organic peroxides: Dicumyl Peroxide (DCP) and Cumene Hydroperoxide (CHP). These two reactive systems are particularly challenging due to their untempered behavior and complex kinetics.

To characterize the physical behavior of DCP and CHP runaways, adiabatic testing was performed in two equipment. Experimental results suggest that:

Scaling up methods used to estimate temperature and self-heating rate profiles on a large-scale, from laboratory data, are inconsistent for fast self-heating rate systems under runaway conditions. Moreover, the use of low thermal inertia or phi factor equipment (more costly and difficult to operate), do not always provide better large-scale estimations. This is due to potential higher heat losses.

Pressure discrepancies of up to 27 times were encountered when the phi factor was increased from 1.1 to 1.8. This finding elucidates the necessity of more efforts to scale up pressure behavior.

Estimation of gas generation rate from different configuration (closed vs open cell) diverges by up to 2.3 times. Principal sources of discrepancies are: open cell gas temperature assumption, pressure influence on vaporization, and gas dissolution.

Due to the complexity of the decomposition reaction of systems under study, grasping knowledge of their thermo-kinetics characteristics by experimental techniques is expensive, time consuming, and probably not possible. In this work, computational quantum chemistry, transitional state theory, and thermodynamic principles are used to achieve a deeper understanding of DCP and CHP decomposition thermos-kinetics. Networks of 12 and 18 reactions for DCP and CHP decomposition, respectively, are proposed. Products of the proposed networks match those reported by analytical techniques. Using this method provides a safe alternative while dealing with complex, highly reactive and unknown systems.

DEDICATION

To

My mother: Vilma Valdes, and

My brother, sister, and nephew: Jorge, Diana and Alejandro

ACKNOWLEDGEMENTS

First and foremost, I want to express my sincere gratitude to my advisor and mentor, Professor Sam Mannan. Dr. Mannan has been supportive since the days when I was doing undergraduate research as an exchange student. He introduced me to the field of Process Safety and motivated me to pursue a Ph.D. in this area. His guidance and genuine trust in my intellectual and personal capacities gave me the courage to aspire and accomplish goals in my professional career. Outside the academic and professional environment, I know that he honestly cares about me and my family's well-being and I do consider him as a member of my family. During these last five years, it was always joyful to stop by his office to have a conversation. The results of those conversations could vary from a good advice, extra and unexpected work, up to a stay in Qatar for almost a year. I could not have asked for a better Ph.D. advisor. Thank you Dr. Mannan.

I am grateful to my co-chair, Dr. Luc Véchot. My Ph.D. project started to get in shape when I was working under his supervision at TAMUQ. Several of the scientific accomplishments of this work are the results of his research interests and curious mind. I also want to thank my doctoral committee members Dr. Perla Balbuena, Dr. Tahir Cagin, and Dr. Chad Mashuga for their support in all stages of my studies and for their constructive criticism during my preliminary exam.

I was very lucky in having encountered Dr. Valeria Casson the first time I went to Texas A&M at Qatar. Since I've met her she has always been there as a mentor and as a friend. She taught me how to safely operate the equipment used in this thesis and most

importantly Valeria was actively involved all the way from the troubleshooting of the equipment to the discussion, revision, and analysis of the last result. Her contributions to this work are countless.

I am indebted to Dr. Simon Waldram, his scientific advices, and support in the moment when I was feeling that none of my experimental results had any sense provided me the intellectual push that I needed to look things from a different angle and to keep motivated. Many of his contributions are reflected in chapter III and IV of this thesis.

I want to thank to Dr. Salvador Moncho. Salvador introduced me to the basics of computational chemistry and contributed in all stages of this part of the project. I am also grateful to his professor Dr. Edwards Brothers, for agreeing to carry out this collaborative research. In this regard I also want to mention the undergraduate intern Emelyn Luna. Her hard work, sharp questions, and ideas made a big impact to the successful completion of chapter VI.

I want to acknowledge Dr. Victor Carreto. I had the fortune of working with him the first year of my Ph.D. and also during my last internship at Shell. His support and technical guidance were key to my success in both places. I am also thankful to my boyfriend and all my friends in both Texas A&M campuses (College Station and Qatar), they added joy to my Ph.D. journey.

I've always been and will always be grateful to my family. My mother, siblings, and nephew are my biggest motivation to achieve my goals and to become a better person every day. I'd like to give special thanks to my mom, I owe all my successes to her immense love and endless support.

TABLE OF CONTENTS

Page

Page

Page

LIST OF FIGURES

Page

Page

LIST OF TABLES

Page

Page

CHAPTER I

INTRODUCTION

Though many advances in terms of regulations and research have been made, reactive chemical incidents continue to occur worldwide. In the United States, a CSB report (2002) [1] identified 167 reactive chemical incidents in a 21 year period (1980-2001), resulting in a total of 108 deaths. An analysis performed by the French Data Bank ARIA [2]showed that between 2005 and 2010 in France, 352 incidents involved sites of polymer production and manufacturing of plastic materials and resins. Between 1962 and 1984, over 169 industrial incidents occurred in the United Kingdom. The aforementioned incidents were attributed to runaway reactions [3]. For instance, Dicumyl Peroxide (DCP) and Cumene Hydroperoxide (CHP) are two organic peroxides widely used in the petrochemical industry as initiators, cross-linking agents, hardeners, and drying accelerators in the petrochemical industry. Their unstable O-O bond is one of the properties that makes them so useful, but it also represents an intrinsic hazard due to the highly exothermic nature of their decomposition. This decomposition can lead to runaway reactions and subsequent explosions [4]. The hazards associated with the processing, transport, and storage of DCP and CHP are clearly reflected in the several incidents that have occurred in the last two decades: Taiwan (2008), Taiwan (2003), Japan (1999), Taiwan (1988) [2].

To deal with chemical reaction hazards, a risk assessment of the process needs to be performed and appropriate safety measures need to be selected, implemented, and maintained. The experimental study conducted in this research, aims to: (1) understand the behavior of the thermal decomposition of DCP and CHP under runaway conditions, (2) identify the influence of experimental conditions, and the accuracy of the correction methods to scale up the parameters obtained at lab-scale, and (3) improve the understanding of the decomposition mechanism of DCP and CHP. The computational part consisted of using computational chemistry and molecular simulations in order to get a better understanding of the thermal decomposition mechanisms of CHP and DCP. By doing this, the intermediates and main products are identified along with their influence on the behavior of hybrid and gassy systems at runaway conditions.

1.1 Problem Statement

Vent sizing and scale-up are two of the most important and challenging aspects in the development of reactive chemical processes. The lack of understanding of the thermo-kinetics of both, intended and unintended reactions, can lead to undersized and/or oversized pressure relief and cooling systems, and ultimately, to catastrophic consequences. The evaluation of the fundamental parameters characterizing a runaway by adiabatic scale experiments, which is a fundamental step in vent sizing methods, is not widely understood [5]. Although a lot of progress has been made in the last two decades, incongruences between data reported at similar conditions can still be found.

These facts were clearly highlighted in the results of the Round Robin test proposed by the Health and Safety Laboratory (HSL) [6]. In this test, information for a

reactor exposed to fire and containing a solution of 40% Dicumyl peroxide in 2,2,4-trimethyl-1,3-pentanediol di-isobutyrate was given to seven different partners including research centers, universities, and consultancy companies. The partners were asked to calculate the suitability of the existing vent area to protect the reactor and to provide the calorimetric data from which this area was calculated. Surprisingly, as observed in Figure 1, due to the differences in the equipment used, configuration of the equipment, and assumption of the behavior of the solution during venting, none of the areas calculated were similar and the smaller and bigger vent areas differed by a factor of 20.

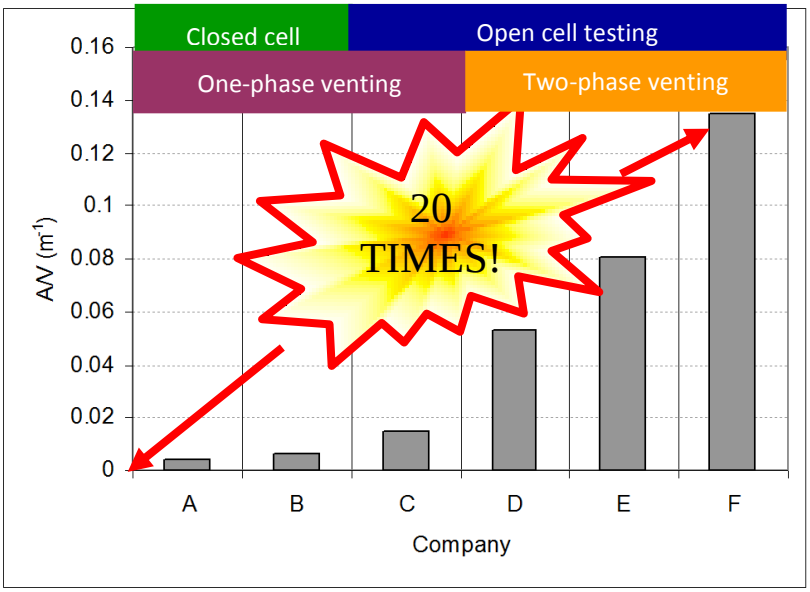

Figure 1 Results of the Round Robin exercise. Adapted from (Vechot *et al*. 2011)

A comprehensive study of the runaway behavior of gassy and hybrid systems using different adiabatic calorimeters and different configurations (open and closed cell) is needed in order to understand the reasons behind current reported discrepancies in

adiabatic data. These discrepancies affect the principal parameters used for vent sizing. In addition, understating the decomposition mechanism will allow addressing the effect that intermediate products have on the runaway behavior, temperature rise, and gas generation rate.

1.2 Objectives and Methodology

The main objective of this study is to characterize the physical, thermodynamic, and kinetic behavior of a gassy system (DCP) and a hybrid system (CHP) under runaway conditions. By combining calorimetric experiments with computational chemistry, we can assess the influence that different experimental conditions and the decomposition mechanism have on the thermal runaway behavior and principal parameters used in vent sizing. In order to achieve this goal, the following specific objectives have been set:

1. To study the thermal decomposition of different concentrations of DCP and CHP under runaway conditions using two different adiabatic calorimeters (Phi-TEC I and Phi-TEC II)
2. To study the influence of concentration, initial fill level, solvent, equipment, and configuration of the equipment used at laboratory scale on:

- The prediction of the severity of the runaway
- Gas generation rate

3. To correct the data obtained at lab-scale with two different adiabatic calorimeters and study how the phi-factor correction affects the prediction of the runaway trajectory on an industrial scale

4. To achieve a better understanding of the decomposition mechanism of CHP and DCP by using quantum mechanics and molecular simulations

The general methodology used to achieve each of the objectives is illustrated in Figure 2, and will be explained in more detail in the following sections.

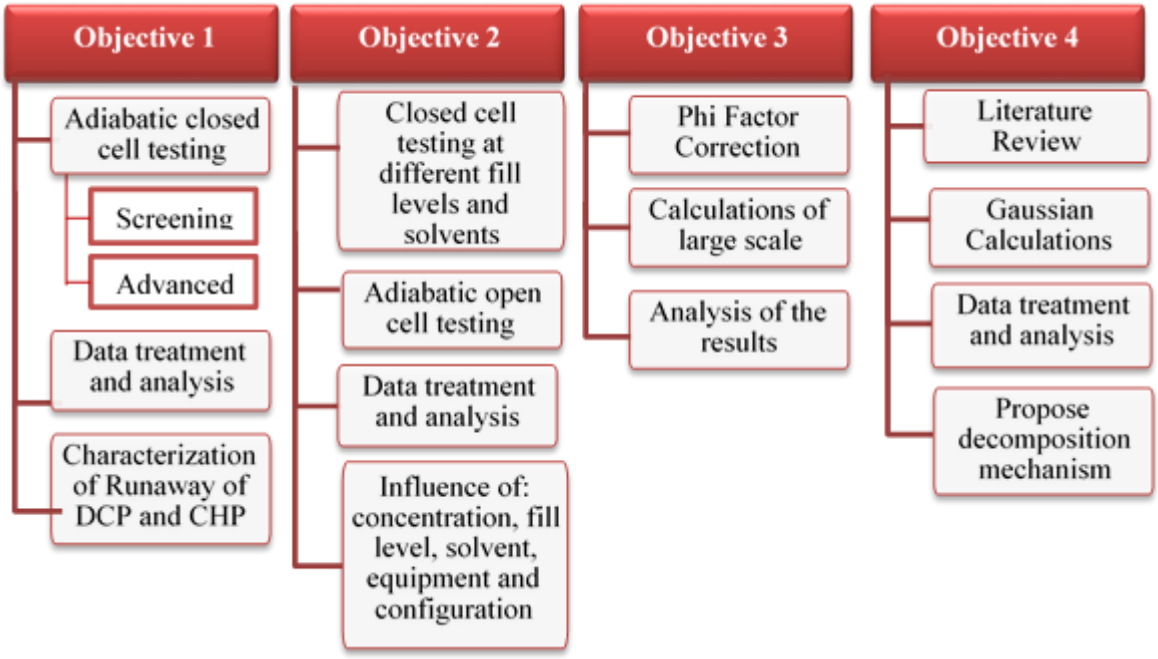

Figure 2 General methodology

1.3 Thesis Outline

- Chapter I introduces this research work and states the problem, objectives and general methodology.
- Chapter II provides background information regarding experimental and computational chemistry methods used to evaluate chemical reactivity and applied in this research. It also presents a literature review of exiting

experimental and computational works relevant to the present study and main gaps identified.

- Chapter III is dedicated to the experimental study of the runaway decomposition of DCP by closed cell adiabatic calorimetry. This chapter describes equipment, calculations and data treatment used for the analysis depicted in Chapters IV to V.
- Chapter IV is oriented to the study of the runaway decomposition of DCP by open cell adiabatic calorimetry. A comparison of the main findings by open cell to closed cell experiments is performed.
- Chapter V is focused to study of CHP runaway decomposition by closed and open cell adiabatic calorimetry.
- Chapter VI is devoted to the application of computational chemistry to study the kinetic pathway of DCP and CHP decomposition. Introduction of this chapter summarizes the main gaps encountered in the experimental study (Chapter III, IV, and V) and proposed a method to fill these gaps using computational chemistry.
- Chapter VII summarizes the main findings of this dissertation by outlining the conclusions and providing recommendations for future work.

CHAPTER II

LITERATURE REVIEW, GAPS AND LIMITATIONS OF PREVIOUS STUDIES

2.1 Runaway Reaction

A runaway exothermic reaction is the direct consequence of overheating in a chemical vessel. This phenomenon is characterized by a positive feedback mechanism that makes large equipment behave similarly to an adiabatic system. A progressive increase of the reaction rate makes the temperature of the reacting mass increase and so the reaction rate keeps rising [7].

The rate of heat removed/dispersed by the vessel is linearly proportional to temperature difference between the vessel contents (TR) and its surroundings (Ta), as the governing mechanism for heat transfer is conduction. The rate of heat produced by the reaction is an exponential function of TR, as it is related to the rate of the reaction (r). The loss of thermal control of the system, and therefore the runway reaction, starts when the rate of heat production exceeds the rate of heat removal, as shown in Figure 3 [8].

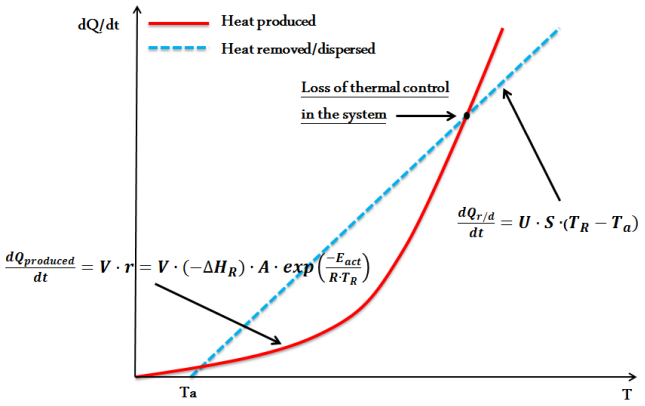

Figure 3 Heat generation rate (solid line) and heat removed/dispersed rate (dashed line) vs. temperature in a chemical vessel. Adapted from (Barton and Rogers, 1997)

A direct consequence of the temperature increase in a vessel undergoing runaway conditions is the pressure increase caused by the vapor pressure of the decomposition of the contents and the thermal expansion. The understanding of the behavior of chemical systems under runaway conditions is of primary importance in order to prevent catastrophic incidents, such as:

- Seveso, Italy (1976): due to a runway reaction during the production of tricholorophenol (TCP), a mixture containing highly toxic dioxin was released, contaminating the environment and exposing thousands of people [9].
- Bhopal, India (1984): a storage vessel containing toxic methyl isocyanate (MIC) was contaminated with water. The contact of MIC with water caused a rapid runaway reaction. More than 40 tons of MIC was released to the atmosphere. The aftermath estimations of deaths triggered by this incident vary from 3,000 up to 20,000. In addition, hundreds of thousands were injured [10].

2.2 Dicumyl Peroxide (DCP) and Cumene Hydroperoxide (CHP)

Dicumyl Peroxide (DCP) and Cumene Hydroperoxide (CHP) are widely used as initiators, cross-linking agents, hardeners, and drying accelerators in the petrochemical industry. However, the use of these peroxides has an intrinsic hazard due to their high instability. Their thermal decomposition reactions, which are usually highly exothermic, can lead to runaway reactions and subsequent explosions [4].

From a pressure relief point of view, DCP and CHP have been classified as gassy [11] (mainly gases are formed during the runaway) and hybrid [12] (vapor and gases are formed during the runaway) systems, respectively. These two kinds of systems typically show an untempered behavior: the temperature increases even after the relief operation.

2.3 Uses of DCP and CHP

Cumene Hydroperoxide (CHP) is a hydroperoxide usually used as a cross linking agent, hardener, drying accelerator in the production of phenol and acetone, and polymerization initiator in particular for the acrylonitrile butadiene styrene (ABS) copolymer [13]. Dicumyl Peroxide (DCP) is a white crystalline solid at ambient temperatures. It is principally used in the polymers and elastomers industries as a curing agent for unsaturated polystyrene and crosslinking agent for polyethylene, ethylene vinyl acetate copolymer and ethylene-propylene terpolymer. It is also applied in different resins to improve the physical properties of electronics, footwear, electrical insulators, decoration, and architectural materials [14].

2.4 Vapor, Gassy, and Hybrid Systems

The design of an emergency relief system can be complicated because of the pressure profile developed during the reaction, which depends on the type of system undergoing the thermal explosion: vapor, gassy, and hybrid. In the vapor system, the total pressure is equal to the vapor pressure. In this case, the reaction is called "tempered" (Figure 4, left) because when the operation of pressure relief occurs the temperature becomes constant in the system. The heat is removed with the vapor outlet from the system as latent heat of vaporization.

In gassy systems, the total pressure is equal to the non-condensable gas pressure. They are called "untempered" (Figure 4, right) systems because when the operation of pressure relief occurs the temperature continues to increase with the increase in pressure. Between these two systems are the hybrid systems, in which both gas and vapor are generated simultaneously such that the total pressure is the sum of the gas partial pressure and vapor pressure. Therefore, these require the knowledge of both rate of temperature and pressure rise for vent sizing. In addition to this, knowledge about how much of the generated pressure is due to vapor pressure and whether the system will temper during the operation of pressure relief [11] is required. Many peroxide systems show untempered behavior when undergoing decomposition [15]. Table 1 summarizes the characteristics of the three systems described above, and the principal parameters used in vent sizing design.

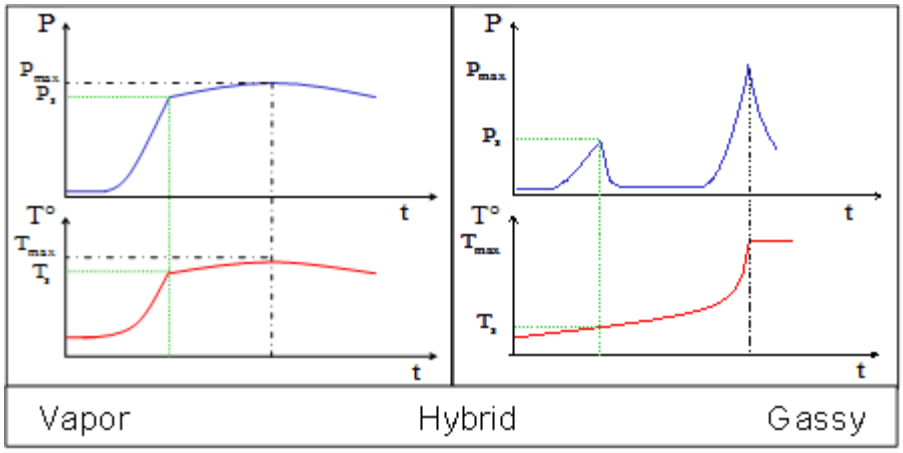

Figure 4 Behavior of tempered (left) and untempered (right) systems during the relief operation

Table 1 Summary of the main characteristics of vapor, gassy, and hybrid systems

Type of System	Behavior	Experimental parameters needed for vent sizing
Vapor	Tempered	Temperature, rate of temperature rise, latent heat of vaporization.
Gassy	Untempered	Pressure, temperature, and rate of temperature rise at maximum pressure rise. Sample mass, volume being pressurized and initial pressure at this volume.
Hybrid	Tempered or Untempered	Data required for vapor system plus data required for gassy systems.

2.5 Experimental Methods to Assess Chemical Reactivity

Calorimetric studies are extensively used for the evaluation of thermal and kinetic parameters of chemical reactions. Data obtained from calorimetric measurements allows finding the rate of reaction, specific heat capacity of the reaction mass and the enthalpy of the reaction, which are scale-independent. Two of the most widely used calorimetric techniques are described below.

2.5.1 Differential Scanning Calorimetry (DSC)

In a DSC the difference in the quantity of heat required to heat up a sample and a reference is measured as a function of temperature. The sample (placed in a sealed metal pan) and reference (empty sealed metal pan) are kept at the same temperature regime through the experiment [16]. The relatively small quantity of chemical used in DSC (few microliters) makes difficult the direct extrapolation of the results to pilot plant scale. Information regarding the heat released by reaction as well as the global kinetics can be obtained from a DSC; however, it does not provide information regarding pressure, and it usually detects an exotherm at temperature much higher than what is expected at pilot and industrial scales. DSC is widely used as a first screening tool to evaluate reactive hazards and the potential need of further and more advance testing [17] DSC can use different principles of measurement, such as power compensation or heat flow.

2.5.2 Adiabatic calorimetry

In an adiabatic calorimetry, both the sample and the vessel are under adiabatic conditions. The most common adiabatic calorimeters are the VSP (Vent Sizing Package), the APTAC (Automatic Pressure Tracking Adiabatic Calorimeter), the ARC (Accelerating Rate Calorimeter) and the PHI-TEC (used in this study). In these devices, heat losses from the sample are minimized by keeping the temperature of the sample and its surroundings as close as possible. Volumes of the test cell volume is usually between 10 and 120 ml. Experimental range is usually from 20 to 500°C for temperature and from 0 to 150 bar for pressure [18]. To obtain a set of data representative of a worst-case

runaway on a large-scale, in addition to being adiabatic, a suitable adiabatic calorimeter should also have a low thermal inertia. The thermal inertia or phi factor (φ) of the equipment is defined as follows:

$$\varphi = 1 + \frac{m_{cell} \times C_{P\,cell}}{m_{sample} \times C_{P\,sample}} \qquad \text{Equation 2.1}$$

Where m is the mass and Cp is the heat capacity.

When adiabatic testing is being performed, both the sample and the reaction vessel (in this case our cell), are in adiabatic condition. Therefore, the heat produced by the reacting sample causes not only an increase in its own temperature but also in the vessel temperature. Sample holders absorb some of the energy from the reaction. How much heat is absorbed depends upon the mass and heat capacity of the sample container. The significance of φ lies in the fact that large industrial reactors have a $\varphi \sim 1$ [19].

2.6 Computational Chemistry to Study Reactive Chemicals

The study of a complex kinetic reaction scheme can be tedious, long and experimentally very expensive [17,20–22], as they involve complex analytical techniques such as IR spectroscopy, GC, and HPLC.

Advances in computational quantum chemistry along with its strong practical elements have promoted its use in chemical reactivity studies. Mathematical models like Density Functional Theory (DFT) and Hartree Fock (HF) are used to predict molecular properties such as vibrational frequencies, activation energies, vibrational temperatures, bond lengths, etc. [23–25].

With these methods, electronic calculations are performed by solving wave functions like equation 2.2:

$$\vartheta\Psi = E\Psi \qquad \text{Equation 2.2}$$

Where, Ψ is the wave function, E a coefficient, and ϑ is an operator that in the case of the prediction of the energy of a molecule is replaced for the Hamiltonian (H), which takes into account the total energy of the molecule (expressed in terms of the kinetic energies of the particles in each atom, the attraction forces, and the repulsion between each electron and nucleus):

$$H\Psi = E\Psi \qquad \text{Equation 2.3}$$

Equation 2.3 is the Schrödinger equation, which mathematically is a type of wave function [26]. DFT and HF give a first approximation of molecular properties in their ground state by expressing them as a function of one system parameter, *e.g.*, the electron density or number of electrons per unit of volume (in the case of the DFT) [27]:

$$\rho(1) = N\int |\Psi|^2 \, d\tau_2 \, d\tau_{3\ldots} d\tau_N \, ds_1 \qquad \text{Equation 2.4}$$

Where, ρ is the density and Ψ is obtained by solving the Schrödinger equation.

During the 70s and 80s the most widely available (and used) method was HF. However, its use showed great difficulties in calculations involving the O-O bond functional group. Organic compounds with the O-O functional group (peroxides, hydroperoxides, and related compounds) were believed to be one of the most challenging functional groups for computational treatment [28]. Estimations concerning O-O bond cleavage were evaluated with extreme caution, conformational properties

studies on hydrogen peroxide encountered difficulties in calculating the O-O rotational barrier [29] [30]. Earlier studies using HF method frequently led to major errors when estimating reaction energies, especially where lone pair electrons, inherent to the O-O bond, are handled [31].

The introduction and extensive use of DFT made it possible to obtain reliable calculations for peroxo systems. In particular, the B3LYP functional had shown good agreement with experimental data when calculating activation barrier of processes involving O-O cleavage [32,33]. Recently the promising ωB97XD DFT functional (based on Becke's 1997 functional to diminish self-interaction and include dispersion correction [34]) have been successfully applied in calculations involving peroxide systems [35] and was chosen to conduct this research.

In this work computational quantum chemistry was used to evaluate stoichiometry pathway of DCP and CHP decomposition reactions by calculating thermodynamic (Gibbs free energy and enthalpy of reaction) and kinetic parameters (potential energy and energy barriers) of stoichiometries and their transition states [36].

2.7 Previous Relevant Work

The current literature search showed that there are very few experimental data available on the behavior of hybrid and gassy systems, especially for hybrid systems [37]. In the case of hybrid systems, most of the studies present in the literature are focused on kinetic descriptions [38–42] or on thermal hazard and runaway prevention using screening techniques [12,43–46] as discussed in the following sections.

2.7.1 Calorimetric studies

In particular, the thermal decomposition of CHP and DCP have been experimentally studied by previous authors using different calorimetric equipment such as DSC [14,47], Reactive System Screening Tool (RSST) [48], Vent Sizing Package (VSP2)[49,50], Accelerating Rate Calorimeter (ARC) [48], Automatic Pressure Tracking Adiabatic Calorimeter (APTAC) [40], or a combination of two or more calorimeters [51,52]. The main experimental results are summarized in Table 2 and Table 3. The gaps identified in the works presented in Tables 2 and 3 are discussed at the end of this section.

Table 2 Selected previous studies on the decomposition of CHP and DCP

Author	Substance	Scan rate [ºC/min]	T_o [ºC]	-ΔH [J/g]	Ea [kJ/mol]	Type of reaction
Wang and Shu [13] (2001)	35% CHP	DSC	135	607.3	Not reported	Not reported
Duh *et al*. [53] (1998)	35% CHP	2	80	618.6	120.6 ± 3.0	n^{th} order=0.5
	50% CHP		90	883.0	---	
	65% CHP		90	1172.6	---	
	35% CHP	4	95	1767	120.6 ± 3.0	
	80% CHP		100	1424.8	---	
Chen *et al*. [47] (2008)	88% CHP	4	105	1500	190	---
Di Somma *et al*. [54] (2008)	80% CHP	5-12.5	---	1219	Ea1=108.52 Ea2=97.19	Autocatalytic
Miyake and O'hama [55]. (2008)	80% CHP	1	137	930	Function of conversion	Autocatalytic
	70% CHP		137	830	---	
	60% CHP		137	590	---	
	50% CHP		137	460	---	n^{th} order
	40% CHP		137	310	---	
Talouba *et al*. [56] (2011)	80% CHP	8-10	~100	1538	Ea1=102±2 Ea2=89±2	Autocatalytic
WU *et al*. [47] (2006)	50% DCP	4	123	597.4	137.05	n^{th} order=0.92
	70% DCP		123	622.1	144.43	n^{th} order=1.01
	94% DCP		124	710.8	112.84	n^{th} order=0.74
S-H Wu *et al*. [51] (2008)	99.3%DCP	1	107	666	132	n^{th} order = 0.85
		2	110	704	139	n^{th} order = 0.94
		4	112	737	130	n^{th} order = 0.88
Lu *et al*. [48] (2010)	98% DCP	4	110.	744.8	124.58	n^{th} order = 1
Talouba *et al*. [56] (2011)	98% DCP	8-10	~100	861.5	135±2	n^{th} order = 1

Table 3 Previous reported adiabatic data on CHP and DCP

Author	System	Equipment	φ	T_o [°C]	T_{max} [°C]	P_{max} [bar]	dT/dt_{max} [°C /min]	dP/dt_{max} [bar/min]
Duh et al. [53] (1997)	12% CHP	ARC	1.27	116	166.26	3.43	0.251*	0.02
	16% CHP		1.29	116	181.98	11.56	1.704*	0.17
	20% CHP		1.31	111	192.44	14.49	3.784*	0.35
	30% CHP		1.30	106	229.44	18.40	46.804*	2.29
	35% CHP		1.28	101	250.51	34.93	336.832*	51.48
Y Duh *et al.* [53] (1998)	15% CHP (56.47g)	VSP2	1.19	100	206.2	---	2.8	---
Y Wang and C Shu [13] (2001)	15% CHP (50 g)	VSP2	1.20	115	223.91	24.39	9	2.76
	35% CHP (16g)	VSP2	1.45	140	248.72	43.99	108	55.16
Wu *et al.* [51] 2008	25% DCP	VSP2	1.1	110	175	20	1.61	0.6
Lu *et al.* [48] (2010)	98% DCP (5g)	ARC	---	---	184.61	20.78	----	----

*Values corrected to adiabatic conditions
--- No reported data

Where,

- T_o: is the onset temperature, defined as the lowest temperature at which the calorimeter detects the exothermic reaction. This parameter depends strongly on the sensitivity of the instrument.
- $-\Delta H$: is the heat of reaction, defined as the difference of enthalpy between the products and the reactants.
- E_a: is the activation energy, defined as the minimum energy required to initiate the reaction.

- φ: is the phi factor; refer to the description and discussion of this parameter in Equation 2.1.
- T_{max} and P_{max}: are the maximum temperature and pressure, respectively, achieved during the runaway under adiabatic conditions.
- dT/dt_{max} and dP/dt_{max}: are the maximum temperature and pressure rise, respectively.

2.7.2 Decomposition mechanism

The general decomposition mechanism of DCP is shown in Figure 5. At first, the homolysis of the O-O bond occurs, and DCP decomposes to produce cumyloxy radicals, which further decompose by a radical-induced mechanism to produce the methyl radical and acetophenone [51,57].

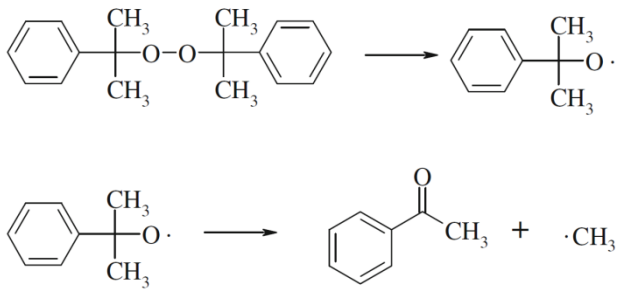

Figure 5 General decomposition pathway of DCP. Reprinted from (Reyes-Valdes *et al,* 2015)

For the decomposition mechanism of CHP, Duh *et al*. (1998) [53], coupled calorimetric techniques (DSC and VSP-II) with Gas Chromatography (GC) and High Performance Liquid Chromatography (HPLC) to propose a free radical decomposition mechanism composed by eight different reactions. Duh *et al*. determined that the

reaction order of CHP in cumene was 0.5, for all peroxide concentrations. The main decomposition products were identified as: acetone, α-methylstyrene acetonphenone, 2-Phenyl,2-propanol, and phenol.

Di Somma *et al*. (2008) [58], (2011) [41,59] and (2012) [60] extensively studied the thermal decomposition of CHP as well as DCP and showed that the decomposition mechanisms of CHP and DCP are much more complex than previously reported . In the case of CHP, they found that the process is regulated by autocatalytic behavior. In the case of DCP, the authors concluded that its thermal decomposition is dominated by first order reaction kinetics when oxygen is not present; otherwise, the reaction is autocatalytic. The decomposition of both peroxides starts with the homolysis of the O-O bond, followed by a series of radical reactions. As DCP is formed from CHP, both of the decomposition networks are composed of a set of 51 different reactions involving 18 chemical compounds and 12 radicals. For industrial purposes, such level of detail is not practical, but on the other hand, simpler decomposition mechanisms proposed earlier can be missing important information.

In the present work, the 51 chemical and radical reactions proposed by Di Somma *et al*. are analyzed by molecular simulations in order to identify the main paths for thermal decomposition of DCP and CHP.

2.7.3 Computational chemistry work

Sebbar *et al*. [61] used Gaussian 03 suite programs to determine the molecular properties of reactants, products and transition states in the decomposition pathway of DTBP, as a result the authors introduced an optimized and synthetized reaction pathway.

Bruneton *et al.* analyzed the reaction pathway of the thermal runaway decomposition of Tetrahydrofurfuryl Benzenesulfonate (TFB) by coupling statistical thermodynamics with computational quantum chemistry. For each of the reaction stoichiometries of previously proposed decomposition pathways the authors estimated Gibbs free energy, enthalpy and entropy of formation. Based on these calculations, infeasible and non-hazardous stochiometries were excluded [62].

Aldeeb [36] proposed a systematic approach to evaluate chemical reactivity of potential hazardous systems. His approach combines experimental (isothermal and adiabatic calorimetry) and computational methods (*i.e.,* group contributions, quantum chemistry, and thermodynamic relations). The author applied this method on di-tert-butyl peroxide (DTBP) [63]. Recently, other authors[64–66] have used computational quantum chemistry either to gain more understanding of the decomposition pathway of a system or to discriminate between two or more than one different pathways reported.

Regarding DCP and CHP decomposition, Lu *et al*. [48] made a first attempt to use quantum chemistry and molecular simulations to analyze the different possible paths of the decomposition reaction of CHP. Their pathway analysis was based on the decomposition mechanism proposed by Duh *et al*. [53]. The authors [48] calculated the Gibbs free energy and enthalpy of reaction of each of the eight proposed reactions and

applied the Marcus equation (Equation 2.5), which addresses the relationship between activation energy and the enthalpy and barrier of reaction:

$$E_a = \left(1 + \frac{\Delta H_r}{4E_a^0}\right)^2 E_a^0 \qquad \text{Equation 2.5}$$

Where E_a is the activation energy, E_a^0 is the barrier of the reaction, and ΔH_r is the enthalpy of the reaction. Based on these three calculations, the authors concluded that the dominant reaction pathway was composed of five reactions. The authors [48] neglected the effect of the solvent in their simulations; however, it has been verified with other peroxides that the presence of solvents affects the thermal decomposition of organic peroxides [67]. Moreover, further research proved that the decomposition mechanism of CHP is more complex that the one from which Lu *et al*. based their simulations.

2.8 Gaps Identified

- As seen in Table 2 most of the studies related to the understanding of the runaway of CHP and DCP are based on screening techniques (they use small-scale isothermal and high-thermal inertia adiabatic equipment). As the name indicates, screening techniques are meant to be used only as a first screening step in risk analysis, and hazard identification. Due to the small size and the large amount of heat loss, they are not capable of simulating real industrial scenarios.
- Only few of the studies found in the literature (Table 3) correct the adiabatic data obtained at lab-scale to address a real worst-case scenario at industrial scale. This correction is extremely important because, as mentioned earlier, industrial

reactors and large storage tanks will usually have a low thermal inertia factor (φ =1). Therefore, the use of the data available in the literature can: underestimate the severity of the runaway when the data is not corrected or overestimate it when the data is corrected [53].

- The few data that are available from adiabatic equipment with low thermal inertia factor (closer to 1) is taken at concentrations below 25% for both peroxides. This is because of the severity of the runaway and fast pressure rise as well as the temperature increase during the decomposition of DCP and CHP. This fact makes it difficult to obtain adiabatic experimental data at high concentrations without damaging the equipment. However, during the processing of DCP, CHP can be found at concentrations up to 83% and DCP at concentrations up to 99.3%. [68] As will be demonstrated further within this document (in the preliminary results), not all the runaway parameters change linearly with concentration; therefore, the results at such low concentrations cannot be directly extrapolated.
- The thermal decomposition mechanism of both CHP and DCP are still not well understood [50]. Different reaction pathways for the thermal decomposition of CHP and DCP have been reported; the simpler pathways miss important information, while the more complicated ones are not fully understood. The identification of the main products and intermediates can help in gaining fundamental understanding of the developed pressure profile and therefore the behavior of the systems.

- None of the previous authors performed a comprehensive experimental study on the influence of different parameters (which can vary in the processing and storage of DCP and CHP), such as initial fill level, solvent, and concentration on the runaway severity, and on the vapor or gas generation rates. These parameters are of paramount importance in the characterization of a runaway reaction.

CHAPTER III*

RUNWAY DECOMPOSITION OF DICUMYL PEROXIDE DECOMPOSITION BY CLOSED CELL ADIABATIC CALORIMETRY

3.1 Synopsis

This chapter describes the study of the behavior of Dicumyl Peroxide (DCP) under runaway conditions using low and high phi factor (φ) calorimeters. Solutions of 20, 30 and 40%, by weight, of DCP in 2,2,4-trimethyl-1,3-pentanediol diisobutyrate and cumene were run at different phi factors experiments($1.8 > \varphi > 1.1$). The results depicted that cumene reduces the severity of the runaway decomposition of DCP, while the phi factor of the experiments showed to have a high influence on the rise of temperature and pressure. Values up to 18 and 27 times higher, respectively, were obtained at same concentration when reducing the phi factor from 1.8 to 1.1. Temperatures and self-heating rates obtained at different phi factor experiments were scaled up to a phi factor equal to 1.0 using the correction method recommended by the Design Institute for Emergency Relief System (DIERS) and developed by Fisher[5]. The results showed that this method works well at low concentrations. However, at the highest concentration, fast heating rates (up to 600 °C/min) were observed in the low phi factor equipment. These fast heating rates, most probably caused the equipment to lose its adiabaticity, and

* This Chapter contains material reprinted from "Experimental sensitivity analysis of the runaway severity of Dicumyl peroxide decomposition using adiabatic calorimetry" by Olga J. Reyes Valdes, Valeria Casson Moreno, Simon P. Waldram, Luc N. Véchot, and M. Sam Mannan, 2015. Thermochimica Acta Jounal, Volume 617, 10 October 2015, Pages 28-37, ISSN 0040-6031. Copyright [2015] by Elsevier

the scale-up of the temperatures and self-heating rates did not any longer give reliable results. This means that the estimation of experimental variables such temperature and self-heating rate (used for vent sizing calculations), directly from the data obtained at lab-scale, even when using an advance low phi factor equipment, can result in under-conservative design calculations.

3.2 Materials and Methods

DCP was studied in solution with 2,2,4-trimethyl-1,3-pentanediol diisobutyrate (DIB) and with cumene (CUM). Some of the known physical properties of DCP, DIB and CUM are shown in Table 4.

Table 4 Solute and solvents physical properties

Chemical	Structure	M.W [g/gmol]	Density at 25 °C [g/ml]	Purity grade [%]	Melting /Boiling point [°C]	Cas No.
DCP	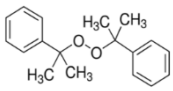	270.37	1.56	98	mp 39-41 -lit	80-43-3
DIB	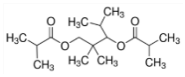	286.41	0.941	≥ 98.5	bp 280 -lit	6846-50-0
CUM	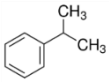	120.19	0.864	98	bp 152-154 -lit	98-82-8

3.2.1 Equipment closed cell

From a theoretical point of view a large-scale vessel under runway condition behaves like low phi factor adiabatic system. So experiments with low heat losses to the

surrounding containment vessel, which can be quantified by the phi factor (φ) (defined by Equation 2.1), are needed.

For all solutions an average heat capacity of 1.845 kJ kg^{-1} $°C^{-1}$ was assumed. The heat capacity of the cells (cell + magnetic stirrer) is that of the stainless steel, a value of 0.41 kJ kg^{-1} $°C^{-1}$ was taken based on vender specifications [69].

In this study, runaway experiments were performed using Phi-TEC I and Phi-TEC II calorimeters[69].

Phi-TEC I (Figure 6-a) cells are 8 ml stainless steel bombs that can withstand high pressure due to the thick walls of the cells themselves. However, the sample cell results in phi factors of up to 1.8 for typical sample sizes and this compromises reliability of the results for extrapolation to the large-scale. Phi-TEC I can operate at temperatures and pressures up to 500 °C and 200 bar. The lowest possible exotherm detection rate is 0.02°C/min. Pressure is measured by an absolute transducer[70].

In the Phi-TEC II adiabatic calorimeter (Figure 6-b), the reactive sample is taken to runaway in a 110 ml thin walled, magnetically (or directly) stirred test cell. Phi-TEC II shows excellent low phi factor adiabatic performance due to the relatively low thermal mass of the cells (very thin walls with $\varphi \sim 1.1$) compared to the thermal mass of the liquid mixture. This ensures that experimental data can closely predict large-scale behavior. In a Phi-TEC II closed cell experiment, the lack of strength of the test cells is compensated for by a flux of nitrogen from the pressure compensation system. Nitrogen is added to, or removed from, the high pressure vessel (in which the cell and heaters are placed) in order to keep a differential pressure between the cell and containment vessel

close to zero bar. The pressure compensation system can track the sample pressure up to 100 bar/min. The sample pressure is determined by a differential transducer, which measures the difference in pressure between the containment vessel and test cell and has a maximum differential range of 14 bars. An absolute transducer is used to measure the pressure in the containment vessel. Phi-TEC II can work up to 500 °C and 120 bar. The lowest possible exotherm detection threshold is 0.02 °C/min.

The main differences between the apparatus used during the experiments are the volumes of the sample cells and the value of φ for the experiments. In both calorimeters, the adiabatic conditions are maintained by controlling a set of heaters (a sample heater wrapped around the test cell and top, side, and bottom heaters – called guard heaters), which can track sample temperature rates at over 100 °C/min. The sample heater is used to provide heat to the test cell (usually in a heat-wait-search mode) until an exotherm is detected. The guard heaters' purpose is to maintain an adiabatic environment during the reaction by adjusting their temperatures to maintain equilibrium with the temperature inside the test cell [70].

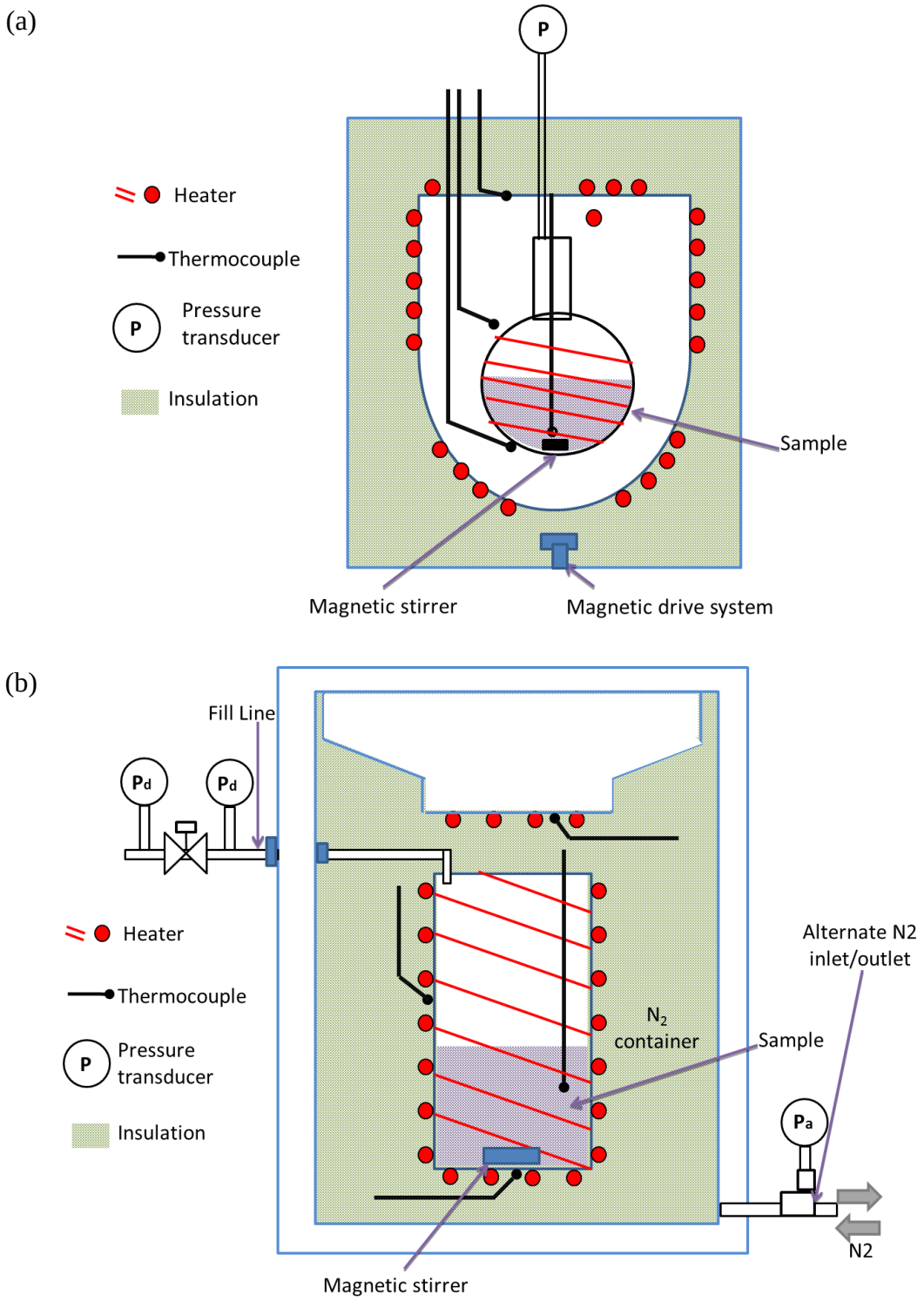

Figure 6 Schematic representation of: (a) Phi-TEC I and (b) Phi-TEC II

3.2.2 Inaccuracies

The thermocouples used to measure sample temperatures, are type K with a resolution of ± 0.1 °C. This inaccuracy in temperature affect the high self-heating rates reported in this study up to 0.5% (± 2.4°C/min at 556.45 °C/min, which is the maximum self-heating rate reported in this study). Absolute pressure transducers have an accuracy of ± 0.1% in a 0 to 200 bar range. Sample weight measurements have an accuracy of ± 0.01 gm.

3.2.3 Experimental plan

Closed cell runaway experiments, were performed using Phi-TEC I and Phi-TEC II. With these experiments the influence of the solvent and φ (which varies between equipment, and because of concentration and initial fill level) on the thermal decomposition of DCP and its runaway severity, were studied.

The influence of the φ factor was studied by performing experiments of DCP within a solution in a high boiling point solvent (2,2,4-trimethyl-1,3-pentanediol diisobutyrate, boiling point 280 ºC). This set of experiments was used also to correct to adiabatic conditions and study the applicability of the correction method proposed by DIERS [5] on the DCP decomposition.

As in industrial processes, DCP is found in solutions with cumene, a comparable set of experiments using DCP in cumene (boiling point 152 ºC) was also done. The influence of these two solvents on the runaway parameters for DCP decomposition is discussed.

The experiments were run in heat-wait-search mode [70] starting at a temperature of 60°C; after a 40 min calibration, the equipment was programmed to gradually heat the sample in 2 °C steps (small steps allow a more accurate detection of the 'onset' temperature). The temperature was then held constant for five minutes, while searching for an exotherm. When the exotherm was detected, the equipment shifted to adiabatic tracking mode and tracked the runaway reaction until completion. After the completion of the runaway, the experiments were stopped and the equipment was left to cool down to ambient conditions. Initial and final temperatures, pressures, and mass of reagents/products were recorded.

3.3 Calculations and Data Treatment

The influence of the experimental variables on the runaway severity of the DCP decomposition at different concentrations was addressed based on the importance from a process safety standpoint of the following parameters:

- T_{max} and P_{max}: maximum temperature [ºC] and pressure [bar] achieved during the runaway under adiabatic conditions.
- dT/dt_{max} and dP/dt_{max}: maximum self-heating [ºC/min] and self-pressurization rates [bar/min].
- T_o: detected 'onset' temperature [ºC], defined as the lowest temperature at which the calorimeter first detects the exothermic reaction. This parameter depends strongly on the sensitivity of the instrument.
- Δn : Moles of gases formed during the runaway [mol].

- ΔT_{ad}: Adiabatic temperature rise [ºC], calculated as the differences between the maximum and onset temperatures, multiplied by the phi factor of the experiment:

$$\Delta T_{ad} = \varphi(T_{max} - T_o) \qquad \text{Equation 3.1}$$

- ΔH: Enthalpy of reaction [J/g]. Calculated as:

$$-\Delta H = C_p \Delta T_{ad} \qquad \text{Equation 1.2}$$

From each test, temperatures (T) and pressures (P) versus time (t) were recorded during the experiment. Using these profiles T_o, T_{max}, and P_{max} were identified; and the adiabatic rise temperature ΔT_{ad}, maximum self-heating and self-pressurization rates dT/dt_{max}, dP/dt_{max}, were calculated. After this, the calculations were performed according to the equations reported below.

3.3.1 Gas production rate and gases generation

From a pressure relief point of view, DCP has been classified as gassy; the nature of main gases formed are methane, carbon monoxide, and carbon dioxide [71–73]. In order to estimate the formation of gases, the specific gas production rate (moles of gas/kg of initial solution) was calculated based on the assumption of the ideal gas law:

$$\Delta n = n_{final} - n_{initial} = \frac{P_{final} \times V}{R \times T_{final}} - \frac{P_{initial} \times V}{R \times T_{initial}} \qquad \text{Equation 3.3}$$

Where Δn is the moles of gases generated; n_{final} is the total moles of gases (initial moles + gas generated); $P_{initial}$, P_{final} , $T_{initial}$,and T_{final} are the initial and final pressures and temperatures (at the beginning of the experiment and after equipment cool down, *i.e*,. at room temperature), respectively; V is the free head space volume in the

cell, which was assumed to be constant; *R* is the universal gas constant; and $n_{initial}$ is the moles of gas present in the cell at the beginning of the test (air moles).

3.3.2 Global kinetics calculations

As already mentioned, the kinetics of the thermal decomposition of DCP have been studied by previous authors mainly by screening techniques, *i.e.,* Differential Scanning Calorimetry *(*DSC) [14,51,74]. The reaction has been reported as an n^{th} order type, with reported values of n varying from 0.5 to 1.0. Adiabatic experimental studies can also be found in the literature; however, these studies do not report the kinetic parameters of the decomposition of the peroxide [5,75]. In the present study, the global kinetic parameters (activation energy, E_a, pre-exponential factor, A, and order of reaction, n) were calculated by fitting the adiabatic experimental data (time and temperature) to an n^{th} order type reaction kinetic model.

For this scope, the following assumptions were made

- Single reaction, with n^{th} order global kinetics.
- Relation between the kinetic rate constant and the temperature is given by the Arrhenius equation.
- Conversion can be expressed in terms of the adiabatic temperature by the Townsend – Tou relation [76].

The rate of reaction (dX/dt), kinetic constant (k), and conversion (X) are given by equations 3.4, 3.5 and 3.6 respectively.

$$\frac{dX}{dt} = k \cdot (X_0)^n = k \cdot (1 - X)^n \qquad \text{Equation 3.4}$$

$$k = A \cdot \exp\left(-\frac{E_a}{RT}\right)$$ Equation 3.5

$$X = \frac{T - T_o}{T_{max} - T_o}$$ Equation 3.6

Substituting Equation 3.5 into Equation 3.6 and taking logarithms,

$$\ln\left(\frac{dX}{dt}\right) = \ln(A) - \frac{E_a}{RT} + n \cdot \ln(1 - X)$$ Equation 3.7

Using the adiabatic data obtained in each experiment, a multiple linear regression was performed on Equation 3.7, to calculate n for each solution tested. Then, the average values of the obtained *n* were used to calculate the activation energies and pre-exponential factors. To do this, Equation 3.6 was differentiated with respect to temperature and substituted into Equation 3.4, to obtain Equation 3.8.

$$\frac{dX}{dt} = k \cdot \left(\frac{T_{max} - T}{T_{max} - T_o}\right)^n (T_{max} - T_o)$$ Equation 3.8

Defining, k^*, as:

$$k^* = k \cdot (X_0)^{n-1}$$ Equation 3.9

Rearranging and taking logarithms,

$$\ln k^* = \ln(A) - \frac{E_a}{R}\frac{1}{T}$$ Equation 3.10

If the calculated n is accurate, the plot of ln k* vs 1/T is linear. Then the kinetic parameters E_a and A can be easily calculated.

3.3.3 Maximum gas production rate and (φ) correction

The maximum gas production rate for the closed cell experiments was calculated from the maximum self-pressurization rate in the test cell using the following equation [77].

$$\left(\frac{dG}{dt}\right)_{max,\varphi>1} = n_g * \left\{\left(\frac{dP}{dt}\right)_{max}\frac{1}{P} - \left(\frac{dT}{dt}\right)\frac{1}{T}\right\} \quad \text{Equation 3.11}$$

Where n_g, is the number of moles of gases formed during the reaction, dP/dt_{max} is the maximum self-pressurization rate in the test cell and P, T, and dT/dt are the values taken at dP/dt_{max}.

To have a better estimation of the maximum gas production rate at an industrial scale, the experimental values of T_o, dT/dt and dG/dt_{max} were corrected to φ =1. The correction method used in this study is described by the following equations [5,77]:

- Adiabatic Onset temperature:

$$\frac{1}{(T_o)_{\varphi=1}} = \frac{1}{T_o} + \frac{R}{E_a}\ln\varphi \quad \text{Equation 3.12}$$

- Adiabatic Temperature:

$$(T)_{\varphi=1} = (T_o)_{\varphi=1} + \varphi(T - T_o) \quad \text{Equation 3.13}$$

- Adiabatic self-heating heating rate:

$$\left(\frac{dT}{dt}\right)_{\varphi=1} = \varphi \exp\left[\frac{Ea}{R}\left(\frac{1}{(T)_{\varphi=1}} - \frac{1}{T}\right)\right] * \left(\frac{dT}{dt}\right)_{\varphi>1} \quad \text{Equation 3.14}$$

where, $\left(\frac{dT}{dt}\right)_{\varphi>1}$ is the experimental temperature rise [K/s].

- Adiabatic maximum gas production rate:

$$\left(\frac{dnG}{dt}\right)_{max,\varphi=1} = \varphi \exp\left[\frac{Ea}{R}\left(\frac{1}{T_M} - \frac{1}{T_{MAD}}\right)\right] * \left(\frac{dnG}{dt}\right)_{max,\varphi>1} \quad \text{Equation 3.15}$$

Where, T_M is the experimental temperature at which the maximum gas generation rate was achieved [K], T_{MAD} is the value of this temperature after correction [K], and $\left(\frac{dnG}{dt}\right)_{max,\varphi>1}$ is the experimental maximum gas production rate [mol/s]. The proposed correction method (Equations 3.12-3.15) can also be applied if the initial temperature of the industrial reaction is different from the initial selected temperature at lab-scale, *e.g.*, in gradually programmed temperature).

3.4 Results and Discussion

The experimental conditions and main results for each of the tests performed are shown in Table 5 and Table 6, respectively.

Table 5 Initial and final condition for all experiments

DIB as solvent								
DCP [% w/w]	φ	Equipment	Cell mass [g]	Sample mass [g]	$T_{initial}$ [°C]	T_{final} [°C]	$P_{initial}$ [bar]	P_{final} [bar]
20	1.82	Phi-TEC I	16.6	4.52	23.7	23.7	1.0	16.8
	1.65	Phi-TEC I	16.4	5.61	24.9	25.6	1.3	20.6
	1.12	Phi-TEC II	43.4	77.38	24.8	22.9	1.0	22.4
30	1.78	Phi-TEC I	16.6	4.7	20.4	22.8	1.0	29.8
	1.15	Phi-TEC II	43.7	64.85	23.5	26.5	1.0	39.1
	1.11	Phi-TEC II	42.2	78.91	22.7	28.6	0.9	57.6
40	1.82	Phi-TEC I	16.6	4.5	24.9	23.9	1.0	41.0
	1.58	Phi-TEC I	16.4	6.23	24.7	24.3	1.0	45.6
	1.14	Phi-TEC II	42.7	69.18	25.5	21.7	0.9	52.6
CUM as solvent								
20	1.87	Phi-TEC I	16.4	4.17	22.5	24.5	1.1	15.1
30	1.97	Phi-TEC I	19.0	4.36	22.7	20.0	0.91	16.1
40	1.92	Phi-TEC I	19.0	4.62	23.8	21.0	0.87	21.0

Table 6 Summary of main experimental results

DIB as solvent								
DCP [% w/w]	φ	T_o [°C]	T_{max} [°C]	ΔT_{ad} [°C]	P_{max} [bar]	dT/dt_{max} [°C/min]	dP/dt_{max} [bar/min]	$-\Delta H$ [J/g]
20	1.82	116.1	156.5	73.6	19.0	0.45	0.17	135.8
	1.65	112.8	163.2	83.1	27.2	0.69	0.33	153.3
	1.12	110.8	175.5	72.4	37.1	2.75	2.75	133.6
30	1.78	111.3	178.8	120.1	30.2	3.72	1.47	221.6
	1.15	105.5	212.6	123.7	48.2	68.9	40.81	228.2
	1.11	101.1	214.1	125.5	69.3	71.17	52.94	231.5
40	1.82	103.8	204.3	182.8	36.2	42.83	16.36	337.3
	1.58	101.3	211.5	174.2	54.4	59.56	34.52	321.4
	1.14	102.3	242.0	159.3	66.7	556.45	280.45	293.3
CUM as solvent								
20	1.87	116.5	151	64.7	15.5	0.27	0.09	119.4
30	1.97	115.5	169.3	105.9	22.7	1.48	0.59	195.4
40	1.92	111	198.8	168.2	29.4	27.35	7.62	310.3

3.4.1 Global kinetics

The global kinetic parameters determined for the thermal decomposition of 20 %, 30 % and 40 %w/w of DCP in DIB and CUM are shown in Table 7 (± symbol represents the standard deviation).

Table 7 Kinetic parameters DCP decomposition

in DIB [% w/w]	n	E_a [kJ/mol]	ln A [1/s]	DCP in CUM [% w/w]	n	E_a [kJ/mol]	ln A [1/s]
20	0.84 ±0.05	147 ±1	34.67±0.27	20	0.77	144	37.15
30	0.80 ±0.10	148±5	35.03±1.39	30	0.77	154	40.50
40	0.83 ±0.09	149 ±2	35.29±0.43	40	0.79	150	49.67

The reaction order (n) was determined to be lower than one. The concentration of peroxide does not seem to have a big influence on n or on the activation energy (E_a).

DCP is commercialized by Arkema as Luperox DC, Arkema Inc. [78] reports an activation energy of 154 kJ/mol (when DCP is dissolved in decane solutions), which is within the range of the values found in this study. The activation energy is expected to be close to the one reported in [78], but not the same as the solvents and DCP concentration used in this study are different.

Using the calculated *n* for each recipe, the plot of ln *k** vs 1/T (Figure 7) showed a good linear correlation. Therefore, the n^{th} order behavior of the reaction suggested by previous authors is reasonable. The modeling of the runaway decomposition by an n^{th} order reaction type and the determined values of activation energies and pre-exponential factor showed good agreement with the experimental data.

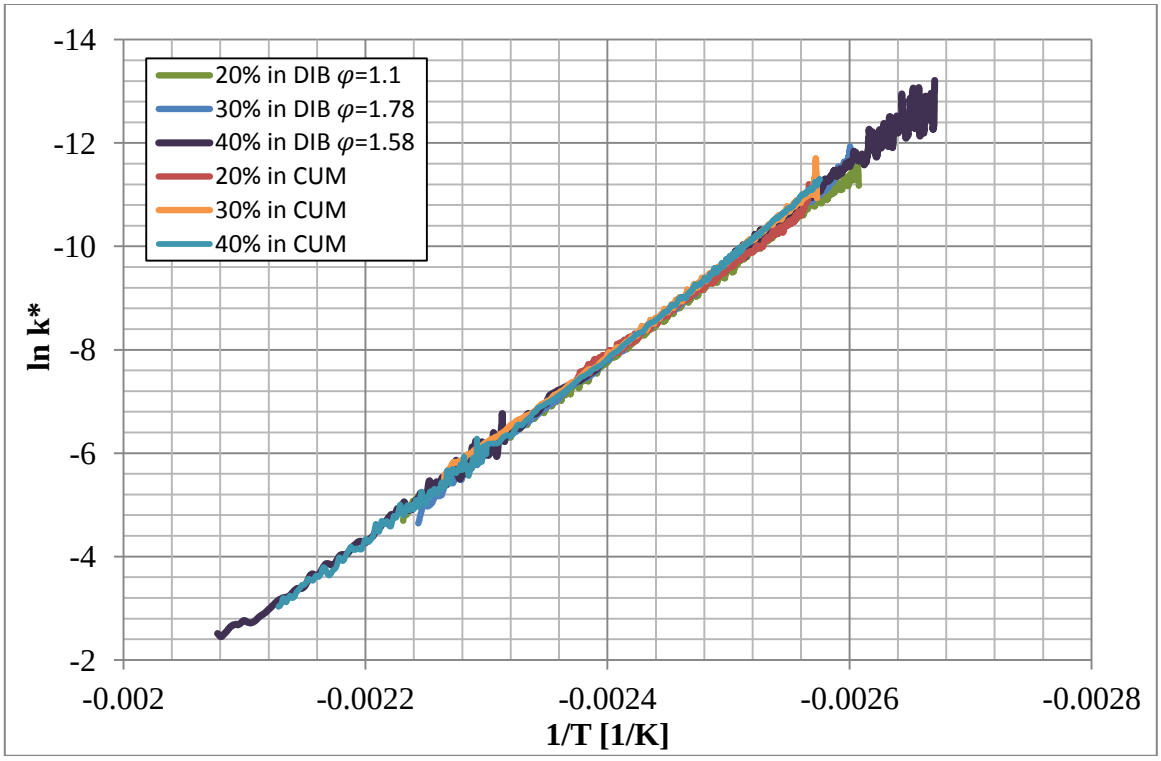

Figure 7 Ln k* (as expressed in Equation 9) vs. 1/T

3.4.2 Influence of the concentration and type of solvent

The runaway temperature and pressure profiles (with time reset to zero at the beginning of the exotherm) versus time obtained for different solutions of DCP in DIB and CUM using the Phi-TEC I are shown in Figure 8.

With these profiles and the data shown in Table 6, the severity of the thermal decomposition in terms of temperature and self-pressurization rate is easily discernable. As expected, the higher the concentration of peroxide, the higher the maximum temperature and the faster the self-heating rate during the runaway. Similarly, the maximum pressure and self-pressurization rate are directly related to the concentration of the peroxide in both solvents.

The severity of the thermal decomposition of DCP was found to be reduced when it is dissolved in CUM rather than DIB. The decomposition of DCP starts with the homolysis of the O-O bond, followed by a series of radical reactions [51,57]. When dissolved in CUM the boiling point of the solvent is within the temperature region of the runaway and CUM starts to react with intermediates radicals and chemicals. Di Somma *et al*. [41] previously proposed a reaction network for the thermal decomposition of DCP in CUM. According to their study, when CUM enters the reaction network it tends to form larger and more stable molecules than the radicals or chemicals with which it initially reacted. This could be the reason why the DCP runaway is less severe when dissolved in CUM. On the other hand, DIB is a stable, high boiling point solvent and a much larger molecule than CUM, so most probably it does not react with any of the radicals or intermediates formed during the decomposition of DCP.

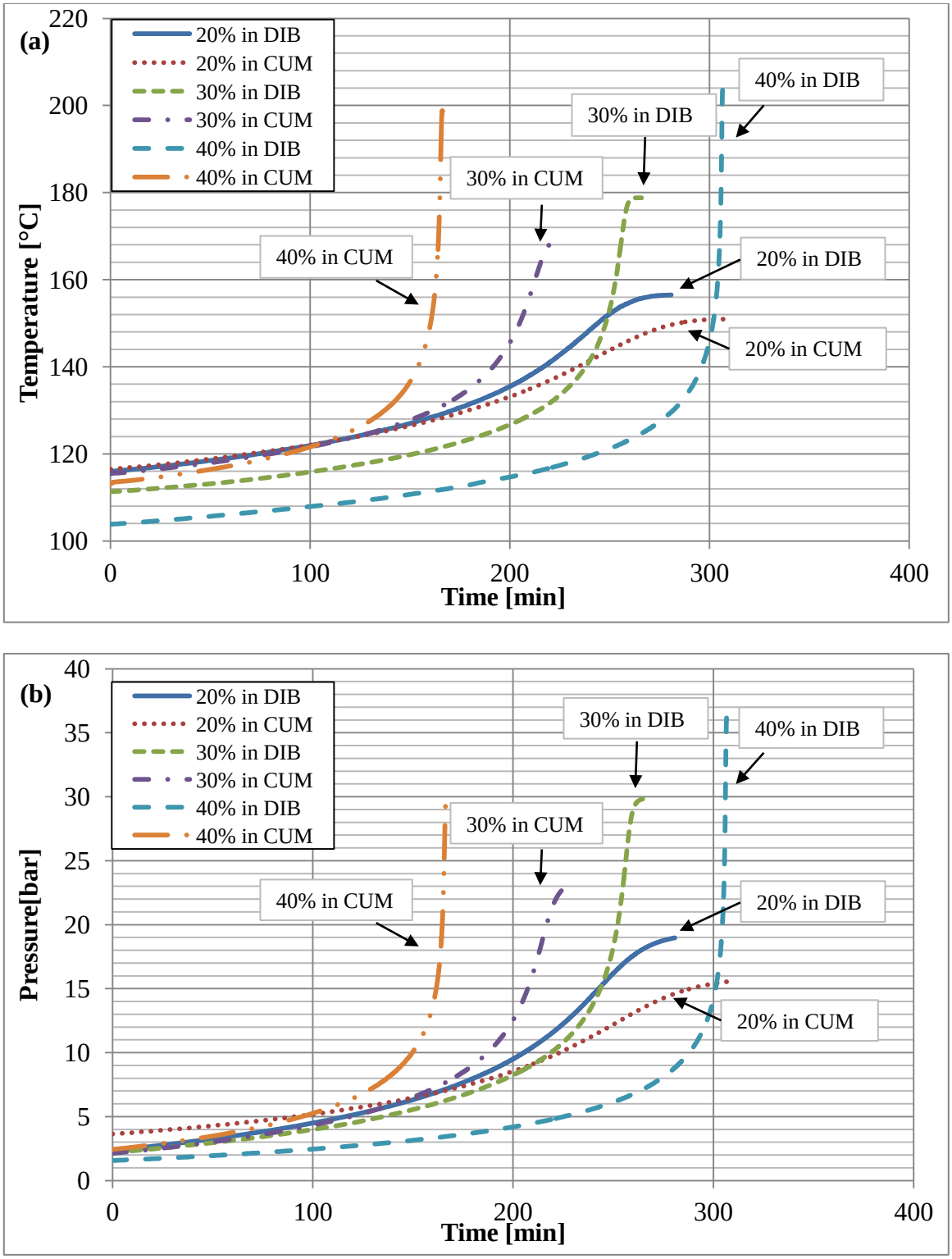

Figure 8 (a) Temperature and (b) pressure profiles of DCP thermal decomposition in DIB and CUM. Influence of the Phi Factor

The influence of φ on the different runaway parameters (P_{max}, $T_{max,}$ dT/dt_{max}, $dP/dt_{max,}$ T_0, moles of gases produced, and gas generation rate) was assessed using the experiments of DCP in DIB. Experiments at different initial solution masses, in both Phi-TEC I and Phi-TEC II where compared to achieve this objective.

3.4.2.1 T_{max} and P_{max}

As seen in Figure 9, both T_{max} and P_{max} are consistently higher for experiments with lower phi factor φ. A lower φ means less heat is absorbed by the cell and states in the sample, therefore higher temperatures are achieved by the reacting mass and consequently also higher pressures. With the increment in concentration, the difference between the measured maximum temperatures at diverse φ experiments becomes wider. This is probably because the heat of reaction release rate was too fast for the tracking heaters to maintain low heat losses. For example, T_{max} increases around 12% at 20% DCP between the lowest and highest φ experiments, while at 40% DCP this increment is around 18 %. The phi factor has a stronger influence on P_{max} than T_{max}. This is because of the gassy nature of the reaction, as the reaction rate goes exponentially with temperature therefore more gases are generated rapidly increasing the pressure of the system.

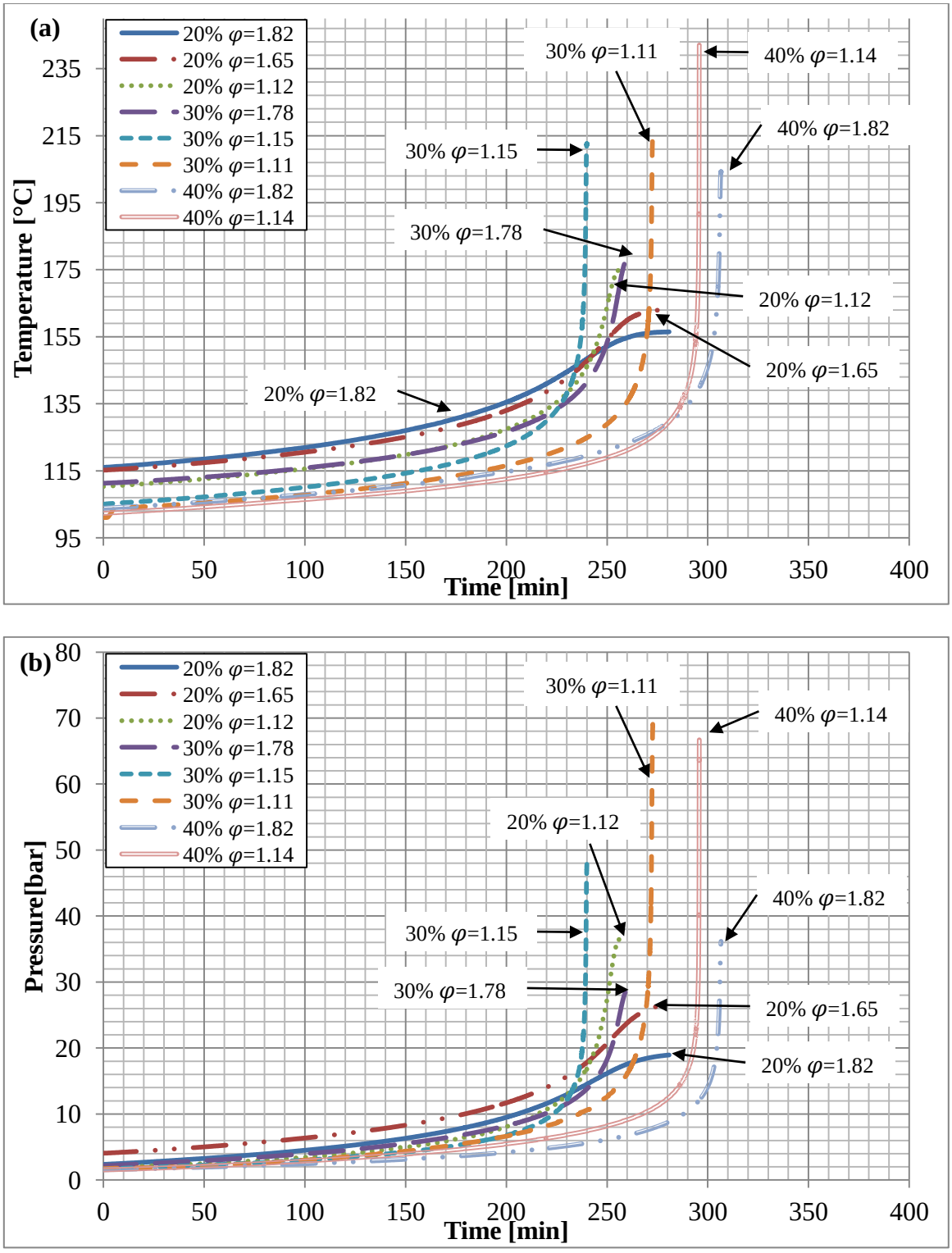

Figure 9 (a) Temperature and (b) pressure profiles of DCP decomposition in DIB

3.4.2.2 dP/dt_{max} and dT/dt_{max}

The maximum self-pressurization and self-heating rates are strongly influenced by the φ of the experiments. As shown in the values measured at the same concentration and same initial fill level, in the Phi-TEC II are much more severe (and closer to industrial scale) than in the Phi-TEC I. This is due to the higher thermal mass of the cell (higher φ) for Phi-TEC I, where the fraction of energy used to heat up the cell wall is significant, leaving less energy to heat up the liquid. It is also linked to the high temperatures at which these properties are measured, which make the heat losses of the Phi-TEC I larger. The values of the maximum self-pressurization rate obtained at the Phi-TEC II are up to 27 times higher than in the Phi-TEC II: in the case of the maximum self-heating rate they are up to 18 times higher. Both dT/dt_{max} and dP/dt_{max} also increase with initial fill level because of the lower phi factor. Experiments at 30% concentration show the highest percentage increase in these runaway parameters when increasing the fill level.

3.4.2.3 Detected onset temperature (T_o)

For all experiments of DCP in DIB, the exotherm is detected between 100 °C and 120 °C. As expected, the *higher the concentration the lower the value of* T_o, for similar φ experiments. This is because more peroxide is decomposing. Under the studied conditions, the phi factor does not show a strong influence on the onset temperature. Lower T_o's were observed at lower φ experiments: the more adiabatic the system is, the lower the temperature at which the decomposition begins. However, at 40% concentration the onset temperature detected in the three different φ experiments does

not have a significant variation. The runaway reaction is detected at lower temperatures when experiments are carried out in the low φ factor equipment (Phi-TEC II), but the differences are minimal. In a previous round robin study, it has been observed that the detected onset temperature is determined by the resolution of the equipment rather than by the value of φ [19].

3.4.2.4 Formation of gases

The observed final pressure of the system, after it had cooled down to ambient temperature (Table 5) is an indication of the formation of non-condensable gases during the runaway decomposition of DCP. As observed, the higher the concentration the larger the formation of non-condensable gases. The phi factor for the experiments does not have a strong influence on the estimation of formation of gases. At the same initial fill level, the gases calculated for the experiments in Phi-TEC II are slightly larger than the ones in Phi-TEC I. However, it is interesting to note (Figure 10) that the formation of gases per unit mass of sample *decreased* when the initial fill level was increased in both Phi-TEC I and Phi-TEC II experiments. The difference was really marked for the tests performed at 40% DCP concentration. The reason behind this could be the higher maximum pressures achieved when the initial fill level is higher force more gas into solution. The higher the initial fill volume, the higher the pressure and therefore the higher the solubility of the decomposition gases in the liquid reaction mixture. This reduction of free volume and its implications is why, for gas generating systems, closed cell experiments are recommended to be done with lower fill fractions than for open cell vent sizing tests [79]. However, closed cell tests show higher pressures and self-

pressurization rate and prevent any possible evaporative losses that could potentially cover thermal activity [37]. As expected, at similar conditions experiments, the higher the concentration of DCP the higher the gas production.

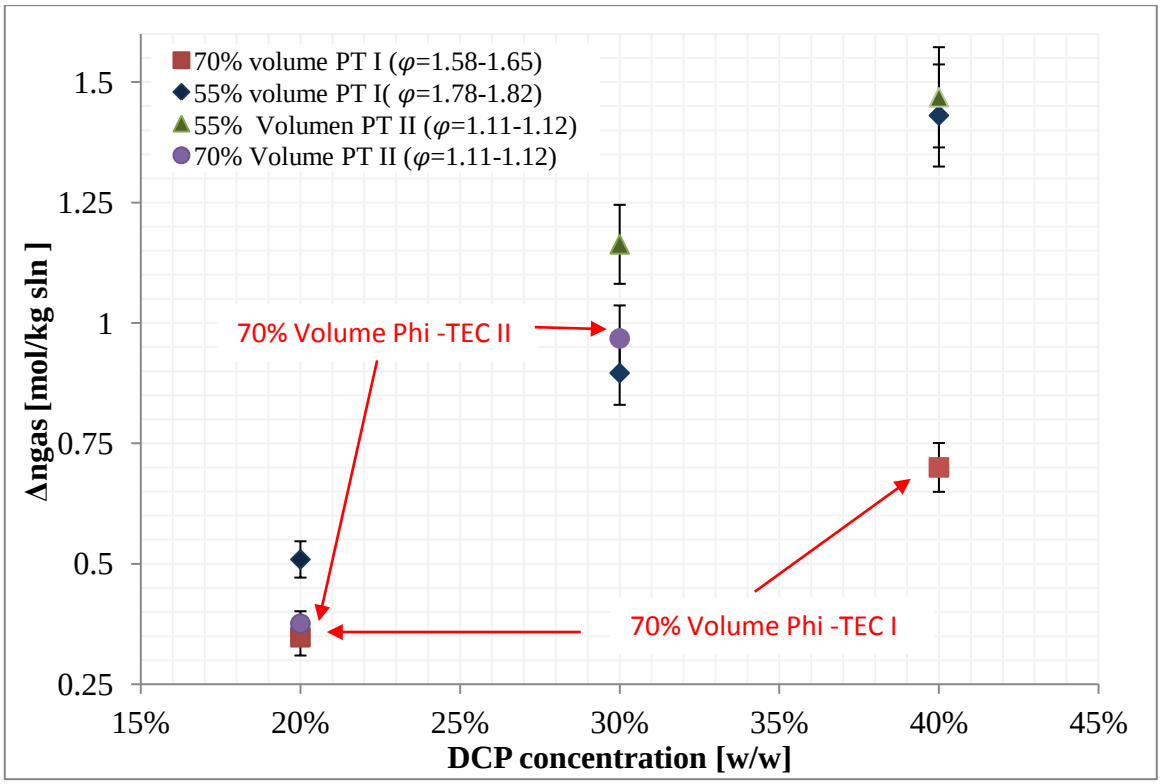

Figure 10 Formation of gases vs. peroxide concentration

3.4.3 Phi factor correction and gas generation rate

In order to compare the accuracy between the prediction of adiabatic behavior ($\varphi = 1$) from the different φ experiments the range of obtained values of T_o, T_{AMD}, dT/dt, and dnG/dt_{max} at φ = 1 are reported in Table 8.

Table 8 Phi factor correction results

DCP [%w/w]	φ	dT/dt at dP/dt_{max} [°C/min]	T_M [°C]	$(dnG/dt)_{max,\varphi>1}$ $*10^{-3}$ [mol/min/kg)	φ	$T_{o,\varphi=1}$ [°C]	$T_{AMD,\varphi=1}$ [°C]	$T_{max,\varphi=1}$ [°C]	$dT/dt_{\varphi=1}$ at dP/dt_{max} [°C/min]	$(dnG/dt)_{max,\varphi=1}$ [mol/min/kg]
20	1.8	0.4	148.8	4.0±0.2	1	110.3-111.0	170.6-175.1	182.5-188.0	5.3 - 6.6	0.11 - 0.16
	1.7	0.6	155.6	4.0 ±0.2						
	1.1	2.7	167.8	28.5 ±1.4						
30	1.8	3.1	171.5	26.9 ± 1.5	1	100.2-106.6	209.1-218.8	226.3-227.6	180.0-221.5	3.80 - 4.24
	1.2	61.5	204.9	681.7 ± 34.1						
	1.1	70.7	200.4	483.9 ± 24.2						
40	1.8	42.4	194.8	380.0± 16.9	1	97.8-101.3	233.0-264.7	261.1-288.0	2035-11854	78.25 - 232.62
	1.6	58.4	199.2	258.6 ± 15.0						
	1.1	506.9	217.3	3403.0 ± 170						

In Table 8 it is observed that at 20 %w/w DCP, experimental dT/dt at dP/dt_{max} obtained from the highest phi factor experiments (taken with the Phi-TEC I) differ with the corrected range of values by about one order of magnitude, while dT/dt at dP/dt_{max} from the lowest phi factor experiment is around half of the mean corrected value. As shown in Figure 11, these differences translate to a corrected maximum gas generation rate that is about three orders of magnitude higher for the high phi factor experiments and two orders of magnitude higher for the low phi experiments. At 30 %w/w DCP, the experimental dT/dt at dP/dt_{max} is about two orders of magnitude lower for the high phi factor experiment, while one order of magnitude lower for the two low phi factor experiments, when compared to the range of corrected values. This leads to a corrected gas generation rate two and one orders of magnitude larger, respectively. The results obtained in this study highlight the importance of correcting the data taken at lab-scale, even when they are obtained at phi factors really close to one. It is important to keep in mind that due to the walls, agitator, coils, baffles, and other accessories; typical industrial equipment, such as a chemical reactor, often has a phi factor of 1.02 to 1.05. When scaling up it is better to be conservative.

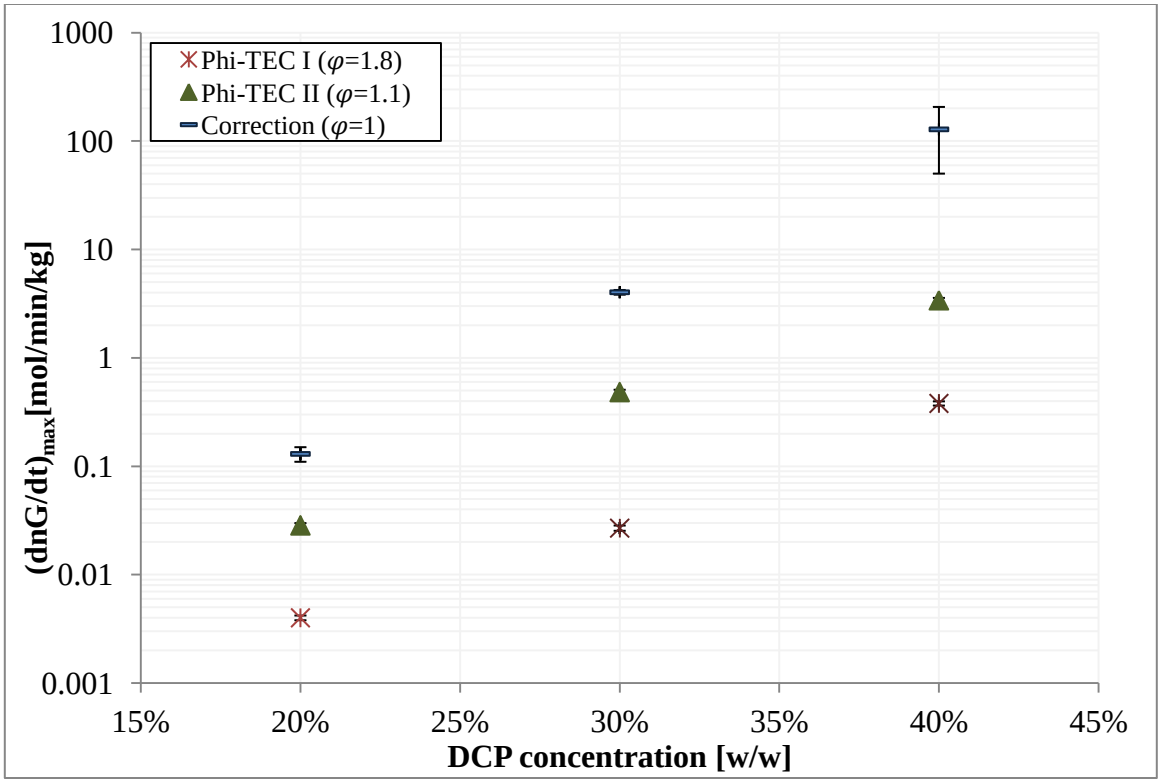

Figure 11 Experimental and corrected maximum gas generation rate

For both 20 %w/w and 30 %w/w the calculation method proposed by DIERS give narrow ranges of corrected self-heating rates and temperature profiles (Figure 12) which leads to a consistent gas generation rate calculated after correction. This indicates that the assumption of an n^{th} order single reaction and the estimated global thermo-kinetic parameters are "appropriate". It also shows that the application of the recommended DIERS method to correct for the temperature and temperature self-heat rate is suitable for the system under study at low concentrations.

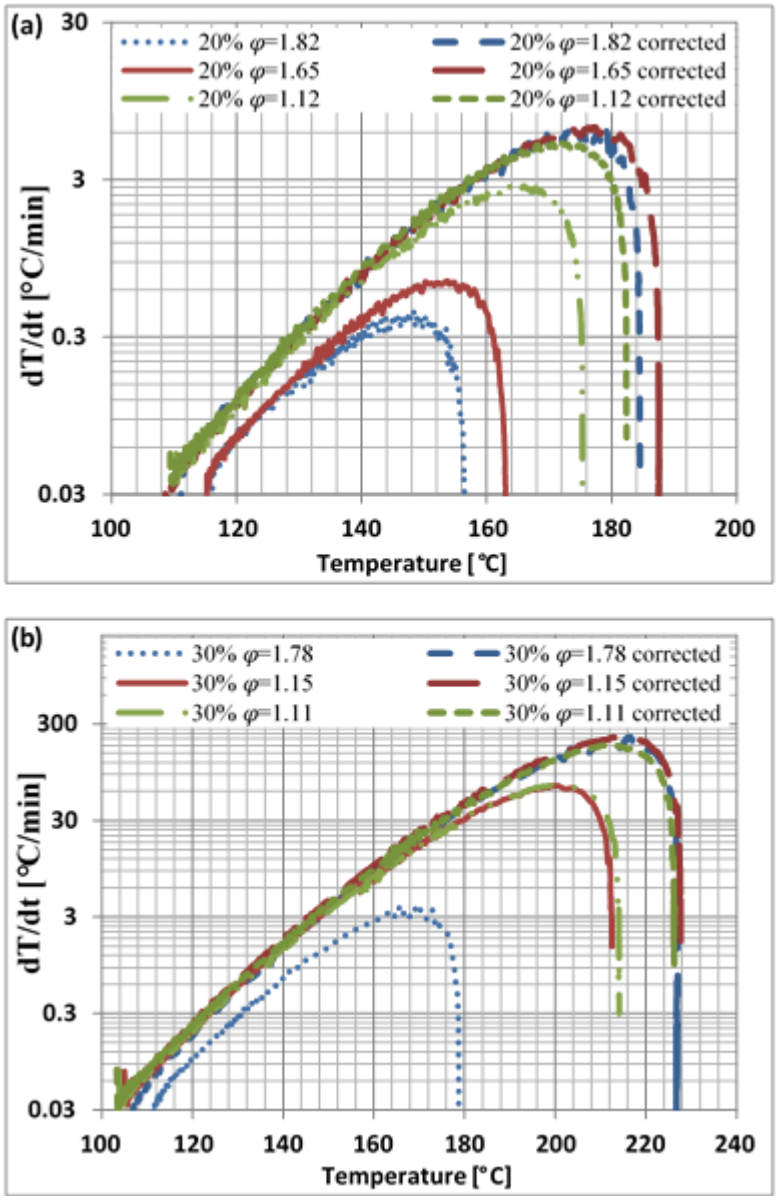

Figure 12 Self heat rates temperature profiles φ correction. (a) 20% (b) 30% DCP

However, in the case of the highest concentration (40% w/w DCP), the range of corrected dT/dt at dP/dt_{max} is really broad (Table 8). The inconsistency is also seen in the corrected self-heating rate and temperature profiles (Figure 13-b), where after correction, maximum self-heating rates go from 1000 °C/min up to 10000 °C/min.

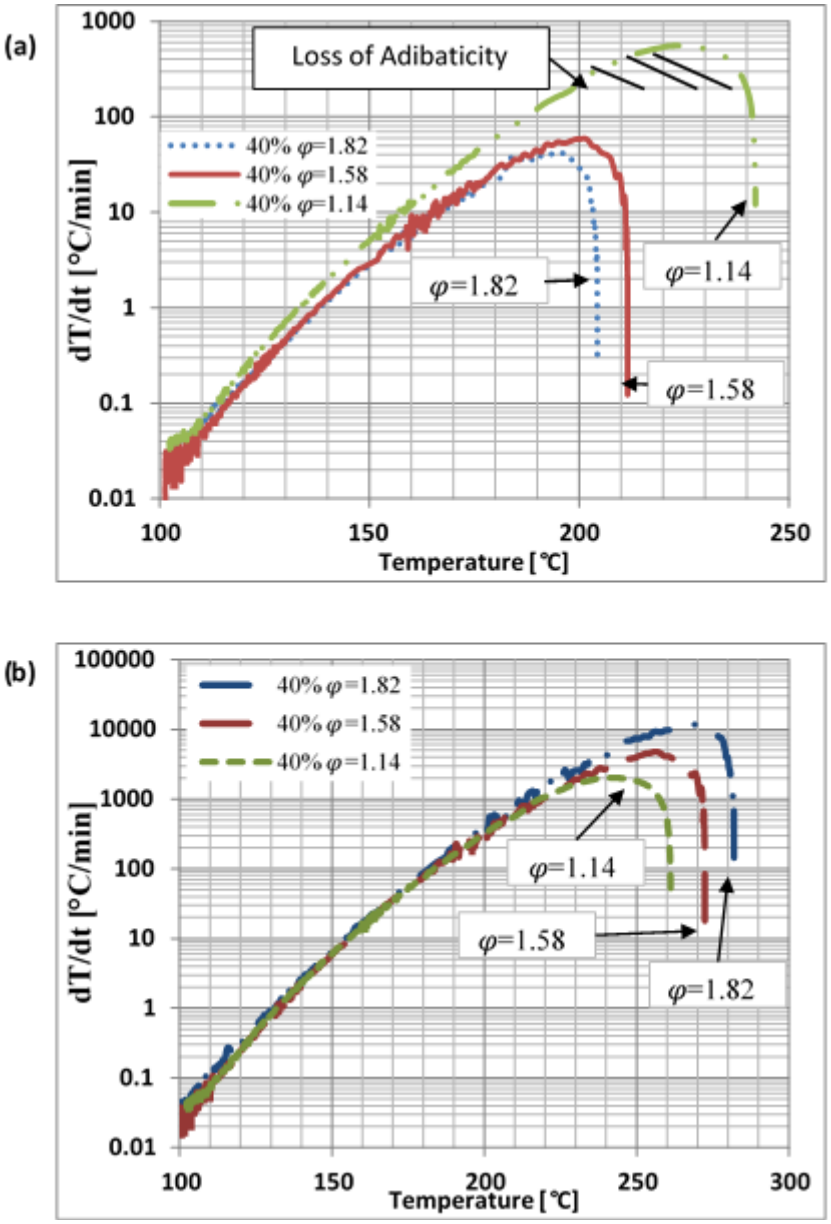

Figure 13 Self heat rate temperature profiles φ correction 40% DCP in DIB. *(a)* experimental data and *(b)* corrected data

These discrepancies affect the principal parameters used for vent sizing, such as the self-heating rate and temperature at maximum self-pressurization rate and can lead to the overestimation of gas generation rate [18]. The consequence of this overestimation is

the oversizing of the resulting relief vent device. This not only means that a more expensive device will be specified, but the equipment downstream of the relief vent will also be oversized (*i.e.*, a larger and more costly venting pipeline and catch tank, waste treatment or scrubber). Similar disagreements when applying this correction method to fast self-heating peroxide systems have been observed previously [80]. There are three possible reasons for these:

- With the Phi-TEC II, maximum self-heating rates up to 600 °C/min are being achieved. However, by design, the heaters of the Phi-TEC cannot accurately track self-heating rates of more than 200 °C/min. Therefore, beyond this value, the equipment is not behaving adiabatically (the surrounding heaters cannot follow this high temperature rise rate). The heat losses in the experiments become increasingly higher and the equipment losses adiabaticty (if possible, a higher phi factor should be use to avoid these high self-heating rates). Therefore, ***for fast self-heating rate*** systems under runaway, the first order correction method suggested by DIERS and used in this work is not applicable.
- In the Phi-TEC I the obtained self-heating rates, are lower than 100 °C/min. As these heating rates are lower than in the low φ experiment, the equipment will not lose adiabaticity (the phi factor will be nearly constant and equal to that used to make the correction). Hence, the corrected values obtained from the high φ experiments may be more accurate. However, as the heating rates are still large and adiabatic conditions are difficult to maintain, the correction should only be trusted up to the temperature at which the experiments where performed.

- At high concentrations, the reaction type/order may change during the reaction or the gas evolution of the reaction affects the phi factor during the runaway. Either of these two factors are considered by the correction method applied within this study [81]. These can be corrected by performing dynamic simulations.

3.5 Conclusions

In this work, closed cell adiabatic experiments were performed to study the thermal decomposition of 20%, 30%, and 40% w/w DCP solutions in a high boiling point solvent and a solvent with a boiling point inside the temperature region of the runaway reaction. In both solvents, the global kinetic parameters calculated by assuming a single n^{th} order type reaction, show a good agreement with the experimental behavior. The nature of the solvent showed no influence on the global kinetics. However, the runway of DCP in DIB seemed to be more severe than when DCP was in solution with CUM (higher temperatures, pressures, and self-heating and self-pressurization rates were achieved).

The runaway of DCP in DIB was studied using the Phi-TEC I and Phi-TEC II, in which the main differences are the sample size and the thermal inertia (phi factor) of the equipment. Experiments at different phi factor were obtained at 20%, 30% and 40% w/w DCP. A strong influence of the phi factor on each experiment on the runaway variables was noticed; the lower the phi factor of the experiment, the more severe the runaway reaction became (higher values of temperatures, pressures, and self-heating and self-pressurization rates). On the other hand, it did not show a big influence on the detected onset temperature or formation of gases.

The experimental data at different phi factors were corrected to a φ =1, using a first order correction method, which relies on the reagent consumption. The maximum gas generation rate was calculated before and after correction. The applied correction method works well at low concentrations. However, as the self-heating rate of the reaction increases (at high concentration) the results don't show consistency. Corrections of high phi factor experiments show much higher temperature and self-heating rates with respect to tests characterized by lower phi factors. The possible reasons for this behavior are: a) loss of adiabaticity in the low phi factor experiments at self-heating rates above 100-200 °C/min, b) less heat losses (due to lower self-heating rates) in the Phi-TEC I, and c) different global kinetic behavior at high concentrations.

The results showed that the estimation of the maximum gas generation rate directly from the data obtained at lab-scale, even when low phi factor equipment was used, can result in non-conservative calculations, due to the heat losses from the equipment, leading to a vent sized devices unable to withstand a worst-case runaway reaction scenario. In cases like this, where vent sizing may not be feasible, instrumentation would be needed in place in order to mitigate hazards and risk mitigation techniques such as LOPA would be used to characterize how good the risk reduction is after instrumentation barriers.

The data reported in this study will be helpful for the sizing of industrial vent safety devices only if the slight traces impurities are the same that the ones tested at lab-scale (here Sigma Aldrich pure reagents). Otherwise, these results shall not be used as a concluding basis and experimental data should be gathered.

CHAPTER IV*

RUNAWAY DECOMPOSITION OF DICUMYL PEROXIDE BY OPEN CELL ADIABATIC TESTING

4.1 Synopsis

Low thermal inertia experiments in the open cell configuration were carried out to perform a comprehensive sensitivity analysis of the parameters affecting the runaway self-decomposition of Dicumyl Peroxide (DCP). This study facilitates a better understanding on how concentration, initial back pressure, and fill level influence DCP runaway severity. The outcome of this experimental study was compared to previous adiabatic closed cell experiments, with the aim of clarifying the discrepancies reported in the literature and contributing to essential knowledge about self-decomposing peroxide systems.

Results showed that the detected onset temperature, maximum temperature, maximum pressures and time to maximum rate are affected by the configuration of the equipment and initial back pressure of the experiments, while the adiabatic temperature rise did not seem to be affected. The roles that the kinetics, fluid dynamics and thermodynamics play on these observations is addressed and discussed through out the chapter.

---

* This Chapter contains material reprinted from "Runaway decomposition of dicumyl peroxide by open cell adiabatic testing at different initial conditions" by Olga J. Reyes Valdes, Valeria Casson Moreno, Simon P. Waldram, Luc N. Véchot, M. Sam Mannan, 2016. Process Safety and Environmental Protection [In press 2016].

4.2 Introduction

Runaway reactions have been extensively studied, many advances in terms of fundamental understanding, science, and regulations have occurred since Bhopal disaster [82]. However, reactive chemical incidents continue to happen around the world. Although, in the last 25 years runaway incidents have reduced in quantity, their consequences in terms of injuries and fatalities have increased by ~300% [83].

Dicumyl Peroxide (DCP) is extensively used in polymer manufacturing and petrochemical industries as a crosslinking agent, initiator, hardener and drying accelerator [14]. However, its use entails an intrinsic hazard due to the presence of the highly unstable peroxy group (O-O bond); when enough energy is available, DCP will readily decompose. Its decomposition is highly exothermic and can lead to a runaway reaction, usually accompanied by a large and fast pressure rise [84,85].

Process units in which this type of hazardous chemical are processed or simply stored, should be equipped with Emergency Pressure Relief Systems (EPRS), *i.e*., pressure safety valves – PSVs or bursting disks) [86] in order to minimize the possibility of equipment rupture and unplanned loss of containment. However, the design of the protective device(s) will depend on the nature of the system under runaway as well as their reliability [87]. There are some cases, where EPRS, might not be suitable (*e.g*., fast reactions that generate gas at a very fast rate upon decomposition as in some batch polymerization reactions) because the size of the relief device could be too large to be economically feasible. For such cases other strategies such as prevention, quenching, inhibition, and dumping are used. Layer of Protection Analysis (LOPA) is also used in

these cases to determine if the runaway likelihood may be reduced by adding additional layers of protection so that the runaway scenario is no longer considered to be possible [88]. LOPA can also be used to determine if adding other, or extra, layers of protection would be cost-effective [89].

From a pressure relief point of view, when dissolved in a high boiling point solvent DCP has been classified as gassy system (mainly non condensable gases are formed during the runaway) [11]; its main decomposition products are methyl radicals, acetophenone and dimethylphenyl carbinol [41]. This kind of system typically shows an untempered behavior during venting, *i.e.*, the temperature continues to increase even after the relief operation [90]. Currently, there are very few experimental data available on the behavior of DCP during an uncontrolled runaway reaction [74,84], [51], [68] most of which were collected at low concentrations and by screening techniques, *e.g.*, small-scale isothermal micro-calorimeters or high-thermal inertia adiabatic calorimeters [14,51,68,74,85].

The importance of experimental data obtained in low thermal inertia equipment has been recently discussed by the authors [80,84] as well as the problem of collecting reliable experimental data for concentrated solutions of peroxide being tested in a closed cell configuration. As the gases formed during DCP decomposition can exert pressure on the test cell at very rapidly increasing rates, it may not be possible to obtain meaningful adiabatic experimental data at a significant concentration in closed cell configuration with a thin-walled, low thermal inertia sample holder (unless the pressure compensation system capabilities are modified). Therefore, the use of the open cell configuration may

be more appropriate as it helps to avoid bursting the test cell. In addition the use of the open cell configuration reduces the solubility and non-ideal behavior of the generated gases [91].

In order to obtain data capable of simulating a real worst-case industrial scenario, the runaway behavior of DCP was studied by performing low thermal inertia experiments in an open cell configuration. DCP was dissolved in 2,2,4-trimethyl-1,3-pentanediol diisobutyrate (DIB) at concentrations of 20% , 30% and 40% by weight. DIB was chosen as a solvent due to 1) its high stability within DCP runaway range of temperatures and 2) to have a comparable set of experiments with data reported in a previous study [84]. Two different initial back pressures and fill levels were tested. The results highlighted the impact that experimental conditions (initial pressure, fill level, concentration, and configuration of the equipment) have on the general kinetics and decomposition behavior of DCP. Discussion of the role of the kinetics, thermodynamics and fluid dynamics of the system on this behavior is presented. A comparison of the behavior of the runaway to closed cell adiabatic experiments previously reported in [84] is made; special attention is given to the results of the maximum specific gas production rate for both configurations.

4.3 Materials and Methods

4.3.1 Chemical samples

Solutions of 20 % (ρ=1.02 g/ml), 30 % (ρ=1.06 g/ml), and 40 % (ρ=1.12 g/ml) by weight of DCP in DIB were prepared by gradually dissolving peroxide in solvent

while stirring the solutions at ambient temperature. Both peroxide and solvent were purchase from Sigma Aldrich with the characteristics presented in Table 9.

Table 9 Characteristics of peroxide and solvent

Chemical	Molecular weight [g/mol]	Density [kg/m^3]	CAS No.	Appearance at 25 °C	Boiling point [°C]	Vapor Pressure at 25 °C [Pa]
Peroxide (DCP)	270.37	1560	80-43-3	Solid	351.4	1.1×10^{-2}
Solvent (DIB)	152.19	941	6846-50-0	Liquid	280	8.8×10^{-2}

4.3.2 Equipment open cell

Experiments were run using the Phi-TEC II adiabatic calorimeter in the open cell configuration [92], in which the minimum threshold value for the detection of the self-heating typical of the runaway reaction is 0.02 K/min. Thin-walled stainless steels cells of 110 ml volume were used. A vent hole of 1/8'' was drilled on the top of the cell (Figure 14-a). The open cell was then placed into the high pressure containment vessel, which can withstand pressures up to 200 bar. Because of the vent, both the vessel and the cell remained at the same pressure and hence a pressure compensation system was not needed. The adiabatic conditions were maintained by using a set of heaters, a cell heater and three guard heaters (top, bottom and side). The temperatures were measured using type K thermocouples, reading the temperature inside the sample cell (with a submerged, internal thermocouple), and those of the guard heaters. An absolute transducer measured the pressure in the containment vessel. A schematic representation of the described equipment is displayed in Figure 14-b.

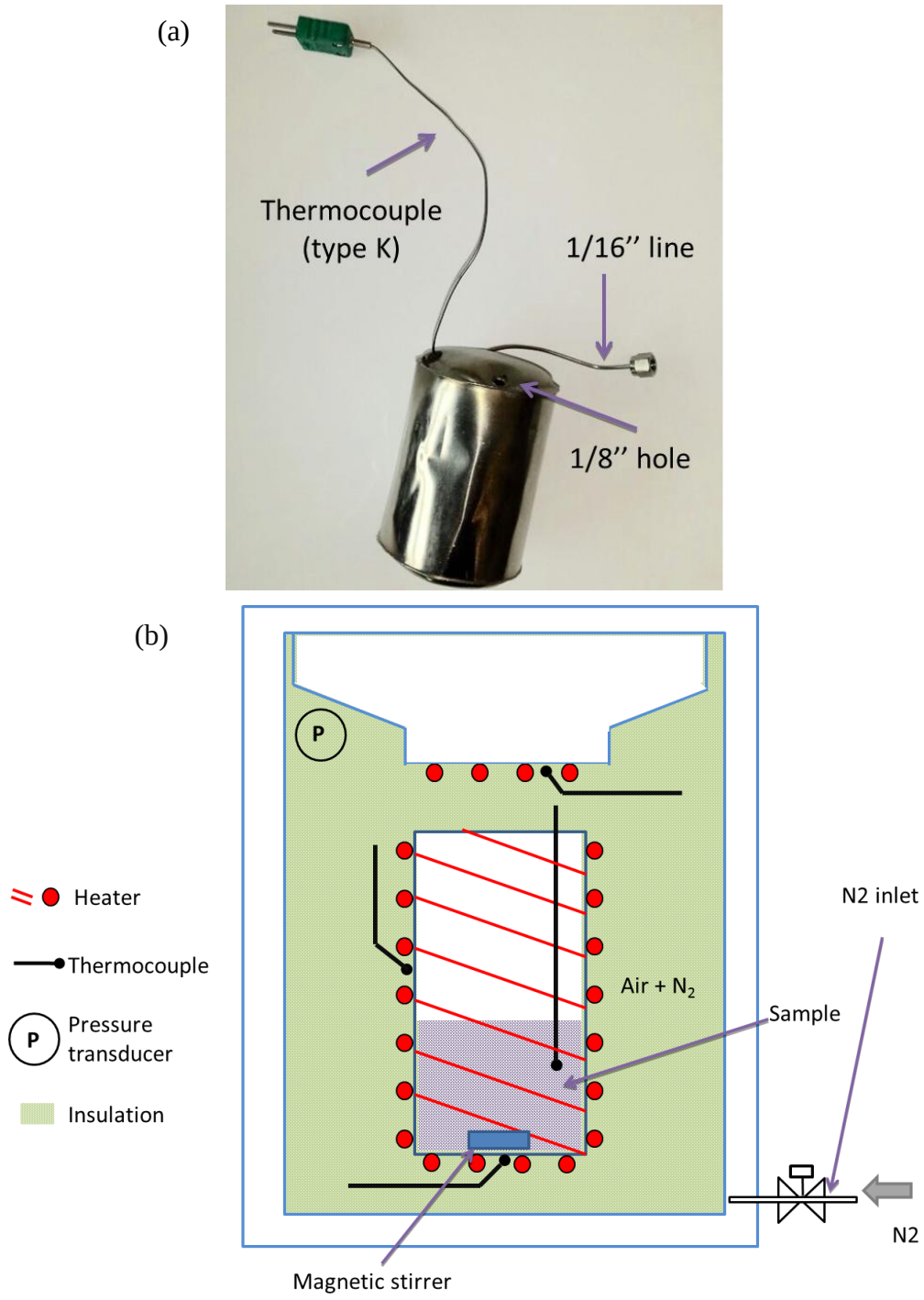

Figure 14 Vented sample holder (a) and schematic representation of the Phi-TEC II open cell configuration (b)

4.3.3 Experimental plan

Runs were started at two different pressures: 1 bar and 5 bar. Tests starting at five bar were pressurized with nitrogen before starting the experiment. This nitrogen pad pressure was used to suppress potential vaporization and consequent tempering and/or boiling effects from the solutions. The experimental plan is shown in Figure 15.

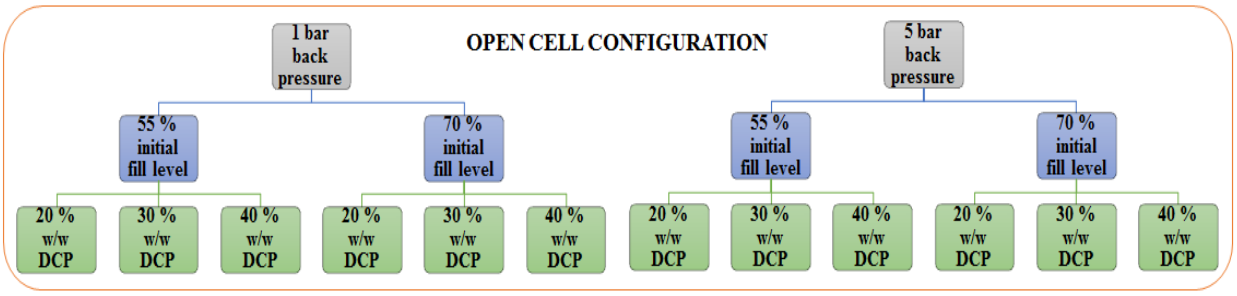

Figure 15 Schematic of the experimental plan carried out in the present study

The equipment was used in a heat-wait-search mode [92]. Samples were heated to 60 °C; then a 40 minutes calibration was performed. After the calibration, the equipment was set to increase the sample's temperature by 2 °C per minute and then hold it for five minutes while looking for any evidence of an exotherm. Once the exotherm was identified, the equipment shifted to an adiabatic mode runaway completion. After the conclusion of the experiments, the apparatus was allowed to cool down to room temperature. Initial and final conditions and mass of the samples were recorded.

4.4 Calculations and Experimental Data Analysis

4.4.1 Kinetics calculations

To estimate the kinetic parameters (activation energy, E_a, order of the reaction, n, and frequency factor, A) the decomposition reaction of DCP was assumed to be an n^{th} order type (based on previous publications [14,51,74]). To calculate *n*, conversion (*X*) was expressed in terms of adiabatic temperature rise [76] and the temperature dependence of the rate constant was assumed to follow the Arrhenius equation. The detailed steps are described in paragraph 3.3.2 [80].

4.4.2 Sensitivity analysis

The sensitivity analysis on the runaway severity of DCP was assessed by analyzing the following parameters [18]:

- Onset temperature, T_o [°C]: The detected onset temperature is defined as the temperature at which the equipment starts tracking the runaway. This parameter was estimated as being the intersection between the tangent of the fast ascending temperature increase and the horizontal tangent of the point where this line starts.
- Pressure build-up in the containment vessel, ΔP_{max} [bar]: As the experiments started at different pressures, the maximum pressure increase instead of the maximum pressure is reported and analyzed. The pressure increase was calculated as the difference between the maximum pressure achieved during the runaway and the initial pressure:

$$\Delta P_{max} = P_{max} - P_{initial} \qquad \text{Equation 4.1}$$

- Adiabatic temperature rise, ΔT_{ad} [°C]: Total temperature increase due to the runaway decomposition under adiabatic conditions. This was calculated as the difference between the maximum and onset temperatures, multiplied by the phi factor of the experiment (Equation 3.1)
- Time to maximum rate, TMR [min]: The TMR is calculated as the time between the onset temperature and the maximum self-heating rate. This parameter is used to estimate the available time for an emergency system to respond with corrective action designed to stop the runaway.
- Maximum self-heating rate and maximum pressurization rate, dT/dt_{max} [°C/min] and dP/dt_{max} [bar/min]: maximum rates of increase in temperature and pressure during DCP runaway decomposition.
- The phi factor, φ*:* defined as the ratio of the sensible heat of the solution and the test cell to that of the solution alone (Equation 2.1)
- Mass loss, $\Delta m/m_s$: The mass loss was estimated as the difference of the mass sample before and after the experiments divided by the initial mass.

$$\frac{\Delta m}{m_s}(\%) = \frac{m_{\text{initial solution}} - m_{\text{solution in the test cell after experiment}}}{m_{\text{initial solution}}} \qquad \text{Equation 4.2}$$

- Moles of non-condensable gases formed, Δn: Moles of non-condensable gases were calculated by using Peng Robinson equation of state (Equation 4.3) and assuming that the gas produced was mainly methane. This estimation was based on the temperatures and pressure of the solution before starting the experiments and at the end (after cooling back to ambient temperature):

$$P = \frac{RT}{V_m - b} - \frac{a \cdot \alpha}{V_m^2 + 2 \cdot b \cdot V_m - b^2} \qquad \text{Equation 4.3}$$

$$a = \frac{0.45724 \cdot R^2 \cdot T_c^2}{P_c}$$

$$b = \frac{0.0078 \cdot R \cdot T_c}{P_c}$$

$$\alpha = (1 + (0.37464 + 1.54226 \cdot \omega - 0.26992 \cdot \omega^2)(1 - T_r^{0.5}))^2$$

$$T_r = T/T_c$$

where P is the pressure difference between the pressure after cooling down and the initial pressure (both at room temperature); V_m is the molar volume of the gas; R is the ideal gas constant; T is the temperature after cooling down; and T_c, P_c, and ω are the critical temperature, critical pressure and acentric factor of the species (in this case methane).

Comparing the obtained moles of gases at dP/dt_{max} using Equation 7, to calculations using an equation of state developed by NIST for methane at pressure up to 1000 MPa and temperatures up to 625 K [93] the percentage of error in molar density is equal to 0.8.Therefore the use of the Peng Robin equation of state is suitable for the purpose of this study.

- Maximum gas generation rate, dG/dt_{max}: this parameter is calculated based on the moles of gas n_g, pressure P, temperature T, and self-heating rate dT/dt at the maximum pressure rise rate dP/dt_{max} using the following equation 3.11. Where n_g was calculated as per Equation 4.3 at maximum self-pressurization rate conditions. The estimation of the gas generation rate not only depends of the equipment and configuration, it also depends on the interpretation of the measured data[6]. When working on closed cell configuration there are gas

dissolution issues, but the liquid and gas temperature are well defined. On the other hand, open cell configuration reduces the gas dissolution effects and prevents bursting the cell, but the measurement of the gas temperature lacks precision and cannot always be assumed equal to that of the liquid. For this reason, the temperature of the gas at the maximum self-pressurization rate (T_{AMD} in Equation 8) is evaluated for three different scenarios:

1. $T_{gas}=T_{liquid}$, and dT/dt = experimental value measured
2. $T_{gas}=T_{av}=(T_{liquid} + T_{ambient})/2$ and and dT/dt_{max} = (dT/dt experimental)/2
3. $T_{gas}=T_{ambient}$ (assumed as 300 K) and $dT/dt_{max}=0$

And the maximum gas generation rate is reported for each of these assumptions.

4.5 Results and Discussion

The experimental conditions and main results presented in this paper are listed in Table 10 and Table 11 respectively. For the sake of comparison

Table 12 summarizes the behavior of the runaway of DCP under adiabatic conditions in a closed cell test under similar conditions (concentration, solvent, equipment and φ) reported in a previous study by the same authors [80]. The moles of non-condensable gases and the moles of gases used to estimate the maximum specific gas generation rate shown in

Table 12 were calculated as per Eq. 7 instead of the ideal gas law. This estimation is more accurate due to the high pressures, high temperature and small volumes that the gas can occupy in a closed cell configuration, especially at the maximum pressure rise.

Figures 16 and 17, display temperature and pressure profiles. The continuous lines represent tests performed at 55 % initial fill level, while the dashed lines denote experiments conducted at 70 % initial fill level.

The profiles of 40 %w/w DCP at 1 bar initial pressure showed a different course at the end of the exotherm, which could be due to: 1) boiling of the solution, 2) another reaction following the decomposition, or 3) calibration problems. These two profiles are analyzed until the point where the curves change their course. As all the analysis performed in this manuscript is solely related with DCP decomposition, the variables reported might not be affected as the curves change their course after the offset.

Table 10 Initial and final conditions of open cell adiabatic tests

#	DCP [% w/w]	Back Pressure [bar]	Fill Level [%]	φ [-]	Cell mass [g]	Sample mass [g]	$P_{initial}$ [bar]	P_{final} [bar]	$T_{initial}$ [°C]	T_{final} [°C]
1	20	1.0 ± 0.1	55 % ± 1.2	1.11	33.67	66.38	1.10	1.99	24.5	26.6
2	30			1.12	33.68	63.32	1.09	2.43	23.4	21.3
3	40			1.11	33.67	66.08	1.09	---	23.8	---
4	20		70 % ± 0.95	1.10	33.68	78.26	1.05	2.29	23.2	22.1
5	30			1.09	33.82	81.75	1.02	2.82	21.3	24.0
6	40			1.09	33.67	85.50	1.00	3.64	25.9	22.3
7	20	5.0 ± 0.1	55 % ± 0.43	1.12	33.67	60.91	5.11	5.88	23.5	22.2
8	30			1.12	33.70	63.46	5.09	6.35	25.0	21.8
9	40			1.11	33.66	66.38	5.04	7.12	23.6	22.6
10	20		70 % ± 2.4	1.10	33.67	78.46	5.06	6.11	24.0	22.4
11	30			1.09	33.67	81.07	5.19	6.81	24.3	21.5
12	40			1.08	33.66	84.94	5.01	7.55	24.4	22.6

--- Due to premature stopping of the experiment, cooling down data was not recorded.

Table 11 Main results from the open cell runaway experiments DCP

#	T_o [°C]	T_{max} [°C]	ΔT_{ad} [°C]	P_{max} [bar]	$(P\text{-}Pin)_{max}$ [bar]	dT/dt_{max} [°C/min]	dP/dt_{max} [bar/min]	TMR [min]
1	105.0	184.6	88.7	2.47	1.21	4.21	0.10	348
2	105.7	213.9	121.0	3.09	1.84	62.31	1.30	259
3	96.5	243.0	163.2	3.66	2.46	591.20	13.28	240
4	107.1	183.2	83.4	2.81	1.49	3.81	0.10	328
5	105.0	212.8	117.7	3.86	2.53	53.56	1.58	250
6	103.6	241.9	150.4	4.51	3.20	504.35	12.62	229
7	113.8	181.0	75.4	7.22	1.48	3.29	0.08	222
8	109.9	212.3	114.6	7.64	1.92	55.71	1.46	215
9	107.9	245.1	152.7	8.43	3.39	644.82	16.69	172
10	115.6	179.2	69.7	7.47	1.74	2.84	0.09	202
11	110.0	212.9	112.0	8.41	2.58	54.77	1.55	209
12	111.4	244.3	143.7	9.26	3.72	553.79	14.61	147

Table 12 Runaway of DCP in DIB for closed cell adiabatic experiments [84]

DCP [%w/w]	φ [-]	T_o [°C]	T_{max} [°C]	ΔT_{ad} [°C]	P_{max} [bar]	dT/dt_{max} [°C/min]	dP/dt_{max} [bar/min]	n * [mol/ kg sln]	dnG/dt_{max}^{*} [mol/(min· kg)]	$dnG/dt_{max,\varphi=1}^{*}$ [mol/(min· kg)]
20	1.12	110.8	175.5	72.4	37.1	2.75	2.75	0.394	0.029	0.050
30	1.15	105.5	212.6	123.7	48.2	68.9	40.81	1.261	0.687	1.964
40	1.14	102.3	242	159.3	66.7	556.45	280.45	1.645	3.429	10.673

*Calculated in this study and different from the original values reported in [80] so as to account for deviations from ideal gas behavior.

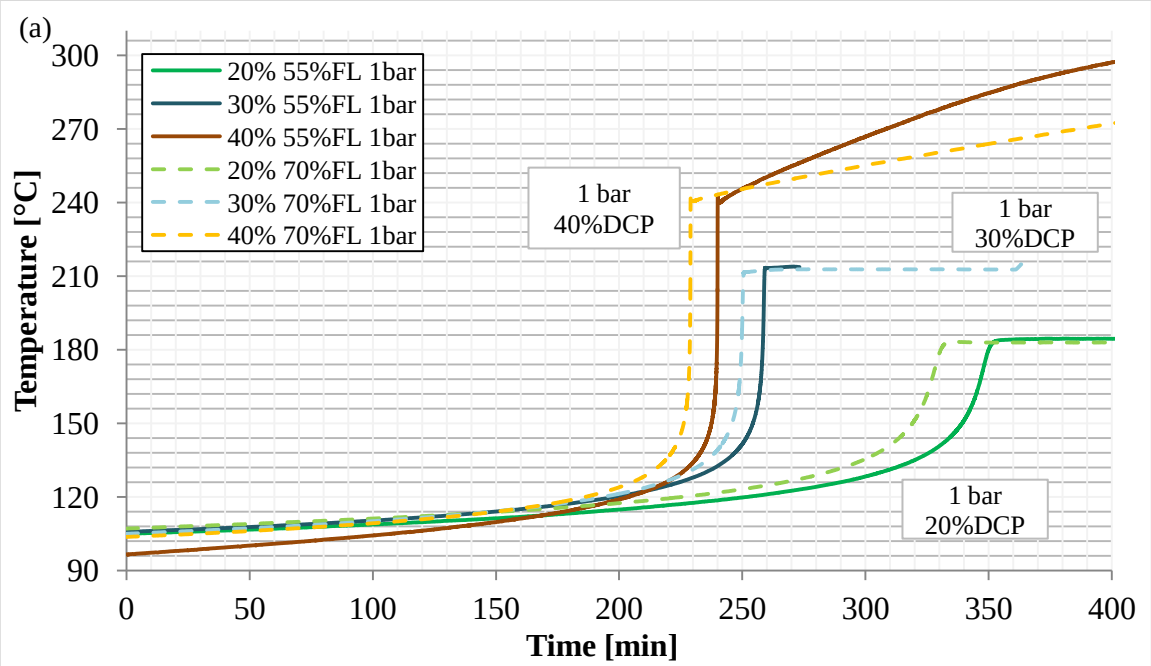

Figure 16 Temperature profiles (a) 1 bar initial pressure (b) 5 bar initial pressure

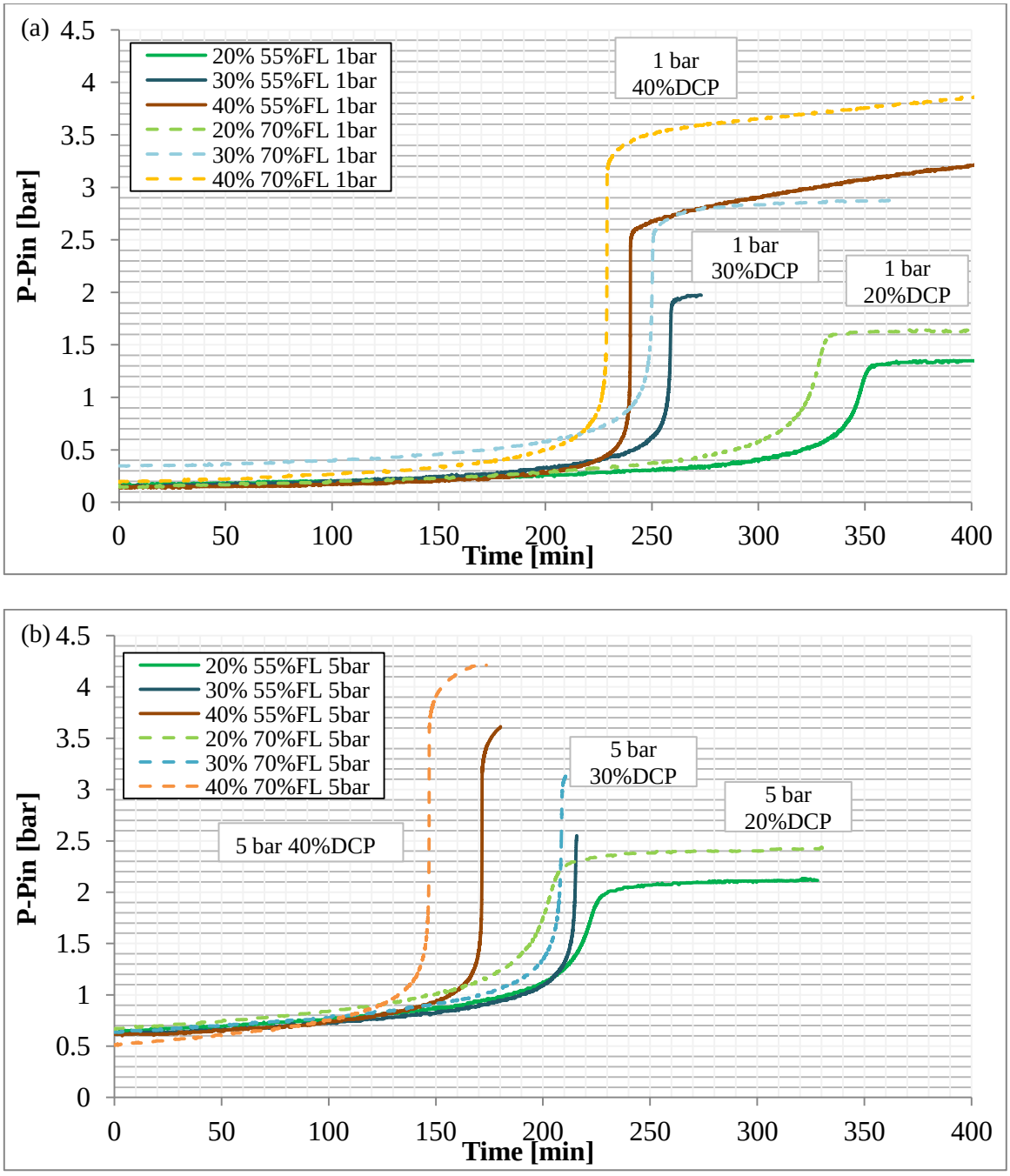

Figure 17 Pressure profiles (a) 1 bar initial pressure (b) 5 bar initial pressure

4.5.1 Kinetics results

The calculated kinetic parameters are displayed in Table 13. An overall order of reaction (n) for all experiments was estimated to be 0.91 ± 0.06. A good linear fit was obtained when plotting ln k* vs 1/T using the calculated n for each concentration (Figure 18). This corroborates that the assumption of nth order type kinetics is valid.

Table 13 Estimated kinetic parameters

DCP [% w/w]	n	1 bar initial Pressure		5 bar initial Pressure		Closed cell [80]		
		E_a [kJ/mol]	ln(A) [1/s]	E_a [kJ/mol]	ln(A) [1/s]	N	E_a [kJ/mol]	ln(A) [1/s]
20	0.93 ± 0.06	140 ± 2.6	32.37 ± 0.73	152 ± 1	35.99 ± 0.38	0.84 ± 0.05	147 ± 1	34.67 ± 0.27
30	0.91 ± 0.04	146 ± 0.9	34.23 ± 0.21	151 ± 0.2	35.72 ± 0.04	0.80 ± 0.10	148 ± 5	35.03 ± 1.39
40	0.90 ± 0.09	146*	34.46*	156 ± 0.6	36.17 ± 0.66	0.83 ± 0.09	149 ± 2	35.29 ± 0.43

*The 40%w/w DCP and 55% initial fill level at 1 bar test was not used to estimate the kinetic parameters due to potential calibration problems.

The order of the reaction was not affected by the concentration of the peroxide nor the filling level in the experiment. Similarly, as previously found out by adiabatic closed cell experiments, the concentration of the peroxide does not have a big impact on the observed activation energy at low concentrations; however, it seems to have a possible impact at higher concentrations.

The initial back pressure does seem to have an effect on the activation energy, resulting in larger activation energies at higher initial back pressures. This result agrees with the higher detected T_o at 5 bar initial pressures, and the possible explanation for this behavior is given below.

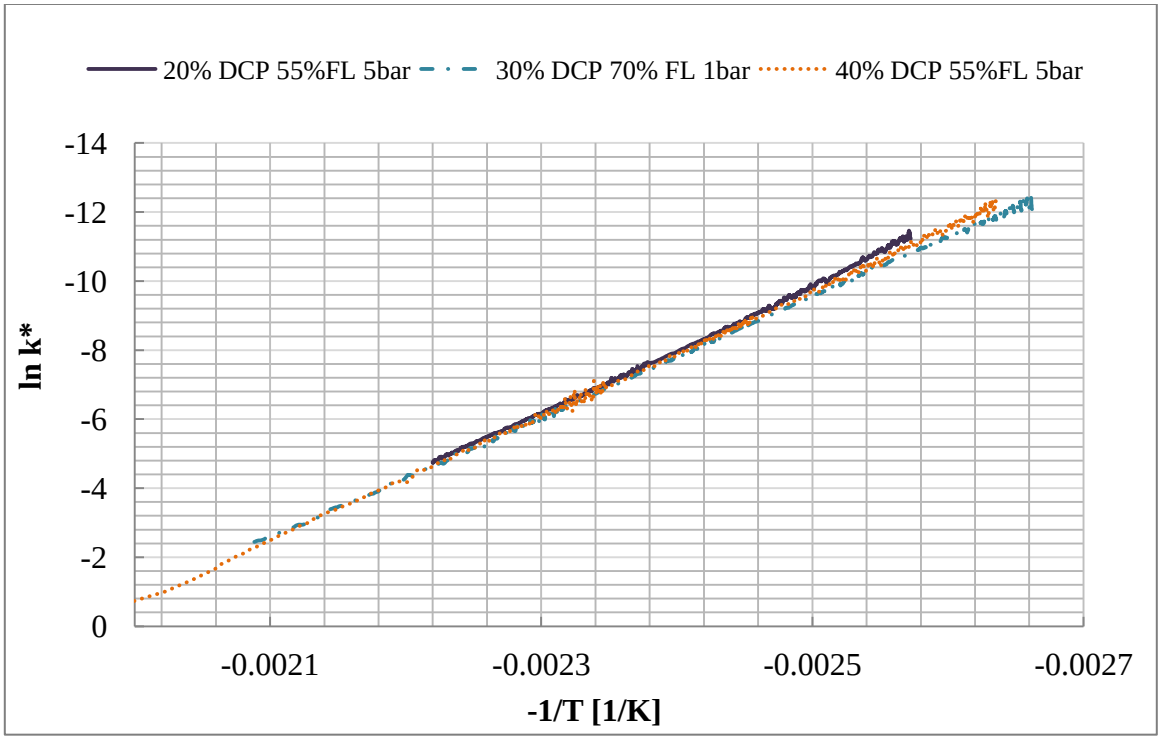

Figure 18 Relation between ln k* vs -1/T DCP in DIB

4.5.2 Sensitivity analysis open cell

The observed influenced of the initial back pressure, fill level and concentration on the kinetics and different DCP runaway parameters are summarized in Table 14. The fill level did not reveal any big impact on the temperature behavior, as the increase from 55% to 70% fill level, only lowered φ by a maximum of 0.03 (as seen in Table 11). However, on the other hand the initial back pressure and concentration were shown to affect the course of the DCP runaway: therefore the sensitivity analysis is focused mainly on the influence of these two variables on the kinetics and the 10 runaway parameters displayed in Table 5. The fill level influence is discussed in the cases where

it was observable. For the non-condensable gases and the maximum gas generation rate, the influence of the equipment configuration is also taken into account (section 4.2).

Table 14 Summary sensitivity analysis: ↑ Increase, ↓ Decrease, - No observable.

Variables (Increasing)	Parameters										
	Kinetics	T_o	T_{max}	Δ_{ad}	ΔP_{max}	TMR	dT/dt_{max}	dP/dt_{max}	Mass loss	n_g	dG/dt_{max}
Initial Back Pressure	Yes	↓	-	↓	↑	↓	-	-	↓	↓	↑
Filling Level	-	-	-	-	↑	↓	-	-	-	-	↑
Concentration	Possible	↓	↑	↑	↑	↓	↑	↑	↑	↑	↑

4.5.2.1 Onset temperature

The exothermic decomposition of DCP was first detected between 95 °C and 120 °C (Table 13). As expected, the higher the concentration the lower the onset temperature (Table 12); this observation also holds for closed cells experiments.

As observed in Table 11, runs starting at 1 bar exhibited a lower T_o than runs starting at 5 bar. In order to understand this behavior, the kinetics and thermodynamics of the studied system must be analyzed. In the general decomposition mechanism of DCP, at first, the homolysis of the O-O bond occurs and DCP decomposes to produce cumyloxy radicals. This first step of the reaction requires energy to occur. Further the cumyloxy radicals, which are highly reactive, exothermically decompose by a radical-induced mechanism to produce mainly methyl radicals and acetophenone [51,57].

From a thermodynamics perspective the energy that is being added to the system in the form of temperature as well as that liberated by the reaction (after the first step), is

utilized for two purposes: 1) to heat the liquid and initiate the homolysis of the O-O bond 2) for the gas molecules being formed to overcome the external pressure barrier and escape from the liquid phase.

In the experiments at 1 bar, less energy is required for this latter step. Therefore, most of the energy added in the form of temperature is used by the system to break the O-O bond and initiate the reaction. Therefore, the equipment can detect the initiation of the reaction at lower temperatures and less activation energy is required.

4.5.2.2 ΔT_{ad} and ΔP_{max}

A linear behavior of the ΔT_{ad} with concentration was observed (Figure 19 -a), this behavior corroborates that the assumption of a single reaction is reasonable.

Figure 19-b displays the pressure buildup of the reaction as a function of DCP concentration. This parameter is related to the quantity of gas produced by the decomposition. As expected, there is a higher pressure build up as the mass of DCP in the cell increases. This is noticeable in the form of increasing the concentration (along the x-axis) or increasing the initial filling volume from 55% to 70%.

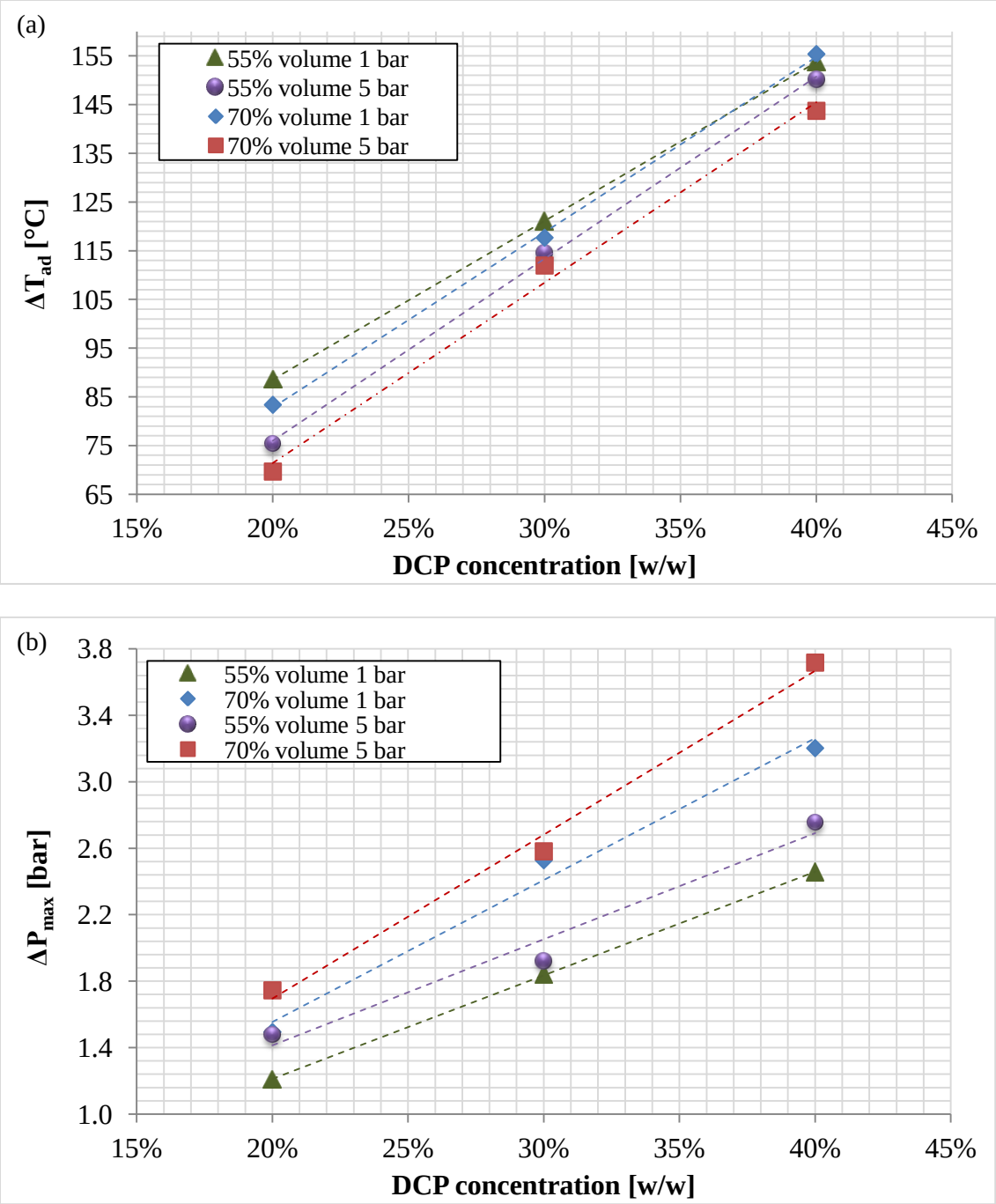

Figure 19 Maximum adiabatic temperature rise (a) and maximum pressure increase (b) vs concentration

It was observed that, in general, runs at 5 bar have higher pressure build up than runs starting at 1 bar (at the same initial fill volume).

This pressure behavior occurs because at higher vessel pressure less mass escapes from the test cell. It means that more reactants stay inside the sample holder and decompose, producing gases which contribute to the increase of pressure. The higher pressure build-up at different starting pressures is more notable for the experiments at highest concentration.

As observable in Table 11, there is not much difference between the maximum temperatures reached by the reacting mixtures. The initial back pressure did not seem to make any significant difference. However, as lower onset temperatures were obtained for 1 bar runs, and the phi factors of the experiments at each recipe are really close, the adiabatic temperature rise is higher for these tests. This adiabatic temperature rise is presented in Figure 19-a.

The different behavior between temperature and pressure can be due to where these measurements are taken and to the fluid dynamics aspect of the system. The temperature is measured directly inside the sample holder, while the pressure is measured within the entire containment vessel. At 1 bar pressure the gases produced by the reaction escape easily from the cell; these gasses can entrain/vaporize some of the solvent and therefore at later times a more concentrated solution can be present inside the can which would increase the maximum temperature attained by the reaction. On the other hand, even if reactants, solvent, or intermediates escape from the cell, they can still

react outside the cell and the effects of the reaction on the pressure inside or outside the cell is being accurately measured.

4.5.2.3 dP/dt_{max} and dT/dt_{max}

Self-heating and pressurization rates as a function of temperature are shown in Figure 20. These two variables showed strong sensitivity to concentration, but not to the initial back-pressure.

In Figure 20 and Table 11, it can be observed that the maximum pressurization and self-heating rates increase by around one order of magnitude when increasing DCP concentration by 10% w/w.

The initial pressure did not show a strong influence on the maximum temperature and pressure rises in the open cell configuration. However, at 40% w/w concentration, an effect of initial back pressure was noticed, with the run at 5 bars having higher self-heating and pressurization maximum rates when compared to the ones at 1 bar. This indicates a possible role of the initial pressure on the reaction kinetics for high concentration solutions of DCP. As expected maximum pressure rises in closed cell configuration are much higher at all concentrations (around an order of magnitude), on the other hand, self-heating rates in open and closed configurations are in the same range at every concentration.

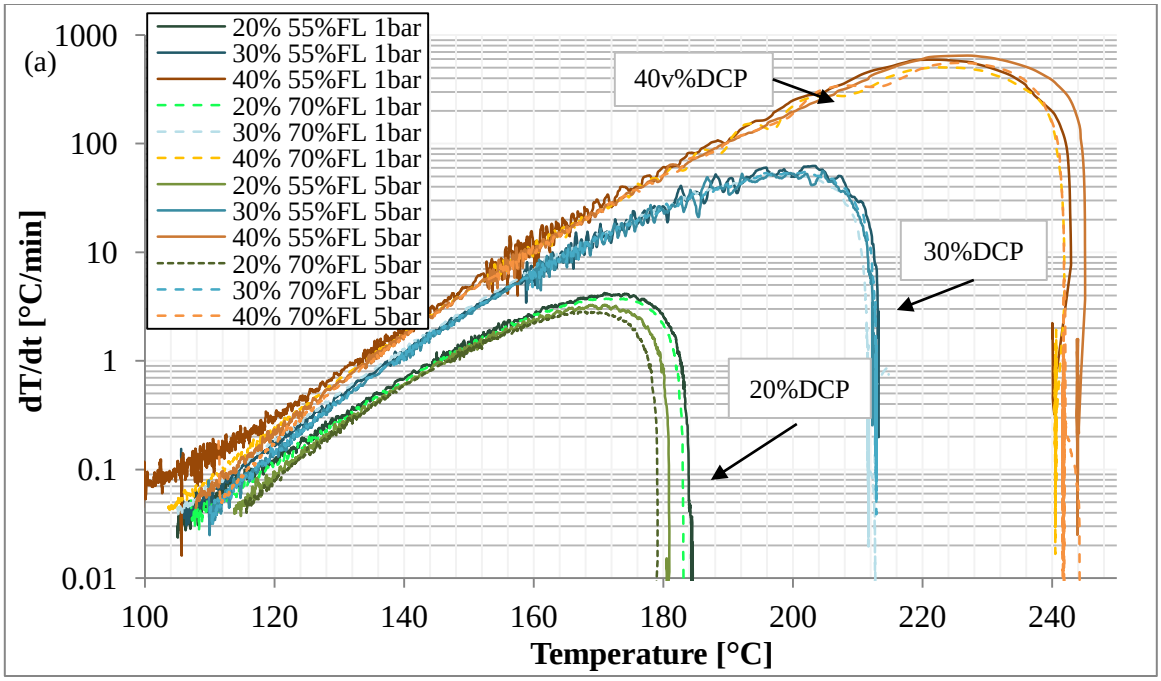

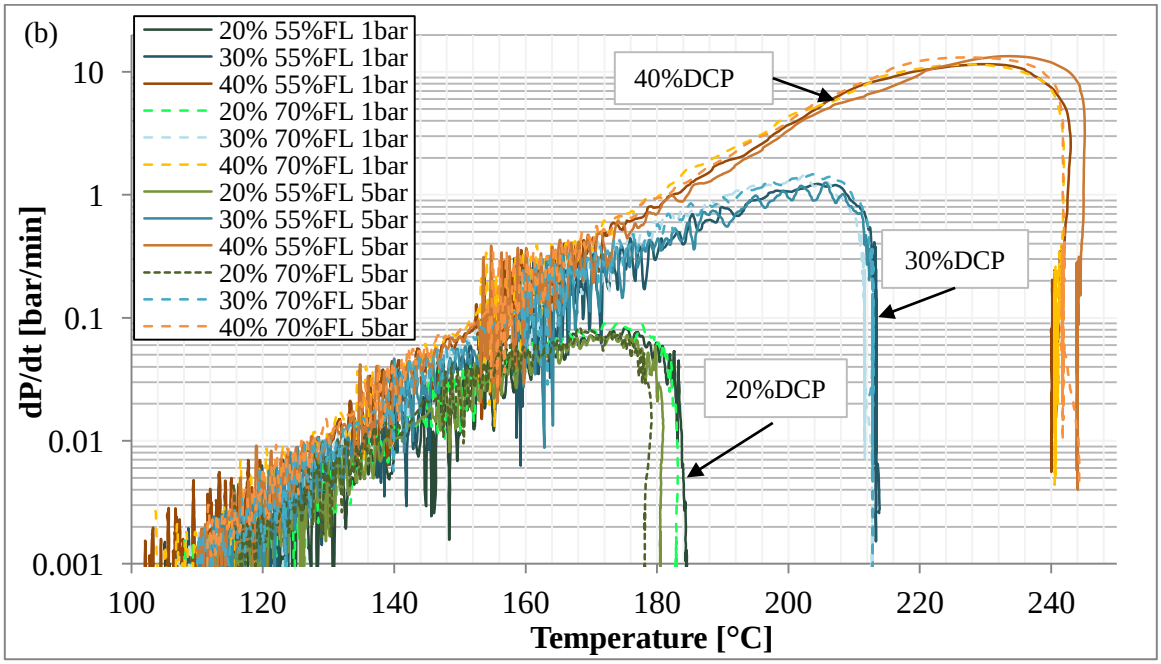

Figure 20 Self-heating rates (a) and pressurization rates (b)

4.5.2.4 Mass loss

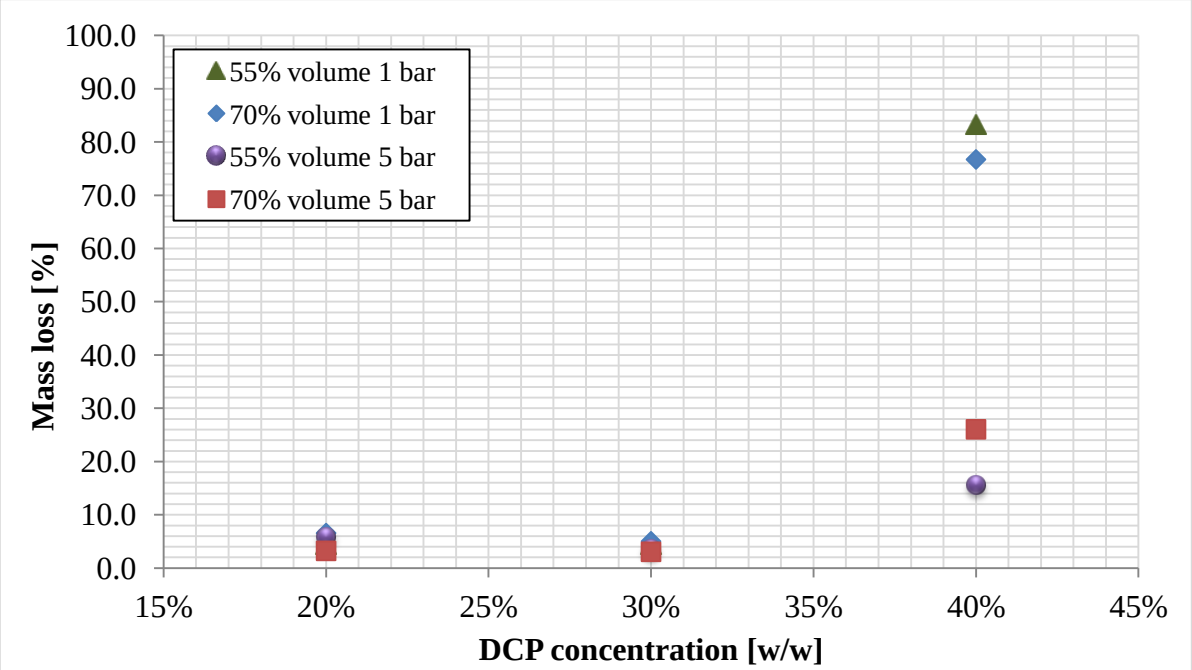

Figure 21 Mass loss percentage

The outcome of the mass losses is displayed in Figure 21, the mass loss depicted a quadratic increase with concentration. The obtained results showed that at low concentrations the initial fill level and starting pressure do not have a strong effect on the mass loss.

The influence of the initial pressure is easily seen in experiments at 40% DCP. Runs at 1 bar have significantly higher mass loss than rust at 5 bars. This could be due to the suppression of level swell at high starting pressures. These results indicate an influence of the initial pressure on the level swell and brings into question the validity of calorimetric tests performed at high concentration and low initial pressures.

The high mass loss for the runs at 40% concentration and 1 bar initial pressure could also be explained by higher maximum temperatures that were achieved after the runaway (which are most probably due to the boiling of the solvent). The loss of the solvent was visible in the viscosity and color difference of the product that was obtained from these runs, when compared to other runs as shown in Figure 22. The light color at low concentrations could also be a sign that the gas is escaping the cell before reacting.

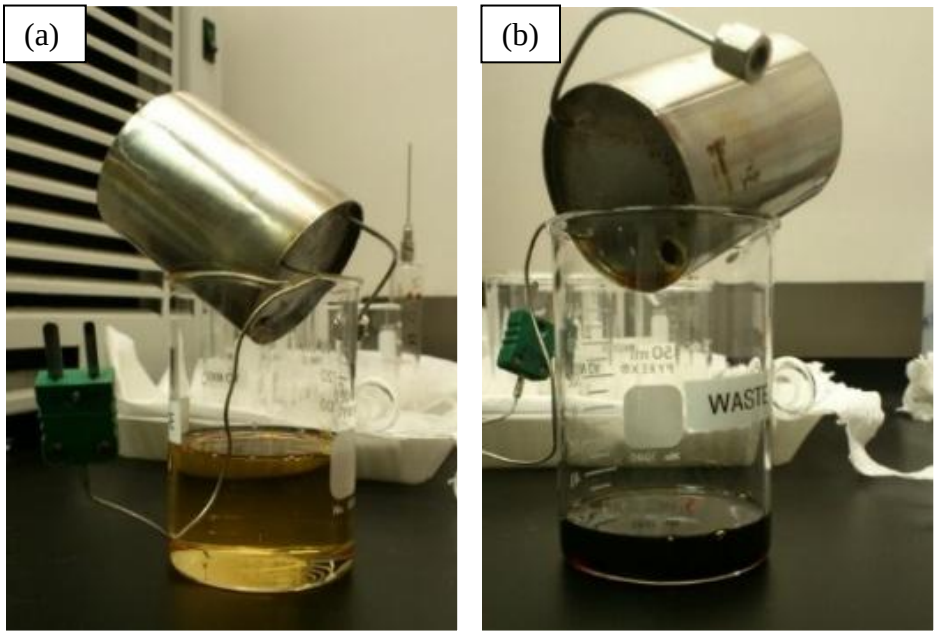

Figure 22 Final product from run of (a) 20% w/w DCP at 1 bar and (b) 40% w/w DCP at 1 bar (right)

4.5.2.5 Time to maximum rate (TMR)

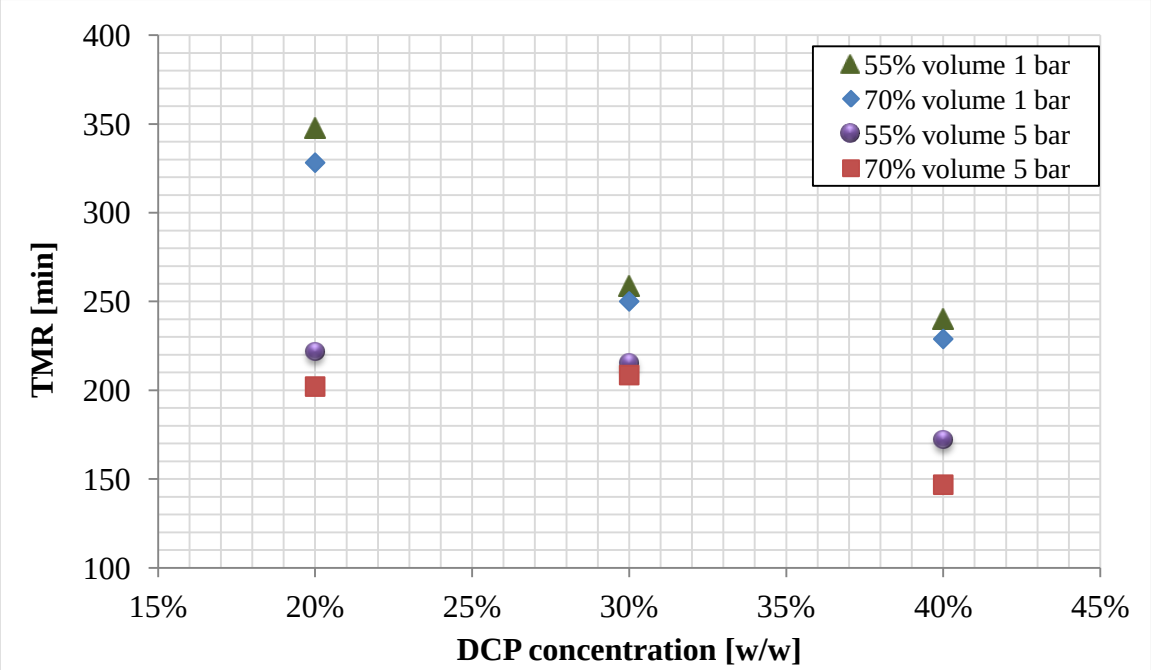

Figure 23 Experimental time to maximum rate

Even with the small increase in fill level (which increases the as expected) runs at 55% initial fill level take a longer time to achieve their maximum self-heating rates.

The experimental TMR was greatly influenced by the initial pressure with runs starting at 1 bar taking a longer time to achieve their maximum heating rate and following a different trend with respect to concentration than runs at 5 bar initial pressure. This can be due to 1) evaporative losses which slow down the reaction, 2) the influence of pressure on the reaction kinetics, and 3) an effect of the initial pressure on the level swell, with runs at 1 bar having higher level swell and therefore a smaller amount of solution during the runaway [94].

To explain the second point, the detailed kinetic and chemical characterization study performed by [41,59] was taken as a basis. Assume that the solvent does not participate in the reaction (as DIB is a large and stable molecule with a high boiling point); the radicals shown in Table 15 can be formed during DCP decomposition.

Table 15 Radicals formed during Dicumyl Peroxide thermal decomposition

Radical	Formula
R1	$C_6H_5CO\bullet(CH_3)_2$
R2	$C_6H_5C^{\bullet}(CH_3)_2$
R3	$CH_3\bullet$
R4	$C_6H_5COO\bullet(CH_3)_2$
R5	$HO\bullet$
R6	$C_6H_5(CH_3)_2(CO)_2(CH_3)(CH_2^{\bullet})C_6H_5$
R7	$C_6H_5C\bullet(CH_3)(CH_2OH)$
R8	$C_6H_5(CH_3)(CH_2\bullet)COOH$
R9	$C_6H_5(CH_3)(CH_2\bullet)COH$
R10	$CH_3OO\bullet$
R11	$HO_2\bullet$
R12	$C_6H_5(CH_3)(CH_2O\bullet)CH$

Increasing the pressure does not affect the homolysis of the O-O bond, as there is only one molecule splitting up in a liquid phase solution. However, as the DCP concentration increases and the concentration of free radicals increase, these later highly reactive species react between each other and will also start attacking DCP molecules by abstracting a hydrogen from the DCP molecule and enhancing its radical decomposition.

Table 16 Reactions between radical species and Dicumyl Peroxide

Regents	Products	E_a [kJ/mol]
R1 + DCP	$C_6H_5C(CH_3)_2OH$ + R6	33.07 ± 4.2
R3 + DCP	$CH_4 + R_6$	55.22 ± 4.2
R4 + DCP	$C_6H_5C(CH_3)_2OOH$+ R6	74.09 ± 4.2
R10 + DCP	CH_3OOH + R6	74.09 ± 4.2
R12 + DCP	$C_6H_5CH(CH_3)CH_2OH$ + R6	83.72

Table 16 depicts the reactions that are feasible between radicals and DCP along with their activation energies [41]. As can be observed the energy required for the reaction between DCP and the formed free radicals is much lower than that required for the O-O bond dissociation (140-156 kJ/mol), as calculated per this study Table 13, and is therefore more energetically favorable. By increasing the pressure to a certain amount (below the pressure where the free radicals are destroyed internally in the gas phase), the rate of radical propagation will increase [95] resulting in faster overall reaction consequently the time to reach the maximum self-heating rate will be much shorter at higher pressures and high concentration, as observed during this study.

4.6 Open Cell vs Closed Cell

For the sake of this comparison of open and closed cell data, the values of gas generation and measured maximum specific production rate were used. Table 17 shows the calculation results of the non-condensable gases and maximum gas generation rate for open cell configuration experiments performed in this study. In order to see how the configuration of the equipment affects the specific gas production rate (a parameter that is of paramount importance for vent sizing calculations), the 55% percent data at both

initial pressures, were plotted and compared to the closed cell adiabatic data shown in Table 12.

Table 17 Formation of non-condensable gases and maximum gas generation rate

#	dT/dt at dP/dt_{max} [°C/min]	T_{MAD} $T_{gas}=T_{liq}$ [°C]	dP/dt_{max} [bar/min]	(P-Po) at dP/dt_{max} [bar]	Δn [mol/ kg sln]	n_g [mol/kg solution]	dnG/dt [mol/(min *kg)] $T_{gas}=T_{liq}$	dnG/dt_{max} [mol/(min *kg)] $T_{gas}=T_{ave}$	dnG/dt_{max} [mol/(min *kg)] $T_{gas}=T_{am}$
1	3.84	448	0.10	1.11	1.05	0.96	0.06	0.08	0.10
2	62.23	476	1.30	1.59	1.58	1.38	0.79	1.03	1.44
3	589.63	495	13.28	2.03	2.35	1.65	7.24	9.71	14.11
4	3.72	445	0.10	1.29	1.08	0.98	0.06	0.07	0.09
5	49.96	475	1.58	2.21	1.54	1.53	0.73	0.96	1.34
6	502.93	496	12.62	2.66	2.15	1.63	5.10	6.94	10.27
7	2.64	448	0.08	1.80	0.93	1.62	0.06	0.07	0.10
8	47.41	478	1.46	2.32	1.46	1.75	0.87	1.15	1.61
9	644.68	501	16.69	2.76	2.25	2.14	8.72	11.88	17.66
10	2.81	441	0.09	1.88	0.99	1.44	0.05	0.06	0.08
11	53.94	476	1.55	2.67	1.40	1.74	0.71	0.94	1.33
12	474.96	493	14.61	3.07	2.08	2.09	5.73	7.95	12.01

4.6.1 Non-condensable gases

The permanent increase in pressure of the system, after the experiments had cooled down to ambient temperature (Figure 24) is a clear indication of the formation of non-condensable gases during the runaway decomposition of DCP.

The normalized formation of non-condensable gases (mol of gas/kg of solution) showed a linear increase with concentration (Figure 25) at all initial back pressures and for both equipment configuration.

The formation of non-condensable gases *slightly decreases* as the initial back pressure *increases*. This could be explained by the increase in the amount of dissolved gas due the higher pressure of the system at the same temperature. The role of the pressure on the gas solubility is even more significant when comparing these results to

closed cell experiments performed under the same conditions (concentration, solvent, equipment, and φ), as depicted in Figure 25, where the formation of non-condensable gases was calculated to be 0.32, 1.16 and 1.47 mol/kg solution for 20, 30 and 40% DCP concentration.

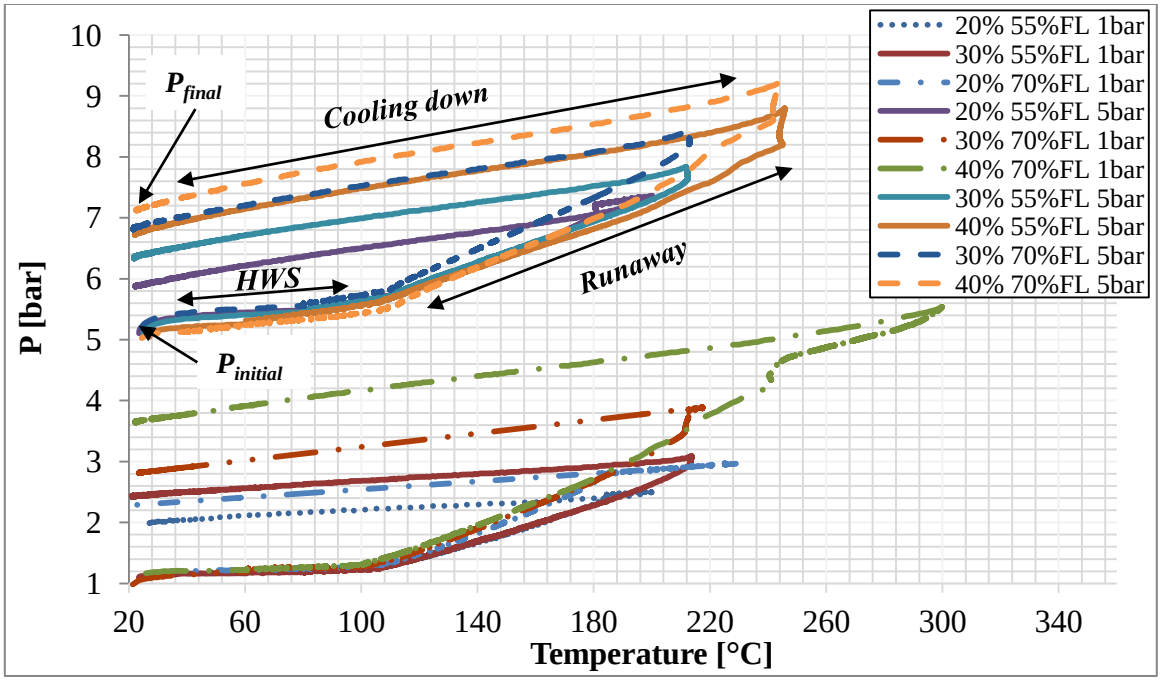

Figure 24 Pressure vs temperature profiles open cell experiments

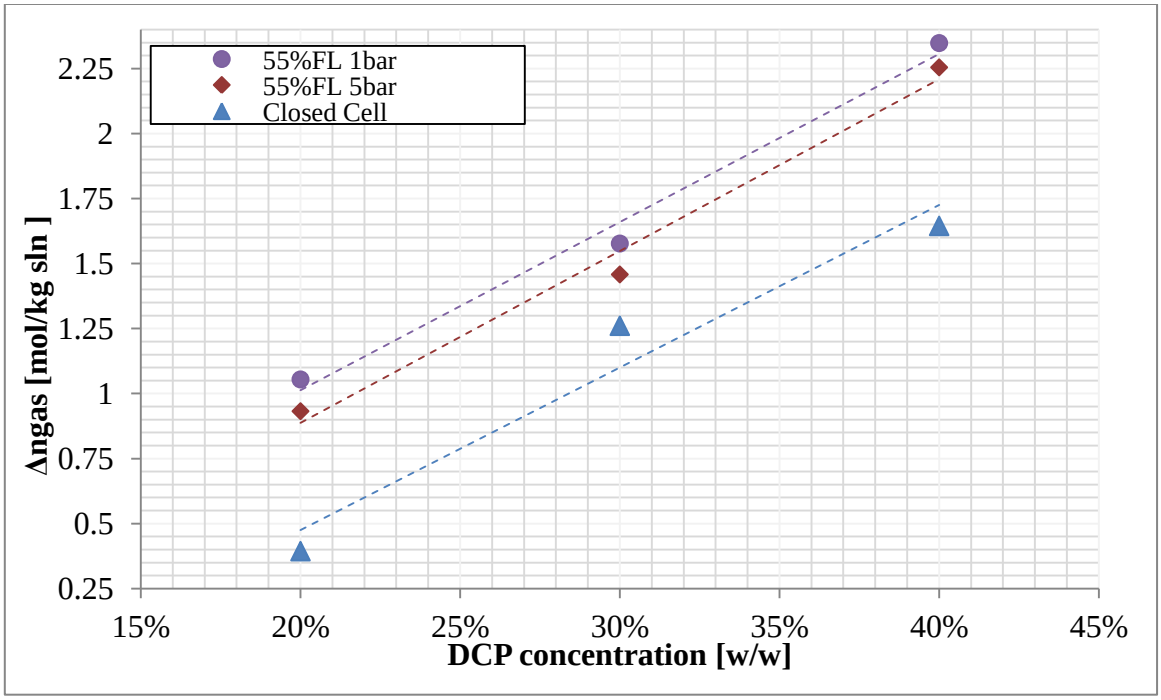

Figure 25 Formation of non-condensable gases per kilogram of solution 55% fill level open cell experiments vs closed cell

4.6.2 Maximum gas generation rate

Figure 26 shows the maximum specific gas production rate (kg of gas produced per kg of solution per minute) for open cell experiments at 55% fill level and closed cell experiments under similar conditions. Estimated gas production rate increases exponentially with concentration at both configuration. For clarity purposes, y-axis of Figure 26 is drawn at different scale for each concentration.

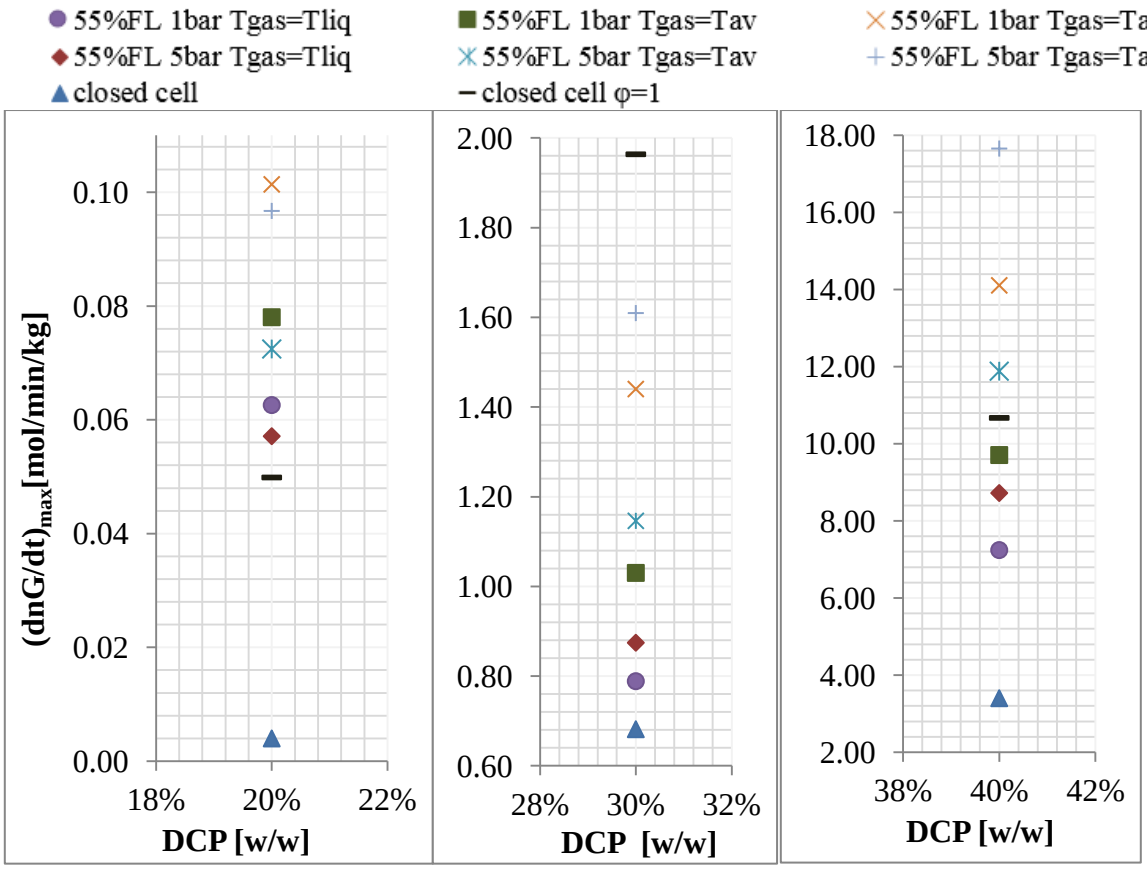

Figure 26 Maximum gas generation rate 55% fill level open cell vs closed cell

4.6.2.1 Temperature assumption

When comparing solely open cell data, the assumption of the gas temperature being equal than that of the liquid underestimates the calculated gas production rate in all cases. While when assuming ambient temperature, the calculated gas generation rate largely increases. This fact has also been observed in previous research [6] and highlights the importance of data interpretation. Results from these two different assumptions differ by factors up to 2.1 (at 40% concentration and 5 bar initial pressure).

For open cell experiments, for a given initial pressure in the containment vessel, the higher the cell initial fill level the lower the maximum specific gas production rate measured (Table 17). This means that a test with a higher initial fill level would be more prone to early level swell and consequently to significant mass loss from the test cell during the runaway. The higher specific gas production rates are therefore obtained with the test with the lower initial mass in the test cell (which may not be as intuitively expected).

For comparison purposes with closed cell data, the estimated gas production rate obtained from the assumption of the gas temperature being the average between the liquid and ambient temperatures is taken as reference (Figure 27). In all cases, lower values of specific gas generation rate were calculated when using raw closed cell data and lower initial pressures (except 20% where the values between the two starting pressures are really close).

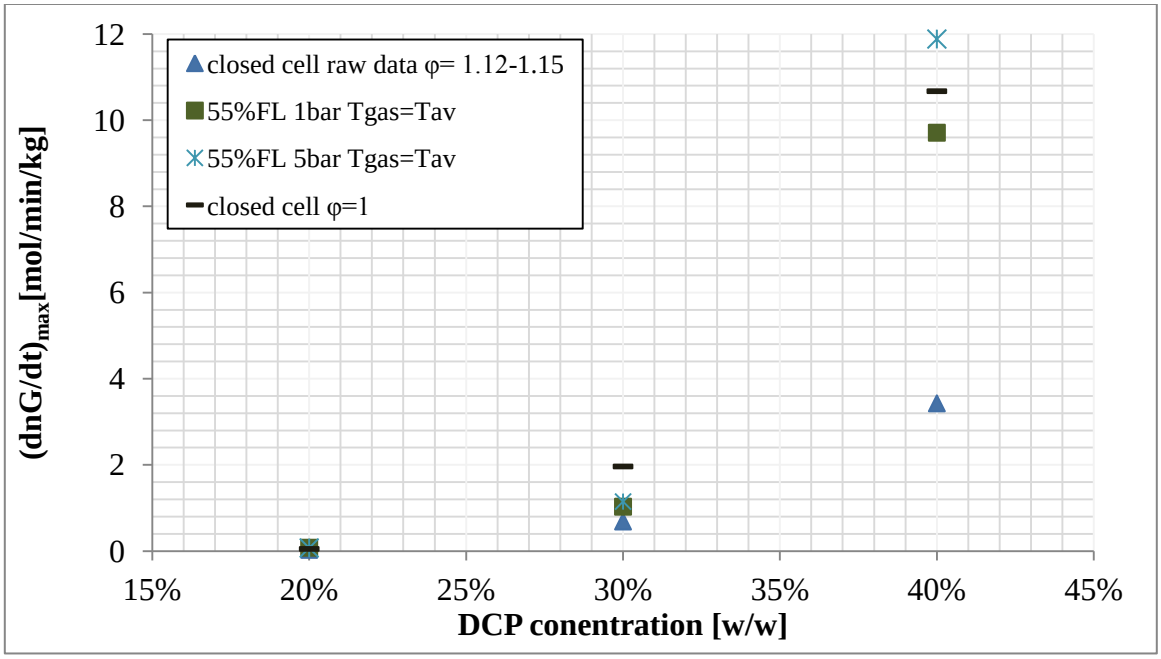

Figure 27 Comparison open vs closed cell maximum gas generation

As concentration increases the estimation of maximum gas generation rate becomes more sensitive to the initial back pressure, configuration, and correction method. At 40% DCP concentration these values are really sensitive to these three parameters. At this concentration, the maximum specific gas production rate can be:

22% higher when increasing the initial containment vessel pressure from 1 bar to 5 bar. This is related to the suppression of boiling and suppression of the level swell (reactant mass loss) at higher pressure as explained above. 347% higher when the test is performed in an open instead of closed configuration. This may be related to the solution of the gas in the liquid in the closed configuration due to the much higher pressures that are developed.

When comparing the estimated gas production rate from closed cell configuration corrected data (by φ), a general trend was not noticed. At 20% concentration the correction seems to still under predict the gas generation rate, while at 30% concentration it seems to overestimate it. At 40% concentration the obtained gas generation rate is comparable with the one obtained from open cell data by assuming an average temperature between the liquid and the ambient as the gas temperature. These observations at 40% concentration are in agreement with previous studies [6]. However a similar study for concentrations other than 40% has not been reported before. The incongruences with corrected data could be due to improper kinetics assumption, dynamic φ factor during the experiment or improper correction method. Deeper investigation and a wider concentration range of experiments should be done in order to get better understanding of these differences.

4.7 Conclusions

A sensitivity analysis on the runaway decomposition of dicumyl peroxide under adiabatic conditions was made by open cell adiabatic testing using the Phi TEC II calorimeter. Solutions of 20 %w/w, 30 %w/w, and 40 % w/w of DCP in DIB were tested. Only the dynamic parameters (those that are dependent on the self-heating rate), namely T_o, T_{max}, P_{max} and TMR were affected by the initial pressure of the experiments. The static parameters (ΔT_{ad} and generation of non-condensable gases) were not dependent on the initial pad pressure.

Regarding the kinetics, the global order of reaction (n) was calculated to be 0.91 ± 0.06. Good linear fitting was obtained when plotting ln k^* vs 1/T, therefore the

assumption that the runaway decomposition of DCP follows an n^{th} order type kinetics is justified, at least over the range of test variables that were studied. The concentration of the peroxide did not display any influence on the activation energy, but, the initial back pressure did; higher activation energies were estimated at higher initial back pressures. Similarly higher detected onset temperatures were observed at higher initial pressures.

Expected general trends of the runaway severity parameters with respect to DCP concentration, initial pressure and initial fill level were observed. The maximum adiabatic temperature rise depended linearly on concentration, while the mass loss displayed a quadratic increase with concentration. The initial fill level was shown to have a big influence on the experimental time to maximum rate with runs starting at 1 bar taking a longer time to achieve their maximum heating rate and following a different trend with respect to concentration than runs at a higher initial pressure.

Comparison of the obtained maximum gas generation rate results with raw and corrected adiabatic closed cell data performed at similar conditions was conducted. Discrepancies were encountered between different initial pressures, as well as with configuration of the equipment and corrected closed adiabatic data. Main source of discrepancies where: *1)* temperature of gas assumed at open cell configuration, *2)* vaporization issues changing with initial pressure at open cell configuration (therefore also with configuration), *3)* configuration at which the test are performed, and 4) correction of data by thermal inertia factor. These discrepancies highlighted the fact that experimental conditions and data interpretation have a high impact on estimation of gas generation rate on a large-scale.

The role of the detailed kinetics, thermodynamics and fluid dynamics of the system under runaway was evaluated and discussed. This analysis contributes to obtain a better understanding of the reasoning behind encountered discrepancies in adiabatic experimental measurements (pressure, temperature, and rate of temperature rise at maximum pressure rise, sample mass, volume being pressurized and initial pressure within this volume). Many of these data are required for vent sizing calculations following the DIERS methodology.

CHAPTER V*

EVALUATION OF THE THERMAL RUNAWAY DECOMPOSITION OF CUMENE HYDROPEXIDE

5.1 Synopsis

This chapter is aimed at a better understanding of the possible consequences of CHP decomposition by analyzing its thermal runaway behavior when dissolved in a high boiling point solvent using two different adiabatic calorimeters. The experimental data obtained allowed us to assess the general trends of the main runaway parameters (*i.e.*, maximum temperature and pressure, gas generation, maximum rise of temperature and pressure rates, and onset temperature). Collected experimental data was also used to characterize the decomposition of the mixture with respect to the peroxide concentration (16%, 20%, 24%, 30% and 32% by weight); and to study the influence of the thermal inertia and configuration of the equipment. Temperature and self-heating rate profiles were corrected to adiabatic conditions. The data generated can assist as guidance for designing limits of operation, controls and safeguards of processes where CHP is involved.

* This Chapter contains material reprinted from "Evaluation of the Thermal Runaway Decomposition of Cumene Hydroperoxide by Adiabatic Calorimetry" by Olga Reyes Valdes, Valeria Casson Moreno, Sam Mannan, and Luc Véchot 2015. Chemical Engineering Transactions, Volume 43, May 2015, Pages 1009-1014, ISBN 978-88-95608-31-1, ISSN 2283-9216. Copyright AIDIC [2015]

5.2 Introduction

Cumene Hydroperoxide (CHP) is widely used as an initiator, a cross linking agent, a hardener and a drying accelerator in the petrochemical industry. However, the use of this peroxide presents an intrinsic hazard due to its high instability nature (class IV) [96] and its thermal decomposition reaction, which is usually highly exothermic. Currently there is very few experimental data available on the behavior of hybrid systems (gases and vapors are formed during the decomposition), such as CHP. This is particularly true for untempered hybrid systems, where most of the studies present in the literature are focused on the description of the kinetic of decomposition [38–40] or on the assessment of the thermal hazards and runaway prevention by *screening techniques* [43,44,97] . The experimental study being conducted in this chapter, aimed to: (1) Collect experimental data to characterize the behavior of the runaway decomposition of CHP when diluted in a high boiling point solvent; (2) identify the main parameters of the runaway decomposition of such untempered hybrid system; and (3) address the importance of following a rigorous methodology while collecting and analyzing experimental data. To achieve these objectives, a series of adiabatic experiments at two different scale calorimeters were performed

5.3 Materials and Methods

Solutions of CHP in 2,2,4-trimethyl-1,3-pentanediol diisobutyrate (DIB) were used to study the runaway decomposition of CHP. Experiments were run at 72.5% ± 2.5% filling level of the sample cells. Closed cell experiments were run at concentrations of 16%, 24% and 32% w/w of CHP. Open cell experiments were run at concentration of

20%, 30% and 40% w/w of CHP. Table 18 displays CHP physical properties. DIB physical properties are those specified in Table 4 of Chapter III.

Table 18 CHP physical properties

Chemical	Structure	Molecular weight [g/gmol]	Purity	Boiling point [°C]	Flash point [°C]	Cas. No.
Cumene Hydroperoxide	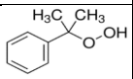	152.19	80%	100-101 (at 0.011 bar)	79 (close cup)	80-15-1

The runaway experiments were conducted using Phi-TEC I and Phi-TEC II in closed cell configuration as described in 3(page 26); Phi-TEC II was also used in open cell configuration as explained in detailed in 4.3.2 (page 59).

5.3.1 Experimental procedure CHP decomposition

Solutions were first quickly heated to 70 °C. After a 40 min calibration, the equipment was programmed to start operating in the heat-wait-search mode, with heating steps of 2 °C/min. Once the beginning of the runaway was detected the equipment shifted to adiabatic mode. After the completion of the runaway, the experiments were stopped and the equipment was left to cool down to ambient conditions, where the final temperature and pressure were recorded. The mass of the final products in the cell was also recorded. The measured initial and final conditions of each of the test performed during this work are shown in Table 19 and

Table 20 20. The 32 % concentration data in closed cell configuration of the Phi-TEC II, could not be recorded as the test cell burst. However, in this research concentrations higher than previous reported adiabatic data at low phi factor was obtained (maximum had been 20.6%) [40].

Table 19 Closed cell CHP adiabatic tests experimental conditions

#	Equipment	CHP [% w/w]	φ	Cell mass [g]	Sample mass [g]	$T_{initial}$ [°C]	T_{final} [°C]	$P_{initial}$ [bar]	P_{final} [bar]
1	Phi-Tec I	16	1.75	19.1	5.7	17.0	17.0	1.01	11.7
2		24	1.65	15.8	5.4	21.1	19.6	0.92	18.7
3		32	1.75	19.1	5.5	21.3	24.0	1.36	27.3
4	Phi Tec II	16	1.12	42.3	79.0	23.0	23.8	1.03	20.7
5		24	1.12	42.3	79.4	26.7	25.4	1.03	29.7
6		32	1.12	42.7	80.2	26.0	24.0	0.92	39.2

Table 20 Open cell CHP experimental conditions

#	CHP [% w/w]	φ	Cell mass [g]	Sample mass [g]	$T_{initial}$ [°C]	T_{final} [°C]	$P_{initial}$ [bar]	P_{final} [bar]
7	20	1.09	33.8	74.1	23.3	26.1	1.02	2.22
8	30	1.10	33.8	72.9	16.5	22.2	1.02	2.61
9	40	1.09	33.8	75.7	23.3	24.2	1.02	2.85

5.4 Calculations and Data Treatment

The experimental data obtained from the Phi-TEC I gave a preliminary estimation on the decomposition behavior of CHP runaway. The following data were recorded: onset temperature (T_{on}), maximum temperature (T_{max}) and pressure (P_{max}) generated. From there the maximum self-heating and self-pressurization rates (dT/dt_{max}, dP/dt_{max}) were calculated. These experiments were used as screening tests to successfully and safely perform experiments in the Phi-TEC II calorimeter. A more

accurate calorimetric study was subsequently performed with the Phi-TEC II providing a more realistic assessment of the runaway characteristics at industrial scale (due to its low φ). CHP runaway decomposition was evaluated following the same approach taken in chapters III and chapters IV.

5.4.1 Activation energy CHP decomposition

The activation energies, order of the reaction and pre-exponential factor of CHP decomposition reaction, were calculated by assuming that:

1. The global decomposition reaction follows an n^{th} order kinetics [40,53,98]
2. Arrhenius relationship holds and,
3. Conversion can be estimated from adiabatic temperature data (Townsend – Tou) [76].

5.4.2 Temperature and self-heating rate profiles

For closed cell experiments, temperature and self-heating rate profiles were corrected by the phi factor to adiabatic conditions in order to estimate a worst-case scenario on a large-scale. Equations 3.12-3.15 specified in chapter III were used. Analysis of the results and discrepancies encountered are highlighted.

The average activation energy calculated for each recipe (16, 24 and 32)% w/w CHP was used to correct the temperature and self-heating rate profiles.

Open cell data was not corrected by the phi factor because the widely-known basis for the correction [99] only considers heat loss to the cell wall, without considering heat loss due to vaporization[100]. Vaporization process becomes much more significant with the larger head space and lower pressures experienced during open cell tests.

5.5 Results

5.5.1 Hazard evaluation by closed cell: Phi TEC I vs Phi TEC II

Temperature and pressure profiles versus time at the three different concentrations resulting from closed cell configuration experiments are displayed in Figure 28.

It is important to recall that during the 32% CHP tests in the Phi-TEC II the cell burst, therefore: (1) the max pressure obtained during this experiment was lower than P_{max} at 24% (61.54 bar). So this value cannot be used for comparisons other experiment; (2) dP/dt_{max}, dT/dt_{max}, and T_{max} (shown in Table 21 and Figure 28) could be much higher; and (3) it is unlikely that a successful test can be done at 32% concentration of CHP in the closed cell configuration at low φ and high filling level in the Phi-TEC II or similar equipment.

Table 21 Results closed cell testing CHP

#	T_o [°C]	T_{max} [°C]	ΔT_{ad} [°C]	P_{max} [bar]	dT/dt_{max} [°C/min]	dP/dt_{max} [bar/min]	TMR [min]
1	145.2	211.6	116.2	21.8	1.6	0.5	212.2
2	130.6	254.2	203.4	37.2	43.5	16.0	304.3
3	121.0	292.9	300.7	45.9	338.3	128.1	280.7
4	147.0	225.0	87.3	48.9	11.1	20.2	162.8
5	130.5	273.2	159.6	71.2	104.5	65.7	305.1
6	124.9	363.5	212.4	61.5	1361.7	325.1	352.1

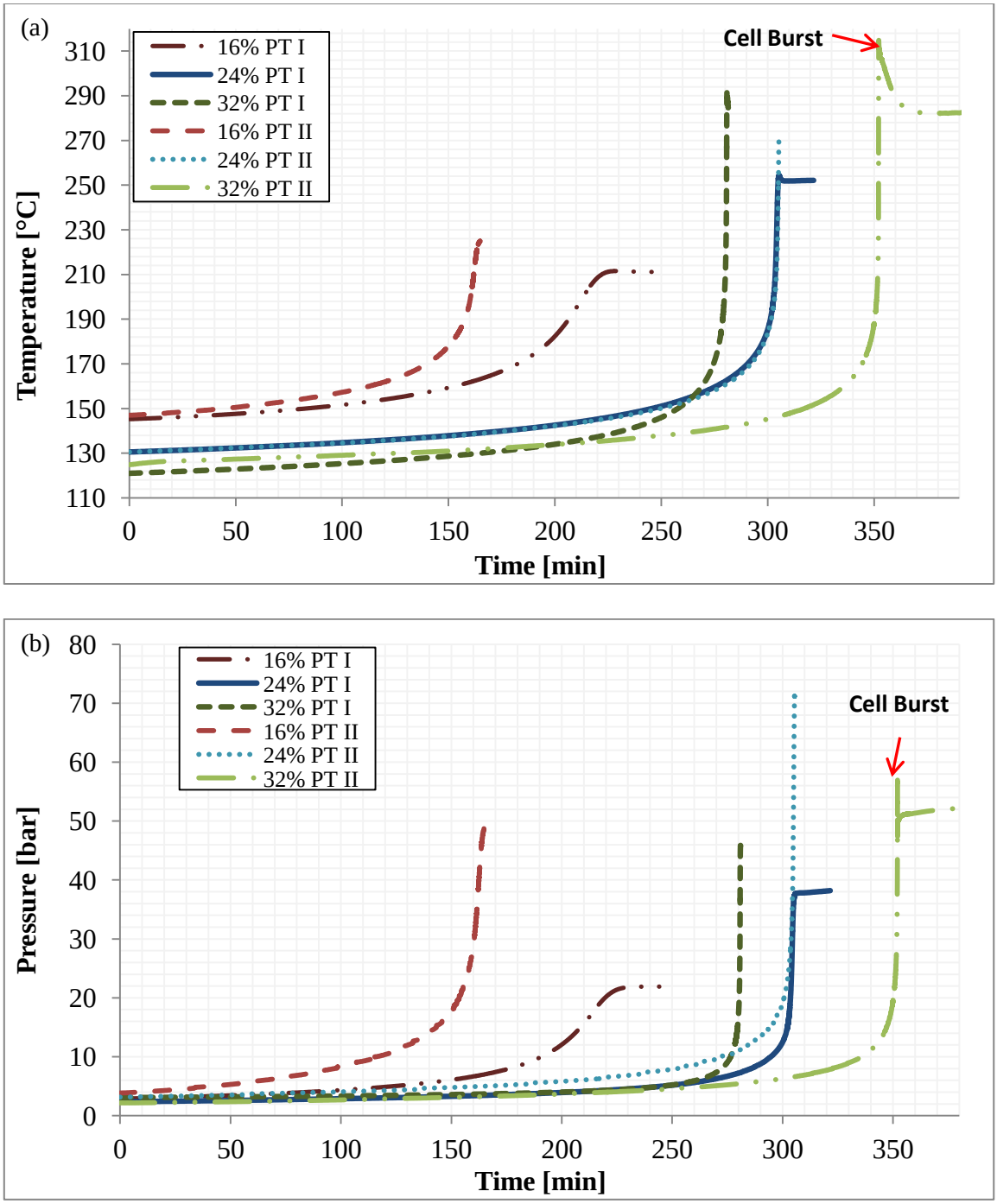

Figure 28 Closed cell (a) temperature and (b) pressure profiles of CHP decomposition in DIB

5.5.1.1 Onset temperature

From Figure 28-a, it can be easily seen that the exotherm is detected when the temperature is about 120°C and higher. As expected, the lower the concentration the higher the onset temperature.

A strong influence of the φ of the equipment on T_{on} was not observed. As observed by previous authors [19] T_{on} is determined primarily by the exotherm resolution detection as well as the equipment adiabaticity, and not by φ. In this study, both the Phi TEC I and Phi TEC II equipment have a threshold detection of 0.02 C/min. Heat losses at the onset temperature may not be that significant to show a major difference in the detected values.

5.5.1.2 Maximum temperature and pressure (T_{max} and P_{max})

Influence of Concentration: In Figure 28 the CHP reactivity in terms of temperature and pressure is easily observable. As expected, the higher the concentration the T_{max} and P_{max} achieved during the reaction. It is worth to point out that the boiling point of the solvent is 280°C. Hence at least some of the pressure generated for the 32% run in both Phi-TEC I and Phi-TEC II can be due to the vapor pressure of the solvent.

Influence of thermal inertia: Low thermal inertia experiments showed an effect in the temperatures and pressures measured during the runaway. It was noticed that φ has a stronger effect on the maximum pressure than on the maximum temperature. However, previous and current research have focused their attention to correction methods for temperature and self-heating rate profiles to account for wall heat losses

[11,81] and vaporization issues [100]; but very little is found on pressure and self-pressurization data corrections.

5.5.1.3 Maximum self-heating dT/dt_{max} and self-pressurization dP/dt_{max} rates

Self-heating and self-heating pressurization rates vs the reciprocal of temperature profiles are shown in Figure 29[1].

Influence of Concentration: Self-heating and self-pressurization rate curves showed similar trends with concentration. As concentration increases the self-heating rate and self-pressurization rate also increase. Self-heating and self-pressurization increment can transform to unreliable data. For example, at high at high self-heating rates, heat losses from the cell will increase as heaters start failing to maintain the adiabatic conditions of the sample so the equipment lose adiabaticity [40]. Therefore, values of self-heating rates above the equipment tracking specification (100 °C/min) could be much higher, and should be carefully analyzed [84]. Flattening shown in the 32% CHP self-heating rate vs the temperature reciprocal at the Phi-TEC II can be the result of: heat losses during the bursting of the cell or time lag of the thermocouples.

Influence of thermal inertia: The thermal inertia of the equipment also showed a strong influence on self-heating and self-pressurization rate curves. The maximum peaks achieved at low thermal inertia experiments are much higher than those at larger thermal inertia experiments.

[1] Phi-TEC II self-pressurization rate profiles are not shown because of noise

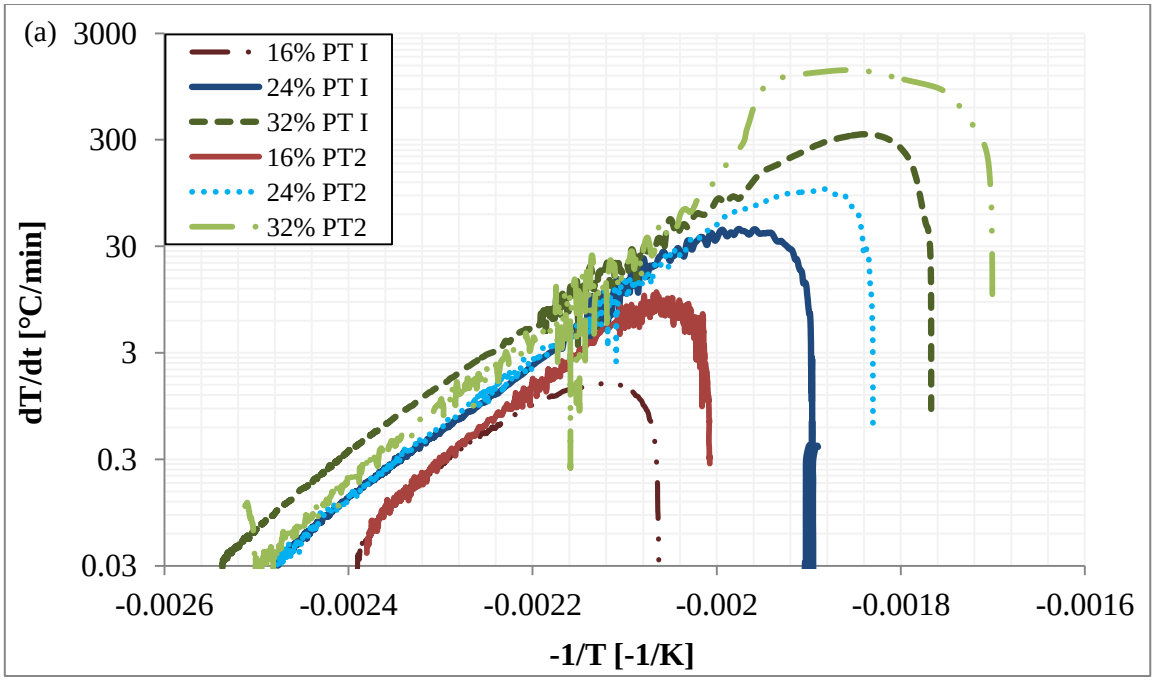

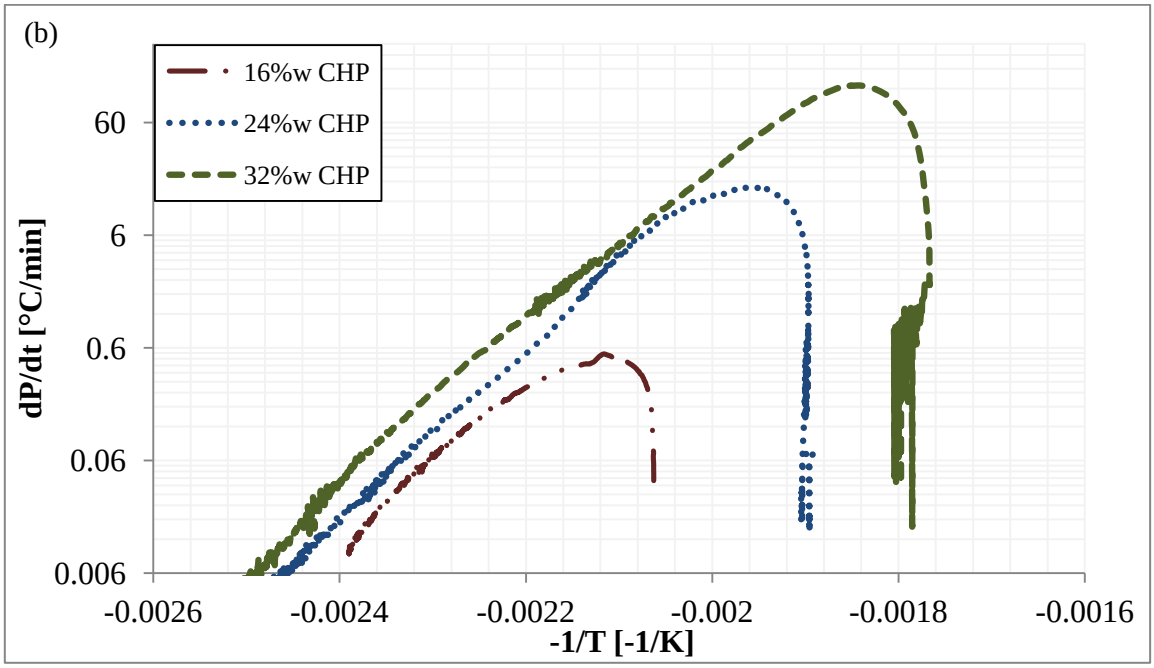

Figure 29 (a) Self-heating rate profiles and (b) self-pressurization profiles vs -1/T

5.5.2 Further observations

When comparing the results obtained in this study to previous adiabatic calorimetric studies at similar conditions, it was observed that the general trends are similar (the higher the concentration and lower the phi factor the higher the T_{max}, P_{max}, dT/dt_{max}, and dP/dt_{max}). However, as shown in Table 22 major discrepancies were observed in the reported values. As concentration increases these discrepancies became more notorious.

Data collected in this study at 32%w/w concentration infer a more severe CHP runaway than previously reported data at 35% concentration, with self-heating rates up to 3 times larger and self-pressurization rates up to 6 times larger.

Table 22 Comparison with adiabatic data available in the literature

Concentration CHP [% w/w]	Solvent	φ	T_{max} [°C]	P_{max} [bar]	dT/dt_{max} [°C/min]	dP/dT_{max} [bar/min]
15%[13]	Cumene	1.20	223.9	24.39	9	2.76
16 % [101]	Not specified	1.29	182.0	11.55	1.704	0.17
16% [This Study]	DIB	1.75	211.6	21.8	1.6	0.5
16% [This Study]	DIB	1.12	225.0	48.9	11.1	20.2
20.6% [40][2]	Cumene	1.25	236.0	51.9	16.9	5.5
35% [101]	Not specified	1.28	250.5	34.93	336.832	51.49
35% [13]	Cumene	1.45	248.7	47.09	108	55.15
32% [This Study]	DIB	1.75	292.9	45.9	338.3	128.1
32% [This Study]	DIB	1.12	363.5	61.5	1361.7	325.1

[2] Highest concentration reported. Authors tested 83.9% CHP concentration, but cell ruptured during test.

The explanation behind these discrepancies could be:

(1) Solvent: study [13] used cumene as a solvent, while study [101] doesn't specify the solvent used. As previously shown with DCP [84] , the solvent can greatly influence the runaway behavior of the peroxide and the runaway reaction of DCP becomes more severe when dissolved in Cumene rather than in DIB. When CHP is dissolved in cumene, the boiling point of the solvent (152 °C) is within the range of the runaway. The differences in temperature noticed with respect to [13] could be due to some of the generated heat being used a latent heat of vaporization and/or to the solvent reacting with some of the radicals created during CHP decomposition and forming more stable molecules. Reported data in [101] predicts a CHP runaway severity much milder than [13] and the present study. These discrepancies highlight the importance of fully specifying the conditions used at lab-scale in order to have data that can be replicated and used for risk assessment purposes.

(2) Pressure leaks: observed differences are much more notorious in the maximum pressures and maximum self-pressurization rates. This could be due to sample cells leakage at high gas generation rates [91]. Pressure is one of the major hazards during a runaway reaction; discrepancies in pressure measurements must be carefully addressed.

(3) Loss of adiabaticity: both temperature and self-heating rate at 32% w/w at the highest phi factor tested in this study are larger than those reported in [13] and [101] at much lower phi factors and lower concentration, which indicate that

potential heat losses in previous data reported could be present. This results was not expected because the thick cell of the Phi TEC I acts as a heat sink absorbing almost half of the heat produced by the decomposition [91].

5.5.3 General trends closed and open cell configurations

Table 23, summarizes the main results of the runaway decomposition of CHP at 20%, 30% and 40% concentration obtained at open cell configuration.

Table 23 Main results open cell experiments

CHP [% w/w]	T_o [°C]	T_{max} [°C]	ΔT_{ad} [°C]	P_{max} [bar]	$(dT/dt)_{max}$ [°C/min]	$(dP/dt)_{max}$ [bar/min]	TMR [min]
20	134.7	250.7	126.9	3.35	59.90	2.13	292.7
30	129.3	277.6	162.5	4.26	312.96	13.14	252.0
40	118.2	291.6	198.8	4.94	656.61	27.27	339.1

5.5.3.1 Onset temperature

In general, in open cell experiments the onset was detected at lower temperatures than in the closed cell experiments (at similar concentrations). This can be due to the lower pressures experienced at this configuration. As demonstrated with DCP (previous chapter) at two different initial pressures, an increase in pressure will, in a way, hold the molecules "more tightly" so more energy would be required to break the O-O bond.

5.5.3.2 Maximum temperature and pressure

The maximum temperature showed a linear increase with concentration at closed cell experiments at both Phi-TEC I and Phi-TEC II (Figure 30-a). At open cell T_{max} also

increase with concentration; however, the increase percentage start to decrease as concentration increases. A possible explanation for this behavior is as follows:

- In experiments run at open cell configuration as the concentration increases, the percentage of mass loss also increases. This is due to gases and vapors escaping from the test cell. For example at 32% CHP concentration, 90% of the initial mass has been lost. The volume of the mixture remaining in the cell at the end of the test at open cell configuration is so low that the cell thermocouple is no longer inside the sample, which could lead to an erroneous temperature measurement and larger phi factor.

The maximum pressure also showed an increase with concentration. As depicted in Figure 30-b, the trends in maximum pressure are similar at closed cell and open cell configuration (which is expected as in open cell configuration the measurement reading is on the containment vessel, not only on the sample holder).

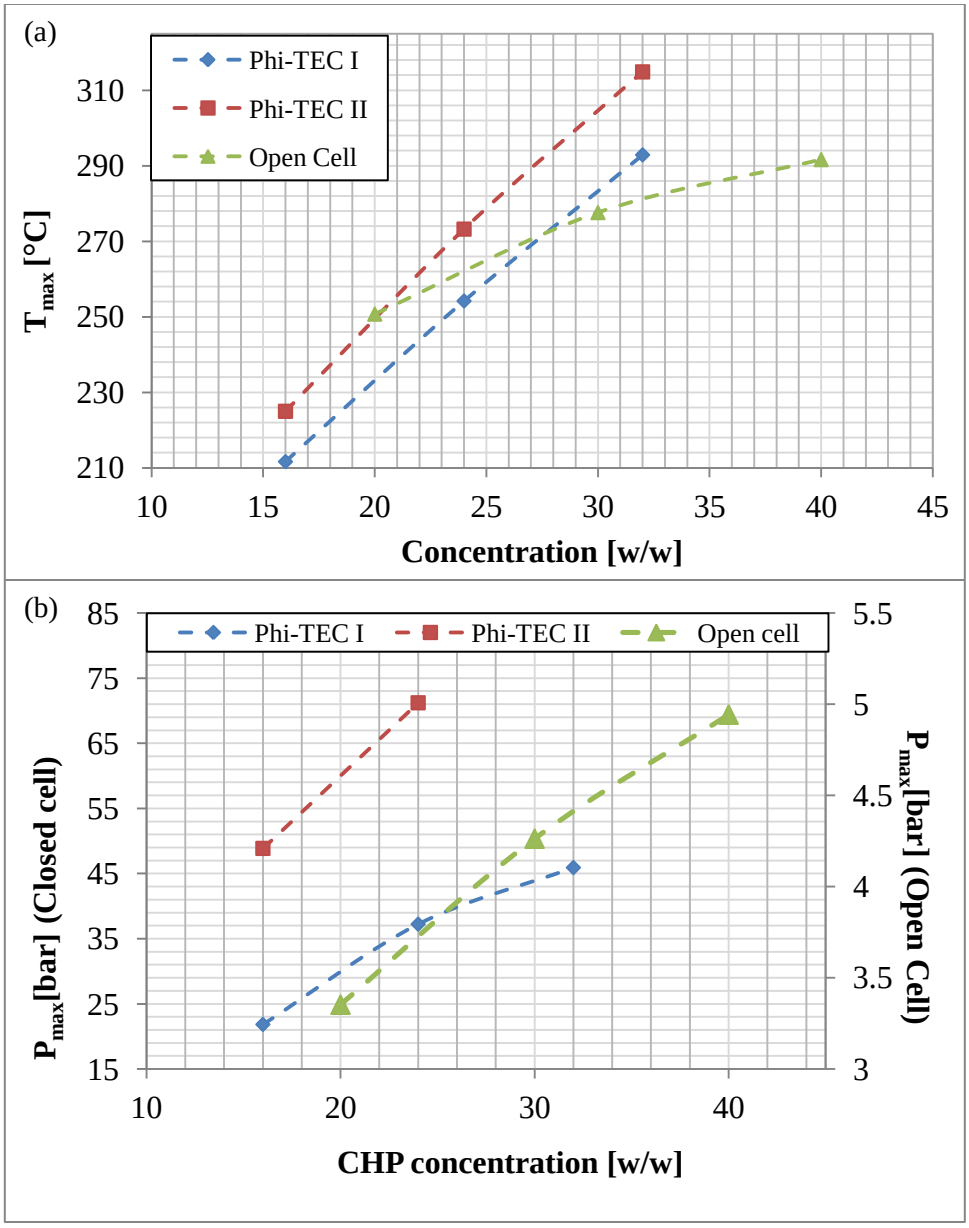

Figure 30 Trends of (a) Maximum temperature and (b) Maximum pressure with respect to CHP concentration

5.5.3.3 dT/dt_{max} and dP/dt_{max}

Increment of self-heating and self-pressurization rates with concentration displayed an exponential behavior at closed cell experiments in both Phi TEC I and Phi TEC II tests. On the other hand at open cell configuration these two parameters showed a linear increase with concentration (Figure 31).

This difference in behavior could be due to:

- At open cell configuration pressures experienced by the sample during the runaway are lower, also there is much more head space, therefore more vaporization occurs [100]. So, some of the produced energy by the decomposition is consumed by more vaporization meaning less changes in temperature.
- Potential erroneous temperature measurement at the end of the runaway due to the low volume of sample mixture remaining within the cell (as most of it escaped from the cell at high temperatures) as explained earlier. This will also make the phi factor increase during the experiment.

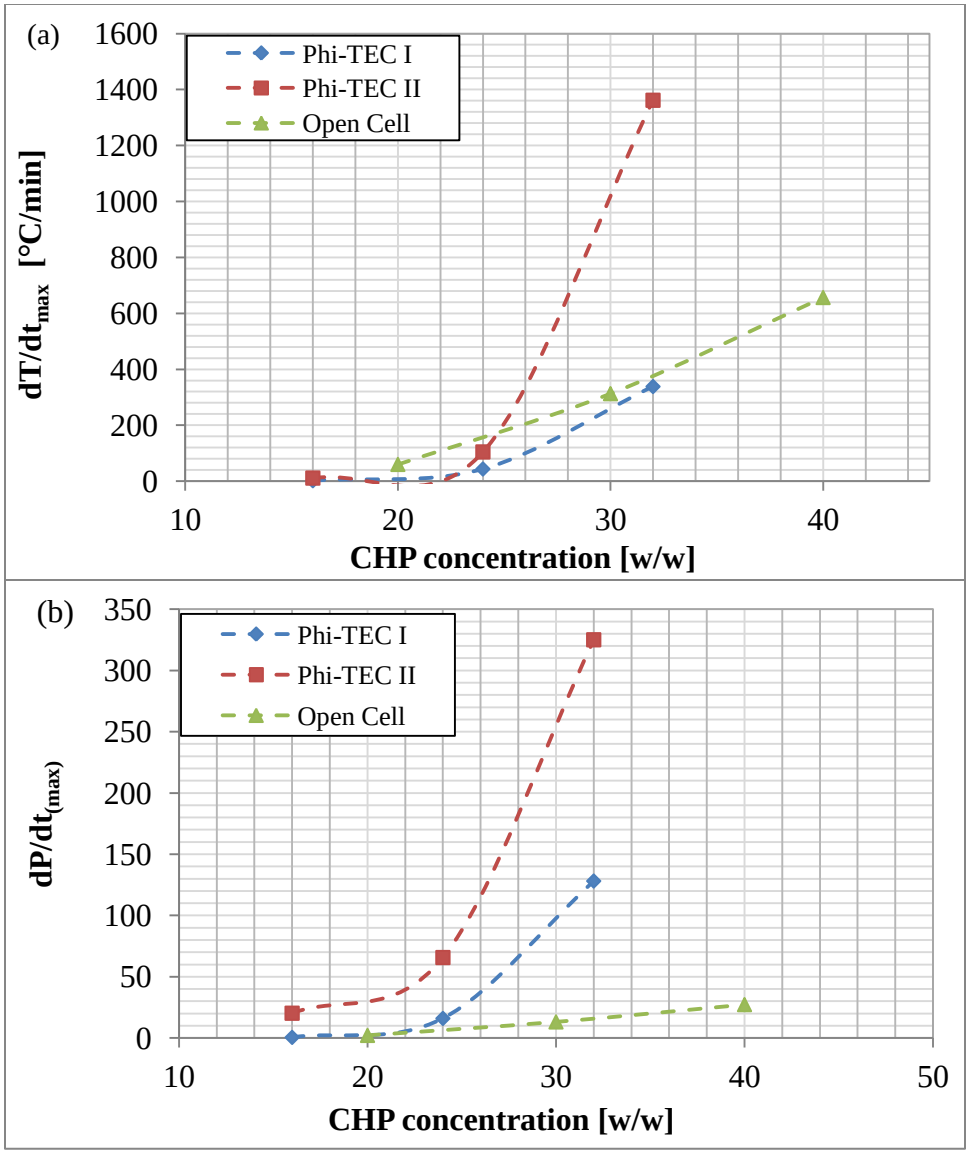

Figure 31 Trends of (a) maximum self-heating rate and (b) maximum self-pressurization rate with respect to CHP concentration

5.5.4 Estimated kinetics

The decomposition reaction of CHP have been described as following n^{th} type 1^{st} order kinetics [40]; nth type 1/2 order [53,98]; as well as autocatalytic kinetics [60,102,103]. In this study by assuming an nth order type kinetics the order of the

reaction was estimated to be ~0.9 when calculated from closed cell data experiments, while closer to ¾ (~0.7) when calculated from open cell data.

Table 24 Kinetics CHP closed cell testing

CHP [% w/w]	n	E_a [kJ/mol]	ln A [1/s]
16	0.89 ±0.04	192 ± 6	39.8 ± 1.6
24		170 ± 3	34.8 ± 0.7
32		153*	31.7*

*Calculated with a single measurement as Phi TEC II data burst during experiment

Table 25 Kinetics CHP open cell testing

CHP [% w/w]	n	E_a [kJ/mol]	ln A [1/s]
20	0.69 ±0.01	171	34.5
30		164	33.5
40		158	33.0

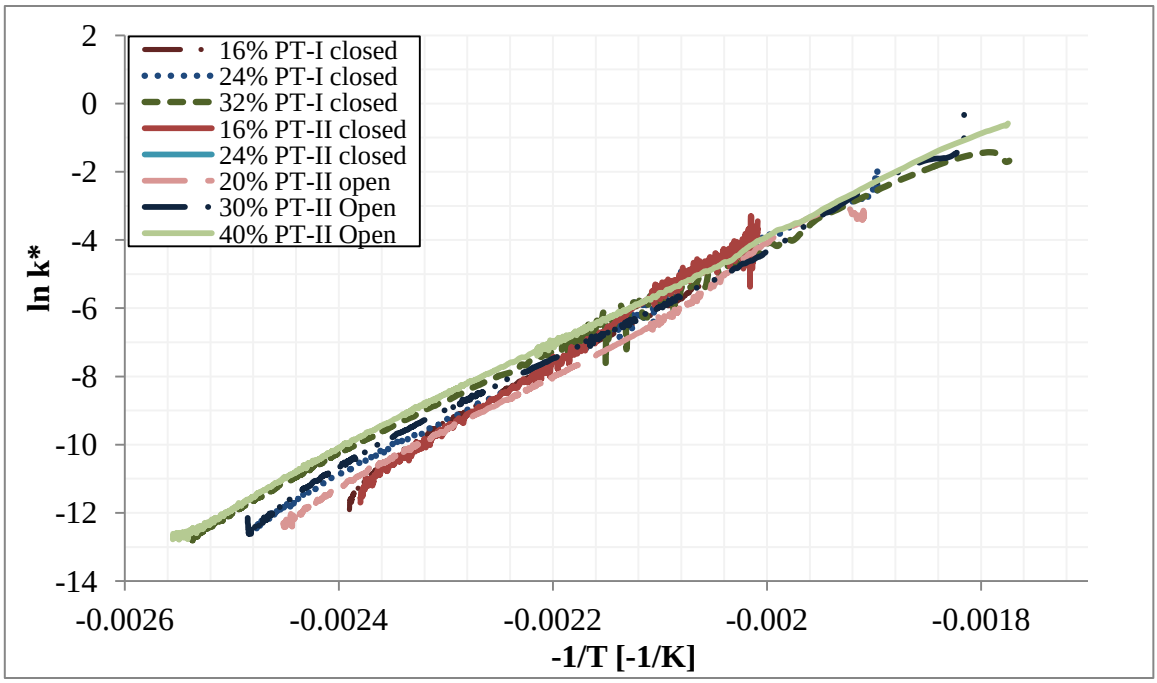

Figure 32 ln *k vs -1/T based on estimated kinetics**

Regarding the activation energy, it was observed that it decreases as concentration of CHP increases. This observation is opposite to what previous studies reported when CHP was dissolved in cumene at concentrations between 12% and 80% [48], where the activation energy was reported to be between (108.6 and 113.4) kJ/mol for concentration 12% to 40% w/w CHP and (136.4-138.7) for 50% to 80% w/w CHP. A possible explanation behind this difference can be the solvent used. In this research DIB (a more stable, heavier and higher boiling point than cumene) was used. As hypothesized previously [84] cumene potentially participates in the reaction forming larger and more stable molecules with radicals from the decomposition. The E_a's estimated in this study are larger than most of the previous reported data of CHP in cumene [53,60,98], which could be due to the larger concentration tested in previous study, equipment used, mode of operation and/or solvent.

5.5.5 Temperature and self-heating rate profiles correction

Results of the temperature and self-heating rate profiles corrected to adiabatic conditions by the phi factor are displayed in Table 26 and Figure 33.

Table 26 Summary of self-heating rate and temperature profiles

#	Equipment	CHP [% w/w]	φ	$T_{o, ad}$ [°C]	P at dP/dt_{max} [bar]	$T_{max, ad}$ [°C]	$dT/dt_{max,ad}$ [°C/min]
1	Phi Tec I	16	1.75	141.0	17.0	257.3	101
2		24	1.65	126.7	30.1	333.1	6828
3		32	1.75	116.2	37.8	421.1	3237
4	Phi Tec II	16	1.12	146.1	41.5	225.0	24
5		24	1.12	129.6	58.7	273.2	319

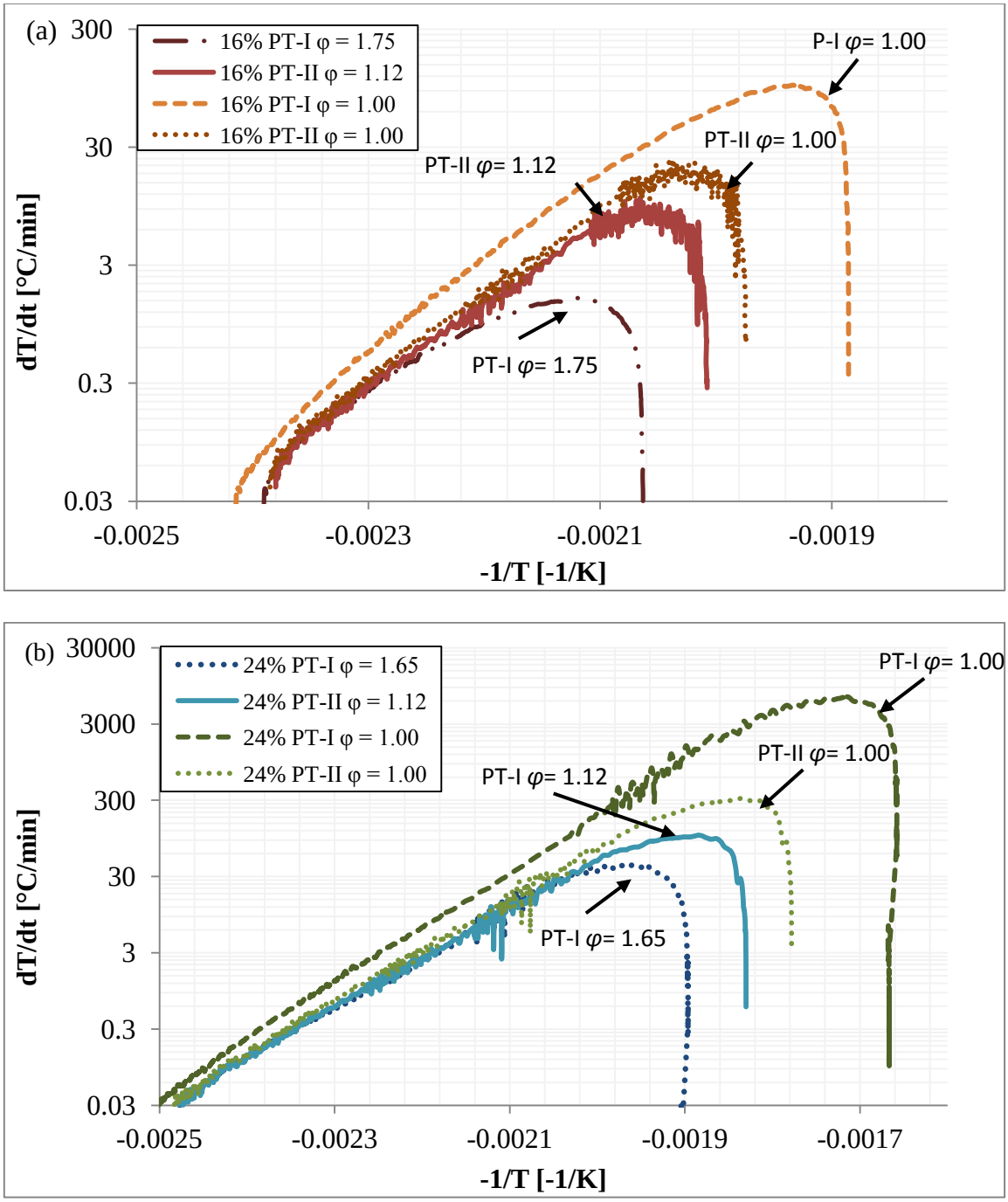

Figure 33 Self-heating rate profiles before and after phi factor correction (a) 16% CHP and (b) 24% CHP

As showed in Table 26, higher values of dT/dt_{max} are obtained from measurements taken with the Phi-TEC II. This is because the lower thermal inertia factor that can be achieved in experiments performed with this equipment; therefore these values are closer to what would be expected when operating on a large industrial scale. However, after considering the correction of this maximum self-heating rate to adiabatic conditions, corrected dT/dt_{max} values corresponding to high phi factor experiments (performed with Phi-TEC I) are much higher than the corresponding corrected values for the lower phi factor experiments (Phi-TEC II data). These differences are by a factor 4.2 and 21.4 for 16% and 24% concentrations respectively. Therefore the higher the concentration, the higher the discrepancies encountered when attempting to estimate temperatures and self-heating rates on an industrial scale scenario from different thermal inertia lab experiments. This observation has also been noticed with a different system (DCP in DIB) under adiabatic conditions [84].

Predicted adiabatic self-heating rates and temperatures from lab-data are frequently used to calculate maximum gas generation rate and to perform vent sizing calculations. As shown in this study the sole use of screening calorimetry (even in adiabatic mode) for vent sizing purposes can lead to under conservative calculations, when the data is not corrected to adiabatic conditions and the sized vent device will not be capable of withstand a worst case scenario. On the other hand, when the data is corrected to adiabatic conditions, the use of screening techniques can lead to over conservative results.

5.6 Conclusions

The runaway decomposition of cumene hydroperoxide at different concentrations in DIB, was studied using pseudo-adiabatic (Phi-TEC I) and adiabatic (Phi-TEC II) tests in close and open cell configurations. The main runaway parameters of the thermal decomposition of CHP were measured. As expected, the data obtained and analyzed showed that the severity of CHP runaway increases when increasing the concentration of the peroxide. This increase shows a linear trend when plotting P_{max}, and T_{max} vs concentration (in closed and open cell configuration); and an exponential trend when dT/dt_{max} and dP/dt_{max} are evaluated against concentration increment in closed cell.

The thermal inertia (φ factor) of the experiments did not show a strong influence on the onset temperature or kinetics of the runaway decomposition of CHP. However, for other parameters (dP/dt_{max}, dT/dt_{max}, P_{max}, and T_{max}) the thermal inertia greatly influenced their value. The comparison of the data obtained from two calorimeters highlighted the importance of performing experiments in a low phi factor calorimeter in order to have representative and confinable data. It was also noted that discrepancies in pressure measurements where larger than temperature when comparing two different φ experiments at similar conditions. However very little research is available on methods for correcting temperature and self-pressurization data.

Unexpected differences in T_o, and trends of dT/dt_{max} and dP/dt_{max} were found when comparing open vs closed cell experiments. These differences are mainly due to: *1)* in an open cell configuration the head-space volume is much larger, this will favor more vaporization of volatile intermediates of CHP decomposition as well solvent when

high temperatures are reached; *2)* errors in temperature measurements when most of the mixture have escape the test cell and/or *3)* dynamic phi factor during the experiment as level (and therefore mass) of the sample remaining in the cell decreases as boiling and evaporation start to be significant.

CHAPTER VI

DFT CALCULATIONS ON THE THERMAL DECOMPOSITION OF DICUMYL PEROXIDE AND CUMENE HYDROPEROXIDE

6.1 Synopsis

In this chapter, DCP and CHP thermal decomposition mechanisms were theoretically studied using computational quantum chemistry, transition state theory, and thermodynamic and kinetic concepts. Analyses were based on the most recent work by Di Somma *et al*. [41,60], in which a network of 51 reactions in total had been outlined. In this work, two simplified networks composed by 12 reactions, in the case of DCP decomposition, and 18 reactions for CHP decomposition, are proposed. Comparison with reported experimental studies showed that these networks accurately predict main products formed during DCP and CHP decompositions. The role of cumene on the autocatalytic behavior reported by experimental research was identified and discussed.

6.2 Introduction

The influence of experimental parameters such as concentration, initial fill level, equipment, calorimetry technique, and configuration of the equipment on the runaway behavior of DCP and CHP [48] [80,84,101] have been previously studied. However, very little is known regarding the physical properties and thermal stability of precursors, intermediates and products of their decomposition. Consequently, the influence that the aforementioned factors have on DCP and CHP runaway decompositions is not fully understood.

As DCP and CHP decompositions involve several elementary steps that occur in gas as well as in solution; getting this understanding experimentally requires the use of analytical and calorimetric techniques. Therefore it becomes costly, time consuming, difficult, and easily influenced by experimental conditions.

Due to these reasons, kinetics (1^{st} order, 0.5 order, autocatalytic) and reaction networks of DCP and CHP decomposition reported by different authors [48,53], are inconsistent.

In this work, the reaction mechanisms for DCP and CHP thermal decomposition are investigated through computational quantum chemistry. As most available experimental studies, including the reference study [40,48,53,60] have characterized their runaway behavior when dissolved in cumene; the present work evaluates their decomposition network using cumene as a solvent. Using transition state theory and thermodynamic calculations, reaction networks for DCP and CHP are proposed. Finally, these networks are discussed and compared with reported experimental data.

6.3 Computational Methods

All calculations were performed using Gaussian 09 suite of programs [104]. Density Functional Theory (DFT) was used, with the ωB97XD functional. This functional uses HF-like exchange in the long range and includes empirical dispersion corrections. Geometries were optimized using the 6-31g basis set and the Gaussian standard tight optimization threshold criteria. Enthalpies and Gibbs Free energies were calculated in fully optimized geometries at 1 atm and at three temperatures: 298 K, 373 K, and 673 K.

Transition states were fully optimized after exploration of the potential energy surface by freezing coordinates. Fully optimized geometries were assigned to minima or transition states according to their number of imaginary frequencies. Intrinsic reaction coordinate (IRC) scans were run to corroborate that computed transition states connect reagent and products of interest [105].

In those reactions where two radicals collapse in a molecule or a molecule breaks in two radicals, the optimization of their transition states was not possible. This is because in the calculation model the two electrons from the bond tend to form a closed-shell system, making difficult to obtain two separated but nearby radicals. In cases like these, it is common to consider the reaction barrier-less. However, in this study estimation of the energy barrier for these cases was improved by calculating relaxed potential energy surfaces for two different spin states. The low-spin state properly describes the bonded system; while the high spin state serves as an estimate of the system with two separated radicals.

Then, the spin-crossing point between the triplet and single states can be considered as an estimate of the energy barrier, as shown in Figure 34.

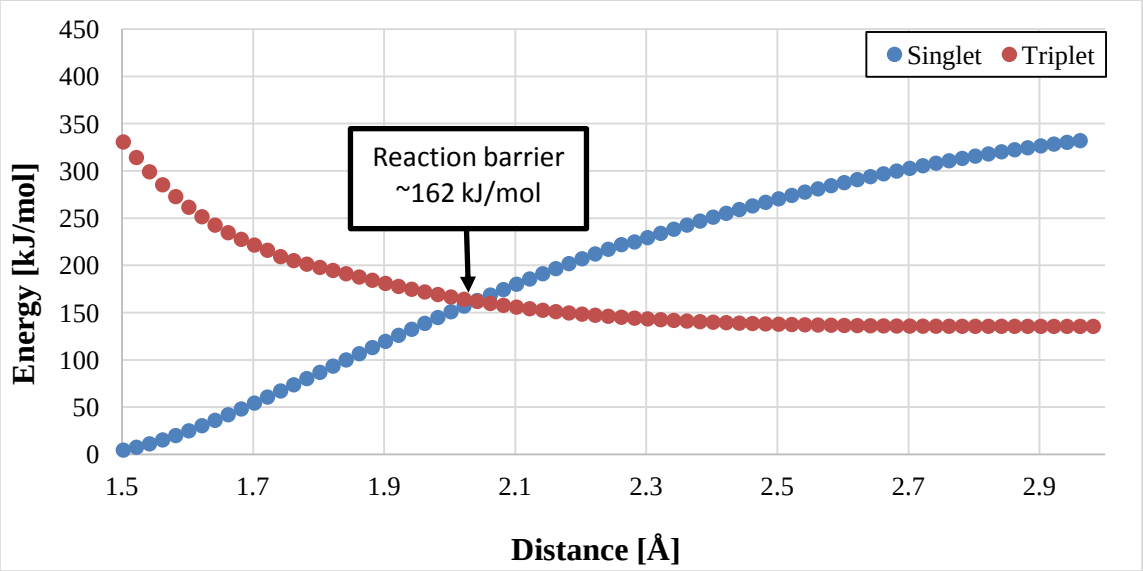

Figure 34 Barrier estimation for O-O bond homolytic cleavage initiation reaction of DCP decomposition (r16). $[C_6H_5C(CH_3)_2]_2 \rightarrow 2\ C_6H_5CO\cdot(CH_3)_2$

As continuum solvent models are computationally more affordable than atomistic solvent models[106]; solvent effects were computed using Polarizable Continuum models (PCM). All calculations were performed using cumene as a solvent. The default parameters for this solvent included in Gaussian were utilized. Transition states in solution were approximated by single point energy calculations. To improve accuracy, single point energies were calculated using a larger basis set 6-311+G(3df,2p). As Gibbs free energies and enthalpies are obtained from vibrational terms (which are only meaningful when computed in fully optimized geometries); energy corrections of reported Gibbs free energies or enthalpies were obtained from the gas geometry optimization. In order to compare the relative accuracy, 19 of the transition states in solution were fully optimized. Activation Gibbs free energy values of transition states resulting from this approach (Equation 6.1) are larger by an average of 7.4 kJ/mol with a

standard deviation of 4.0 kJ/mol than those obtained from fully optimized transition states.

6.4 Methodology

6.4.1 Preliminary analysis: thermodynamic feasibility

Geometrical optimization for all chemicals and radicals participating in the 51 elementary reactions proposed by Di Somma *et al*. [41,60], were computed. Then enthalpies, entropies, and Gibbs free energies of each reaction were estimated. As entropy contribution can become more significant as temperature increases; Gibbs free energy of reaction was estimated at standard conditions and also in the temperature range at which the adiabatic thermal decomposition of CHP and DCP occur (100 °C - 400 °C) [80,84].

Transformations that were thermodynamically feasible at any temperature between 25 °C and 400 °C ($\Delta_r G < 0$) were considered for the pathway analysis. The only exception of the aforementioned statement were DCP (r16) and CHP (r1) initiation reactions. Although these two reaction were endergonic, they were still considered because their driving force is the high reactivity of the formed radicals. These radicals quickly start a propagation phase forming new radicals and product molecules by highly exergonic reactions. As pressure influence on analyzed thermodynamic parameters is almost negligible compared to temperature effects, it was not considered[62].

6.4.2 Transitions states: Gibbs free energy of activation

Transitions states of all thermodynamically feasible steps were calculated at standard conditions. In order to take into account enthalpy and entropy contributions,

reaction barriers were estimated using Gibbs free energies. Gibbs free energies of transition states in solution G_{TS}^{sln} were approximated using fully optimized gas phase calculations by:

$$G_{TS}^{sln} = E_{TS}^{sln} + G_{TS}^{gas} - E_{TS}^{gas} \qquad \text{Equation 6.1}$$

Where E_{TS}^{sln} is the potential energy of the transition state in solution; G_{TS}^{gas} is the calculated gas free energy of the transition state; and E_{TS}^{gas} is the potential energy of the transition state in the gas phase.

6.4.3 Reactivity analysis

Chemical reactivity of radicals participating in the decomposition network was analyzed. As seen experimentally in previous chapters, once the decomposition initiates the overall reaction develops quicker and quicker as temperature increases. Hence, during the propagation phase of the reaction, steps to be considered achievable must be fast. According to the collision theory, how fast a reaction proceeds depends on: 1) number of collisions, 2) required energy to overcome the activation energy, and 3) collisions orientation. In the present work, the first two factors were considered to analyze competitive steps that share a radical precursor.

Factor one was qualitatively considered based on the reagents concentration participating in each reaction. Consequently, elementary reactions where the second precursor was any of the starting peroxides or the solvent were favored. Second factor was considered by comparing the Gibbs energy of activation, therefore transformations with large activation barriers were discarded.

6.4.4 Proposed DCP and CHP decomposition reaction networks

After performing the preliminary analysis (discarding less probable steps by their thermodynamic energies or its compatibility with the experimental knowledge) and analyzing the reactivity of each of the propagating radicals (based on transition states energy barriers); simplified reaction networks for the runaway decomposition of DCP and CHP are proposed and discussed.

6.5 Results

Optimized geometries and energy results (at standard conditions) of chemicals and radicals participating in the mechanism proposed by Di Somma *et al.* [58–60] are shown in Figure 35 and Figure 36. Zero point energy corrections for potential energies are included in the reported values.

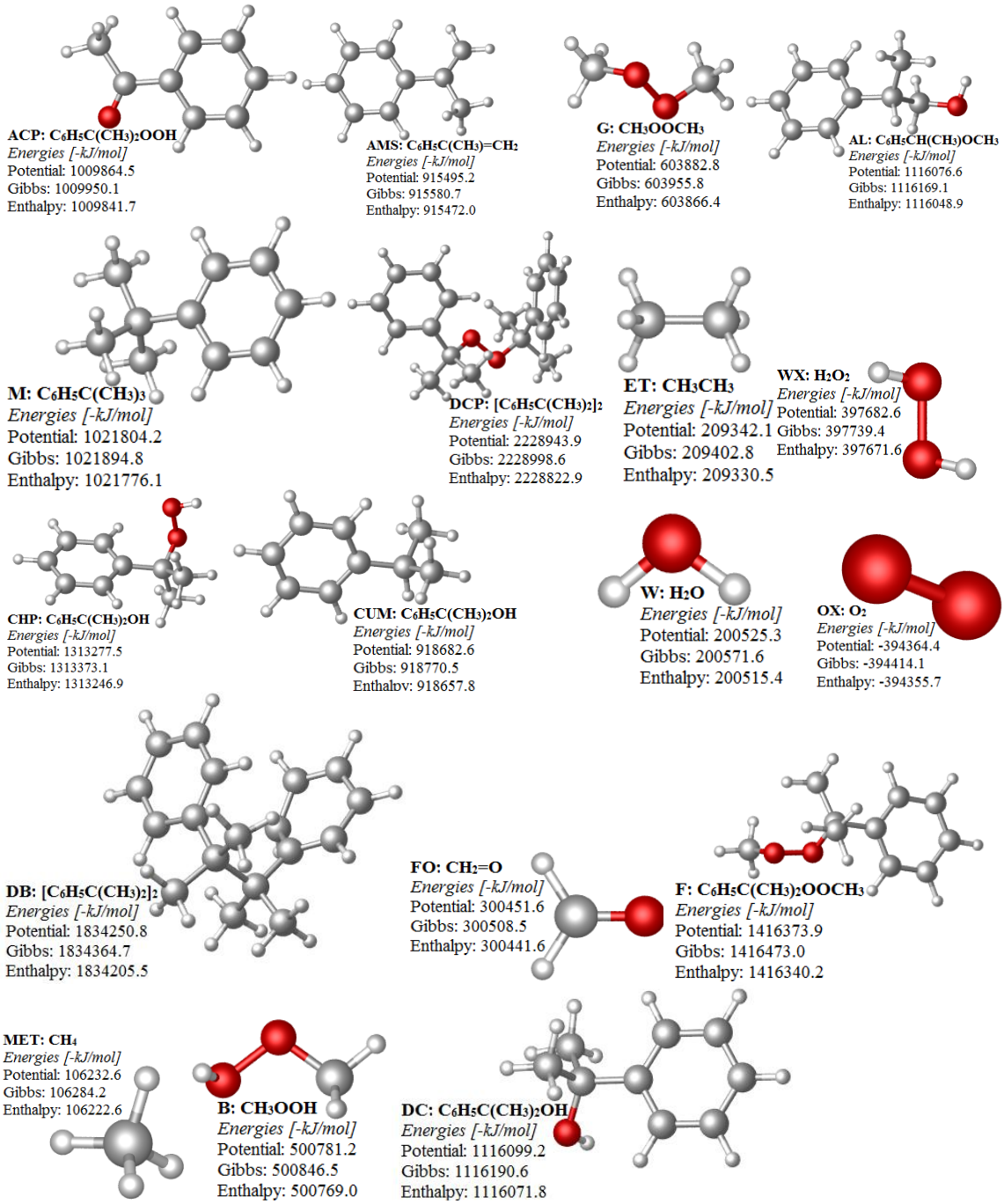

Figure 35 Optimized structures of the chemicals participating in DCP and CHP decomposition mechanisms. Images prepared with CYLview software [107]

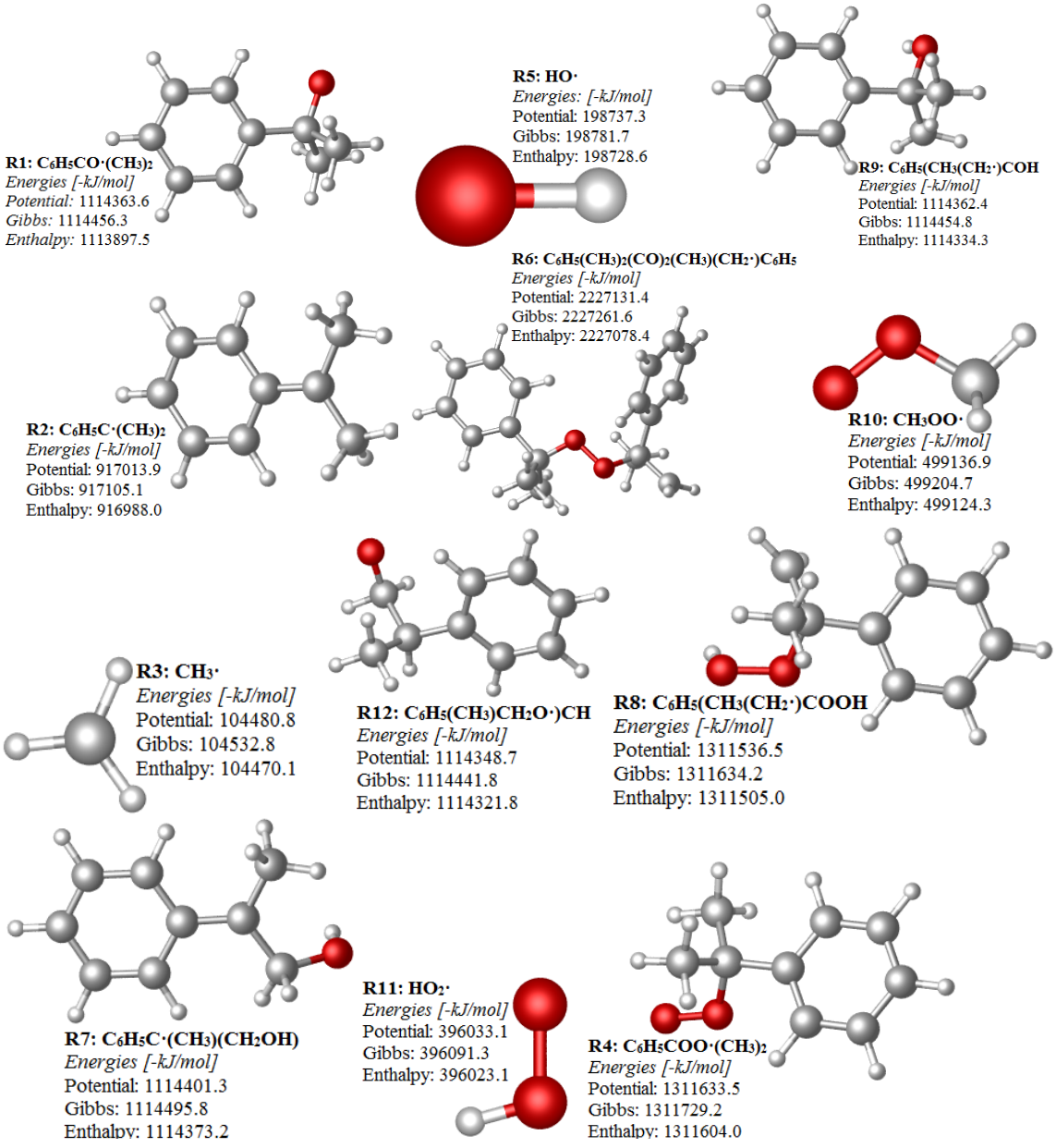

Figure 36 Optimized structures of the radicals participating in DCP and CHP decomposition mechanisms. Images prepared with CYLview software [107]

6.5.1 Preliminary analysis

Computed reaction enthalpies and Gibbs free energies of all 51 reactions in gas as well as in solution phase are displayed in Table 27. For convenience the reaction number given in this table will be used in all the subsequent parts of the manuscript. Because of the large number of reactions considered, the complexity of the reaction network challenges its analysis. For this reason, before proceeding to include the kinetics of each step, some of the reactions were discarded based on thermodynamic calculations.

Table 27 Set of reaction proposed by [41,60] and energies calculated in this work

#	Reagents	Products	Gas phase				In Solution			
			ΔH_r	ΔG_r [kJ/mol]			ΔH_r	ΔG_r [kJ/mol]		
			100 °C [kJ/mol]	25 °C	100 °C	400 °C	100 °C [kJ/mol]	25 °C	100 °C	400 °C
r1	CHP	R1+R5	182.6	135.1	123.2	75.2	160.6	116.3	104.4	56.4
r2	2CHP	R1+R4+W	38.5	-11.0	-23.3	-72.7	3.2	-39.0	-51.3	-100.8
r3	AMS+CHP	R7+R1	9.6	1.6	-0.3	-8.6	-0.9	-3.6	-5.6	-13.8
r4	R1+CHP	DC+R8	6.8	4.6	4.1	0.1	-6.9	-4.1	-4.6	-8.6
r5	AMS+CHP	DCP	-103.9	-44.9	-30.0	28.8	-75.0	58.5	73.4	132.2
r6	R4+CHP	CHP+R8	99.8	95.0	94.0	88.2	91.2	86.9	85.8	80.1
r7	R10+CHP	B+R8	98.1	97.0	93.8	88.4	85.0	86.7	83.5	78.1
r8	R3+CHP	MET+R8	-10.7	-12.5	-12.9	-14.5	-16.7	-13.5	-13.9	-15.5
r9	R5+CHP	W+R8	-44.4	-51.0	-52.5	-59.7	-66.2	-68.4	-70.0	-77.1
r10	R11+CHP	WX+R8	94.2	90.8	90.1	85.7	77.5	78.3	77.6	73.2
r11	R1+CHP	DC+R4	-93.0	-90.5	-89.8	-88.1	-98.1	-91.0	-90.3	-88.6
r12	R3+CHP	MET+R4	-110.5	-107.5	-106.8	-102.7	-107.9	-100.3	-99.6	-95.5
r13	R5+CHP	W+R4	-144.1	-146.0	-146.5	-147.9	-157.4	-155.3	-155.8	-157.2
r14	R10+CHP	B+R4	-1.6	2.0	-0.1	0.1	-6.2	-0.1	-2.3	-2.0
r15	R12+CHP	AL+R8	16.4	11.6	11.9	7.7	0.5	0.2	0.5	-3.7
r16	DCP	2R1	150.5	86.0	69.8	5.2	127.3	-9.1	-25.3	-89.9
r17	R4+DCP	CHP+R6	102.4	93.1	90.9	80.5	98.0	14.9	12.6	2.3
r18	R1+DCP	DC+R6	9.4	2.7	1.0	-7.6	-0.1	-76.1	-77.7	-86.3
r19	R3+DCP	MET+R6	-8.1	-14.4	-16.0	-22.2	-9.9	-85.4	-87.0	-93.3
r20	R10+DCP	B+R6	100.8	95.1	90.7	80.6	91.8	14.8	10.4	0.3
r21	R12+DCP	AL+R6	19.0	9.1	8.8	0.0	7.3	-71.7	-72.7	-81.5
r22	R1	ACP+R3	24.9	-26.6	-39.5	46.1	15.8	-35.8	-48.7	37.0
r23	2R2	DB	-229.6	-154.6	-135.6	-60.1	-208.9	-133.8	-114.8	-39.3
r24	R4+R2	DCP	-230.8	-164.3	-147.6	-81.2	-207.0	-69.4	52.6	53.7
r25	2R3	ET	-392.3	-337.1	-323.5	-266.3	-395.6	-339.6	-326.0	-268.8
r26	2R5	WX	-215.6	-176.0	-166.2	-125.6	-198.6	-158.9	-149.1	-108.4
r27	R5+R2	DC	-356.0	-303.9	-290.9	-239.4	-338.4	-285.7	-272.7	-221.2
r28	R2+R3	M	-319.1	-256.9	-241.4	-178.3	-366.3	-252.1	-236.6	-173.5
r29	R6	AMS+R4	1.4	-48.2	-60.9	-109.3	-23.0	-73.4	-86.1	-134.5
r30	R8	AMS+R11	8.8	-37.8	-49.7	-94.9	-7.2	-54.1	-66.0	-111.2
r31	R9	AMS+R5	133.5	92.5	82.1	41.4	114.8	73.6	63.3	22.6
r32	R4+R3	F	-267.2	-210.9	-196.9	-139.8	-260.3	-202.7	-188.7	-131.6
r33	2R4	DCP+OX	29.4	45.7	49.8	129.7	42.0	129.8	134.0	213.8
r34	2R10	G+OX	26.6	39.4	42.7	119.0	35.6	50.3	53.6	129.9
r35	R7	R12	51.2	54.0	54.6	57.7	62.7	64.3	65.0	68.0
r36	R4	AMS+R11	0.6	57.3	44.3	-6.7	84.0	32.8	19.8	-31.1
r37	2R11	WX+OX	19.1	29.0	31.6	104.9	19.3	30.0	32.5	105.9
r38	R3+CUM	MET+R2	-83.0	-86.0	-86.8	-89.4	-85.9	-88.1	-88.9	-91.5
r39	R1+CUM	DC+R2	-65.4	-68.9	-69.7	-74.8	-76.2	-78.7	-79.6	-84.6
r40	R4+CUM	CHP+R2	27.5	21.6	20.1	13.4	22.0	12.2	10.8	4.1
r41	R5+CUM	W+R2	-116.6	-124.5	-126.4	-134.5	-135.4	-143.0	-145.0	-153.1
r42	R7+CUM	AL+R2	-4.7	-6.8	-7.4	-9.5	-6.1	-10.1	-9.6	-11.7
r43	R12+CUM	AL+R2	-55.9	-60.7	-62.0	-67.2	-68.7	-74.4	-74.5	-79.7
r44	R5+AMS	R7	-173.0	-133.5	-123.5	-83.7	-161.5	-119.9	-110.0	-70.2
r45	R10+AMS	R12+FO	-167.0	-165.0	-164.5	-162.5	-170.6	-167.6	-167.1	-165.1
r46	R2+OX	R4	-260.3	-210.0	-197.4	-210.9	-249.0	-199.2	-186.6	-200.1
r47	R3+OX	R10	-299.6	-257.7	-247.3	-268.1	-302.4	-261.2	-250.8	-271.6
r48	R4+DC	CHP+R9	95.4	92.0	91.2	87.9	91.6	84.2	83.4	80.1
r49	R3+DC	MET+R9	-15.1	-15.6	-15.7	-14.9	-16.3	-16.1	-16.3	-15.5
r50	R1+DC	DC+R9	2.5	1.5	1.3	-0.3	-6.5	-6.8	-7.0	-8.6
r51	WX	2R5	215.6	176.0	166.2	125.6	198.6	158.9	149.1	108.4

6.5.1.1 Thermodynamic feasibility

The systems under analysis include two coexistent phases (gas and solvent). In gas phase, the discarded reactions were: r4, r6, r7, r10, r15, r17, r20, r21, r31, r33, r34, r35, r37, r40, r48 and r51. On the other hand, according to the Gibbs free reaction energy in solution, reactions r5, r6, r7, r10, r24, r31, r33, r34, r35, r37, r40, r48, and r51 are thermodynamically infeasible. Therefore, they were also discarded.

6.5.1.2 Other discarded reactions

In addition, reactions, r23, r28, r32, and r45 were discarded because either tert-butyl-benzene (M), 2,3-dimethyl-2,3-diphenylbutane (B), molecule F, or formaldehyde (FO) (Figure 35) have not been reported as products in any previous experimental study. Moreover, calculations performed in this study suggested that they are not competitive. For example, the potential energy barrier of r28 and r32 in gas phase were estimated to be 239.0 kJ/mol and 308.6 kJ/mol, respectively. These are higher value than most calculated energy barriers.

As step r45 is the only process forming R12, reactions where R12 is a precursor were also eliminated: r15, r21, and r43.

Ethane (ET), product of r25, is not present in the system or formed by other reaction, so r25 was eliminated. This reaction describes the collapse of two methyl radicals, these radicals are very reactive and its concentration is very low; therefore, this collision is statistically difficult despite its low activation energy.

Reactions r10 and r37 are the only two reactions where R11 is consumed, but both of these reactions are thermodynamically unfeasible in gas and solution phases. For

this reason, the feasibility of the reactions that form this radical must be considered carefully. R11 is formed by two different proposed steps:

- $R8 \rightarrow AMS + R11$ (r30)
- $R4 \rightarrow AMS + R11$ (r36)

Reaction 36 is highly endothermic ($\Delta H >> 0$), thermodynamically infeasible at standard conditions and at 100 °C. As it becomes only barely feasible at 400 °C, this reaction was also discarded. However, at this point, r30 cannot be discarded, as it is feasible at all of the evaluated temperatures. Therefore, the formation of R11 must not be discarded and we need to consider at least one reaction consuming it. For the consumption of radical R11 the reverse of reaction 36 is proposed:

- $AMS + R11 \rightarrow R4$ (r-36)

A similar analysis was done for radical R8, which is one of the reactants in reactions r6, r7 and r10, which are thermodynamically unfeasible. R8 can be formed by reactions r4, r7, r8, and r9, which are thermodynamically feasible (in one or both phases, as seen in Table 27). Consequently the reverse of these reactions (r-6, r-7 and r-10) are also considered. The other participant reactants (CHP, B, and WX) are also present at some point in the system either from the beginning or because they are formed in internal steps.

6.5.2 Transition states: Gibbs free energy of activation

Table 28 shows the Gibbs free energy transition and energies of spin crossing profiles (from singlet and triplet scans) at standard conditions. Those steps discarded on the preliminary analysis are omitted from table 2. Reaction r2 is also omitted and the

explanation for its omission is given in the description of the final proposed CHP decomposition mechanism.

As reactions r17 to r21 are assumed to be elementary, negative values of Gibbs activation barrier imply that these reactions occur with no energy barrier. Note that a negative activation barrier is not physically correct because the transition state is a saddle point, but this is an acceptable result because the geometry optimization is done in the gas-phase potential energy. Gibbs free energies of activation calculated in this study are larger than accepted experimental values. Similar discrepancies have been reported in earlier computational studies [108] and are discussed elsewhere [109]. However, the computational results presented important qualitative understandings on the decomposition pathway of DCP and CHP.

Table 28 Gibbs of energy barriers[3,4]

Reaction #	Reagents		Products		Gas phase E_a ΔG^{+}_{gas} [kJ/mol]	In solution E_a ΔG^{+}_{sln} [kJ/mol]
r1	CHP		R1	R5	178.3*	179.9*
r3	AMS	CHP	R7	R1	309.5	332.5
r4	R1	CHP	DC	R8	Non-feasible	95.5
r5	AMS	CHP	DCP		175.3	Non-feasible
r-6	R8	CHP	CHP	R4	137.2	159.0
r-7	R8	B	CHP	R10	131.4	155.0
r8	R3	CHP	MET	R8	89.3	100.0
r9	R5	CHP	W	R8	29.4	169.8
r-10	R8	WX	CHP	R11	124.6	146.9
r11	R1	CHP	DC	R4	26.5	61.7
r12	R3	CHP	MET	R4	41.7	54.5
r13	R5	CHP	W	R4	17.9	41.0
r14	R10	CHP	B	R4	Non-feasible	98.5
r16	DCP		2R1		161.8*	163.0*
r17	R4	DCP	CHP	R6	Non-feasible	-21.6
r18	R1	DCP	DC	R6	78.3	-73.2
r19	R3	DCP	MET	R6	80.7	-79.9
r20	R10	DCP	B	R6	Non-feasible	-24.7
r22	R1		ACP	R3	57.5	51.8
r24	R4	R2	DCP		251.0*	Non-feasible
r26	2R5		WX		~0*	~0*
r27	R5	R2	DC		120.0	125.0
r28	R2	R3	M		186.1	185.7
r29	R6		AMS	R4	52.6	51.9
r30	R8		AMS	R1	57.5	59.9
r-36	R11	AMS	R4		115.3	115.4
r38	R3	CUM	MET	R2	81.9	91.1
r39	R1	CUM	DC	R2	37.8	60.7
r41	R5	CUM	W	R2	19.8	31.7
r42	R7	CUM	AL	R2	93.7	124.4
r44	R5	AMS	R7		---	---
r46	R2	OX	R4		~0**	~0**
r47	R3	OX	R10		~0**	~0**
r49	R3	DC	MET	R9	81.6	91.3
r50	R1	DC	DC	R9	64.7	85.5

[3] (*) Values estimated by spin crossing point profiles and
[4] (**) values based on other researchers findings [60]

6.5.3 Analysis of radicals reactivity

In this section, the reactivity of radicals involve in the reaction networks is discussed. This is done by comparing all the reactions that have them as a precursors. Less probable reactions are discarded.

6.5.3.1 Radical R1

Reactions that can take place from R1 are shown in Table 29. These reactions can be classified as:

1. Decomposition: R1 loses a methyl radical to form acetone (ACP), r22. As ACP is not a reagent in other reactions, it will appear as a final product.
2. Radical abstraction of a H atom on other molecule:

- From a reactant molecule: r4 and r11
- From a DCP molecule: r18
- From cumene: r39
- From the DC: r50

Table 29 Radical R1 reactivity

Reaction #	Reagents		Products		Gas phase ΔG_r [kJ/mol]	Gas phase E_a ΔG^+_{gas} [kJ/mol]	In solution ΔG_r [kJ/mol]	In solution E_a ΔG^+_{sln} [kJ/mol]
r4	R1	CHP	DC	R8	4.6	Non-feasible	-7.6	95.5
r11	R1	CHP	DC	R4	-90.5	26.5	-92.3	61.7
r22	R1		ACP	R3	-26.6	57.5	-37.2	51.8
r18	R1	DCP	DC	R6	2.7	78.3	-180.8	-73.2
r39	R1	CUM	DC	R2	-68.9	37.8	-76.6	60.7
r50	R1	DC	DC	R9	1.5	64.7	-8.8	85.5

As an example, a more detailed discussion (including a graphic) of the comparison between reactions r4 and r11 is included. These two reactions have the same precursors but differ in the products. As observed in Figure 37, both reactions are thermodynamically favorable but the energy barrier required for r4 to occur is bigger than that for r11. So r4 will occur faster. .

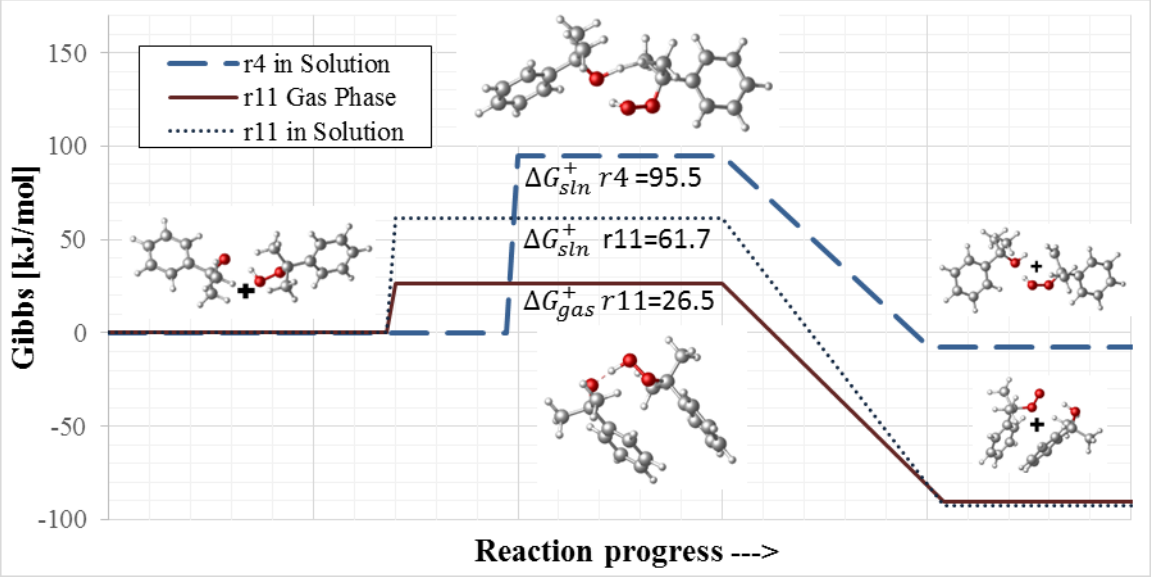

Figure 37 Barrier reactivity analysis R1 reactions r4 and r11

Reaction r18 and r50 are not spontaneous in gas phase at 25°C or 100°C. They become just likely at 400°C, when R1 most probably would be already consumed. For this reason, these two reactions are discarded from the reaction pathway in the gas phase. On the other hand, as observed in Table 29, although r50 is still possible in solution, the activation energy is much higher than the activation energies (in the same phase) of r11, r22, r18, and r39. At the same time it is less exergonic. Therefore r50 is also eliminated

from the solution pathway. Reaction r18 is highly exergonic and does not have barrier in the solution phase, therefore it is still considered in solution.

Gibbs energies of H-abstraction in the solvent and the reactant, are energetically favorable and also by concentration more probable, at least at the beginning of the reaction. So the main radical products from R1 propagation will be: R6 and R2 (in DCP decomposition), R4 and R2 (in CHP decomposition). In both cases the main molecular product will be DC.

6.5.3.2 Radical R5

Elementary steps from where R5 propagates are shown in Table 30. ΔG^{+} in gas and solution phases of r27 and ΔG^{+}_{sln} of r9 is more than 4 times bigger than all the other estimated barriers. Thus, these were discarded.

In reaction r26 two radicals R5 collapse to produce hydrogen peroxide (WX). Though this reaction has not a barrier associated with it, WX is extremely reactive and at the conditions of DCP and CHP decomposition will easily decompose in 2R5, favoring other reactions where R5 participates.

Although the TS of r44 could not be found, this reaction was also discarded because: 1) it was proposed by the reference paper assuming that AMS was present in the system as contaminant, and 2) estimated activation energies of other reactions where AMS participates as precursor (r3 and r-36) are much larger than activation energies shown in Table 30. Main radical products of R5 propagation are R4, R2, and R8 (only in gas phase); and the main the main molecular product is W.

Table 30 Radical R5 reactivity

Reaction #	Reagents		Products		Gas phase ΔG_r [kJ/mol]	Gas phase E_a ΔG^+_{gas} [kJ/mol]	In solution ΔG_r [kJ/mol]	In solution E_a ΔG^+_{sln} [kJ/mol]
r9	R5	CHP	W	R8	-51.0	29.4	-70.2	169.8
r13	R5	CHP	W	R4	-146.0	17.9	-154.9	41.0
r26	2R5		WX			~0*		~0*
r27	R5	R2	DC			120.0		125.0
r41	R5	CUM	W	R2	-124.5	19.8	-140.7	31.7
r44	R5	AMS	R7		-133.5	---	-161.1	----

6.5.3.3 Radicals R2 and R4

Table 31 displays reactions that can take place from R2 and R4. These kind of reactions are:

1. Radical abstraction of an H atom from DCP (r17): this reaction is only possible in solution phase. If r17 is assumed to be an elementary, it will have no barrier.
2. Radical collapse to form DCP (r24). Though the estimated barrier of this reaction is high, it is still considered because radicals R2 and R4 are among the main radical products from other propagation reactions, so r24 is favored by concentration.
3. Oxidation of radical R2 to form R4 (r46): based on previous authors observations [60], this reaction occurs with no barrier. This study showed that the reaction is also highly exergonic. So in the presence of oxygen R2 will easily oxidize to R4. These R4 will catalyzed reactions r17 and r24.

The main products of R2 and R4 propagations are CHP and R6 in solution and DCP in gas phase.

Table 31 Radicals R2 and R4 reactivity

Reaction #	Reagents		Products		Gas phase ΔG_r [kJ/mol]	Gas phase E_a ΔG^+_{gas} [kJ/mol]	In solution ΔG_r [kJ/mol]	In solution E_a ΔG^+_{sln} [kJ/mol]
r17	R4	DCP	CHP	R6	93.1	Non-feasible	-88.5	-21.6
r24	R4	R2	DCP		-164.3	251.0*	33.6	Non-feasible
r46	R2	OX	R4		-210.0	~0**	-200.2	~0**

6.5.3.4 Radical R6

This radical decomposes to form AMS and R4 (r29). The activation Gibbs activation energy of this reaction is 52.6 kJ/mol and 51.9 kJ/mol in gas and solution phases, respectively. As these values are comparable with other considered reactions and the products are pretty stable, so this reaction is still considered.

6.5.3.5 Radical R3

Table 32 shows R3 reactivity. From R3 the following reactions can take place are: 1) radical abstraction of a H atom from CHP, DCP or DC: r8, r12, r19, r38 and r49; and 2) oxidation to form R10: r47

Reaction r8, r12 and r38 are favored by concentration in CHP decomposition, similarly r19 and r38 are favored in DCP decomposition. The estimated activation energy of r49 is relatively high compared with other reactions where DC participates and have not been discarded (Ea<40kJ/mol). Consequently, this reaction was eliminated from the decomposition pathway of both CHP and DCP. Similarly in gas phase r19 is omitted from the decomposition pathway of CHP and r8 is eliminated from the decomposition pathway of DCP. The main products of R3 propagation are R2, R4, R6, R8 and MET.

Table 32 Radical R3 reactivity

Reaction #	Reagents		Products		Gas phase ΔG_r [kJ/mol]	Gas phase E_a ΔG^+_{gas} [kJ/mol]	In solution ΔG_r [kJ/mol]	In solution E_a ΔG^+_{sln} [kJ/mol]
8	R3	CHP	MET	R8	-12.5	89.3	-16.4	100.0
12	R3	CHP	MET	R4	-107.5	41.7	-101.0	54.5
19	R3	DCP	MET	R6	-14.4	80.7	-189.5	-79.9
38	R3	CUM	MET	R2	-86.0	81.9	-86.8	91.1
47	R3	OX	R10		-257.7	~0**	-259.8	~0**
49	R3	DC	MET	R9	-15.6	81.6	-16.3	91.3

6.5.3.6 Radical R8

Table 33 shows estimated activation energy required for reactions involving R8. These are quite large compared to previous reactions evaluated. Moreover, the only reaction favored by concentration is r-6, but the barrier is much higher than other reactions involving CHP. So, the only reaction that will be considered in the decomposition pathways of CHP and DCP is r30. Consequently, main products from R8 propagation are AMS and R1.

Table 33 Radical R8 reactivity

Reaction #	Reagents		Products		Gas phase ΔG_r [kJ/mol]	Gas phase E_a ΔG^+_{gas} [kJ/mol]	In solution ΔG_r [kJ/mol]	In solution E_a ΔG^+_{sln} [kJ/mol]
-6	R8	CHP	CHP	R4	-95.0	137.2	-84.7	159.0
-7	R8	B	CHP	R10	-97.0	131.4	-83.0	155.0
-10	R8	WX	CHP	R11	-90.8	124.6	-77.0	146.9
30	R8		AMS	R1	-37.8	57.5	-6.1	59.9

6.5.3.7 Radical R10

This radical propagates by an H abstraction from CHP and DCP. Reaction barrier of r14 is relatively high so it will be considered only in the decomposition mechanism of

CHP where, it is favored by concentration. The main products of R10 propagation are molecule B and radicals R4 and R6.

Table 34 Radical R10 reactivity

Reaction #	Reagents		Products		Gas phase ΔG_r [kJ/mol]	Gas phase E_a ΔG^+_{gas} [kJ/mol]	In solution ΔG_r [kJ/mol]	Solution Phase ΔG(ts-reagents) [kJ/mol]
14	R10	CHP	B	R4	2.0	Non-feasible	-2.3	98.5
20	R10	DCP	B	R6	95.1	Non-feasible	-90.1	-24.7

6.5.3.8 Radicals R7, R9, R11, and R12

Based on the above analysis R7, R9, R11 or R12 are not formed. However as r-36 and r42 are thermodynamically feasible the activation energy of these reactions, was calculated. ΔG^+_{gas} and ΔG^+_{sln} of reactions r-36 and r42 are approximately 115 kJ/mol and 100kJ/mol, respectively. In the case of r-36, unless α-methylstyrene is present in enough concentration (*e.g.*, as a contaminant), this reaction will not occur. In the case of r42, even when CUM is the solvent (therefore part of the system), the activation energy required by this reaction to occur is much higher than the corresponding value of other stoichiometries where CUM participates. Thus none of these reactions are further considered.

6.5.3.9 Reactions between molecules

Reactions r3, r5 were discarded because 1) the activation barrier is much higher than any of the other estimated barriers and 2) they were proposed in the reference paper considering α-methyl styrene was present in the system as impurity.

On the other hand, r16 (creation of 2R1 by DCP o-o homolysis) will not be considered in CHP decomposition, although DCP is one of the formed products. This, because: 1) the activation barrier is too high, and 2) DCP formation requires overcoming a high activation barrier (r24), therefore it is not favored by concentration.

6.5.4 Proposed reaction networks

Based on the thermodynamic and kinetic analysis performed above, the following reaction networks to study the global decomposition process of DCP and CHP are proposed and discussed.

6.5.4.1 DCP decomposition

According to the present analysis, DCP global decomposition network is composed by 13 reactions. It initiates by the homolysis of DCP O-O bond (r16) to form the active radical R1. The activation barrier in both phases was estimated to be around 162 kJ/mol. This Ea is within the range of activation energies reported experimentally (from 125 kJ/mol [48] to 174 kJ/mol [110]). Final proposed reaction network is depicted in Figure 38. Products are highlighted in bold. List of reactions are displayed in Table 35.

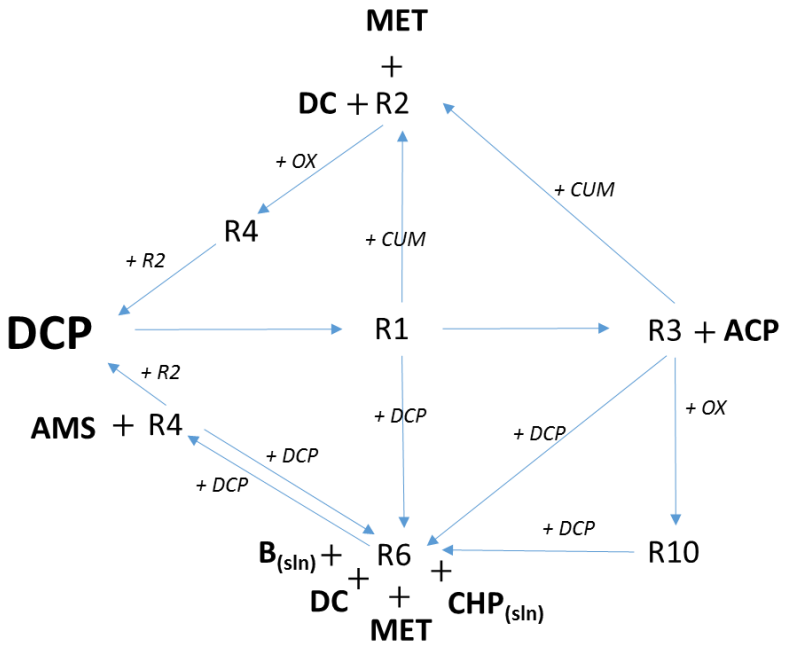

Figure 38 DCP decomposition: reaction network

In Figure 38 it is easily observable that the presence of oxygen creates autocalytic cycles as:

- It allows the formation of R10, which by an H abstraction from DCP creates R6. R6 at the same time propagates to R4, and R4 combines with R2 to form more DCP in both gas and solution phases.
- It oxidizes R2 to form R4 and their combination produce DCP.

However, it is also important to notice that according to the present analysis, R2 is only formed when cumene is present in the system (*i.e.*, when DCP is dissolved in cumene). *This explains why experimental studies have reported DCP decomposition as*

autocatalytic when dissolved in cumene [41,58] *but as a first order when dissolved in 2,2,4-trimethyl-1,3-pentanediol diisobutyrate* [84] *or when studied 98% pure* [48,56].

According to this proposed network, the main DCP decomposition products are acetophenone, α-methyl-styrene, 2-phenyl-2-propanol and methane. It is important to note that methyl hydroperoxide and cumene hydroperoxide are also depicted as products, although these peroxides are less stable than DCP, their concentration may not be enough to favor their decompositions.

Table 35 Complete list of reactions of proposed networks

DCP Decomposition		CHP Decomposition	
Reagents	Products	Reagents	Products
DCP	2R1	CHP	R1 + R5
R1	ACP + R3	R1 + CHP	DC + R4
R1 + DCP	DC + R6	R1	ACP + R3
R1 + CUM	DC + R2	R1 + CUM	DC + R2
R3 + DCP	MET + R6	R5 + CHP	W + R8
R3 + CUM	MET + R2	R5 + CHP	W + R4
R3 + OX	R10	R5 + CUM	W + R2
R6	AMS + R4	R4 + DCP	CHP + R6
R2 + OX	R4	R4 + R2	DCP
R4 + R2	DCP	R2 + OX	R4
R4 + DCP	CHP + R6	R3 + CHP	MET + R8
R10 + DCP	B + R6	R3 + CHP	MET + R4
		R3 + DCP	MET +R6
		R3 + OX	R10
		R3 + CUM	MET + R2
		R6	AMS +R4
		R8	AMS + R1
		R10 + CHP	B + R4

6.5.4.2 CHP decomposition

The initiation phase can occur by two possible reactions:

- $CHP \rightarrow R1 + R5$ (r1)
- $2CHP \rightarrow R1 + R4 + W$ (r2)

The first reaction is a homolytic cleavage of the O-O bond, where two radicals are created. The second reaction involves an O-H cleavage in a second molecule of CHP, giving place to the formation of one molecule of water (W) and the radical R4. Reaction r2 activation energy has been reported as 108.8 kJ/mol [111]. This values is lower than Ea value found in this study and in previous experimental studies [80,98]. However, the energy of the O-H bond (>439 kJ/mol) is much stronger than that of the O-O bond (146-168 kJ/mol) [98]. Based on theory more energy should be needed to break apart the O-H bond and consequently r2 would require more energy than r1 to occur. Moreover, r2 requires the collision of 2 CHP molecules in the proper orientation while the occurrence of r1 is not restricted to collisions. For these reasons and because the products of r2 are formed in subsequent propagation reactions following r1; it was concluded that initiation of CHP decomposition is dominated by r1. The Gibbs free energy of activation of r1 was calculated to be 178.3 kJ/mol and 179.9 kJ/mol in gas and in solution phases respectively, this value is comparable with the experimental findings (153kJ/mol-192kJ/mol) reported in Chapter V and in [80]. Figure 39 depicts the other reactions forming the network for CHP decomposition proposed in this study.

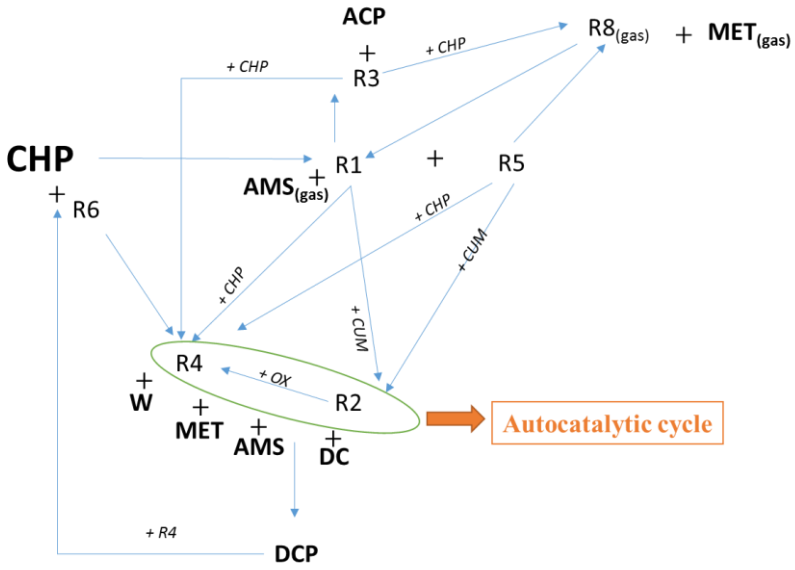

Figure 39 Proposed reaction network for CHP decomposition

In Figure 39, a clear autocatalytic cycle can be identified. This cycle is formed because:

- several reactions form R2 or R4
- R2 oxidizes to form R4
- combination of R2 and R4 form DCP
- R4 radical abstraction from DCP forms CHP and R6
- R6 propagates to R4 and AMS

The kinetics of CHP decomposition by other methods of study (mostly experimental) has been reported as an n^{th} order as well as an autocatalytic. The results obtained in this research supports the latter. Although the solvent used for the present analysis favors the autocatalytic cycle described above, it can be seen that even if this solvent is not present, the reactive system would conserve its autocatalytic nature.

The decomposition products of the proposed network are acetophenone, methane, α-methyl-styrene, water, 2-phenyl-2-propanol and dicumyl peroxide (in really small quantity as some of it reacts with R4 to form CHP).

6.6 Conclusions

Molecular simulations combined with transition state theory and basic thermodynamic and kinetic concepts were successfully applied to get simplified decomposition reaction networks for Dicumyl Peroxide and Cumene Hydroperoxide. This approach was also useful to get a better understanding of the role that cumene (the most widely used solvent for these two peroxide) plays in the runaway decomposition of these two organic peroxides.

The proposed reaction networks are composed by 12 and 18 reactions for the decomposition of DCP and CHP respectively. It was qualitatively noted that as Cumene molecule possesses hydrogen atoms, which are easily abstracted by several of the radicals participating in DCP and CHP decomposition mechanisms; DCP decomposition becomes autocatalytic when studied in this solvent. This observation agrees with experimental studies and gives an explanation of our previously published experimental results [84] where it was found that DCP decomposition in cumene was more hazardous than DCP decomposition in DIB. In the case of CHP decomposition cumene also favored autocatalytic cycles, however they are also formed without cumene presence. In both cases the decomposition products are in agreement with experimental findings.

In order to corroborate the qualitative observations performed on the proposed reaction networks, future experimental and theoretical work needs to be done.

Experimental work should test CHP and DCP at different concentrations in cumene and in other solvents, and fit the data to a specific type of kinetics. Theoretical work should focus on 1) utilizing the proposed set of equations to predict the behavior experimental behavior and 2) studying by molecular simulations to understand the decomposition mechanism in another solvent.

CHAPTER VII

CONCLUSIONS AND FUTURE WORK

7.1 Conclusions

In this dissertation, the physical, kinetic, and thermodynamic behavior of two untempered peroxide systems *i.e.,* dicumyl peroxide (DCP) and cumene hydroperoxide (CHP), were studied under runaway conditions, by experimental and computational techniques. Experimental tests were carried out by using two adiabatic calorimeters of different thermal inertia (phi factor). The computational study was performed using Gaussian 09 software.

The experimental work allowed characterizing the physical behavior of the runaway decomposition of these two peroxides. The influence of experimental factors on the runaway severity was assessed by performing a comprehensive sensitivity analysis. Experimental variables of this analysis were: thermal inertia of equipment, peroxide concentrations, solvent, equipment configurations, initial fill levels, and initial back pressures during open cell testing. By carrying out experimental measurement at different phi factor equipment (from the same vendor), the reliability of current methods used to scale up temperature and self-heating rate profiles, was assessed. The theoretical study contributed to a better understanding of the thermo-kinetics characteristics of the studied systems. In addition, the application of quantum computational chemistry to assess decomposition mechanisms of reactive systems in gas and solution phases were

examined. The computation approach, followed in the present study, gives an alternative to:

1. study the decomposition mechanism of extremely reactive (and hazardous) systems, which are difficult and un-safe to test experimentally,
2. explore the reactivity behavior of complex systems for which calorimetric and analytical experimental studies are time-consuming, expensive, and do not always provide reliable results, and
3. perform screening analysis of new chemicals for which reactive properties are unknown.

The main conclusions and contributions of this PhD work are summarized as follows:

A reliable and comprehensive set of adiabatic data for Dicumyl Peroxide and Cumene Hydroperoxide runaway decompositions are reported as result of this study. Low thermal inertia data at closed cell configuration, which simulates better runaway behavior on a large-scale, was successfully obtained at higher concentrations than previously reported data. Linear trends of temperature vs concentration were identified, while self-heating rates and self-pressurization rates depicted an exponential increase with concentrations.

It was found that current methods for assessing temperature behavior on a large-scale, based on laboratory measurements, are not consistent for fast self-heating rate systems under runaway. Moreover, it was elucidated that estimation of large-scale temperature behavior from high thermal inertia experiments (less costly and less time

consuming) can be better than from low thermal inertia experiment. Specially, in runaway cases where self-heating rates much larger than 100 ° C/min are encountered.

Major discrepancies on maximum gas generation rate, from the same equipment but at different configurations (open vs closed cell) were found. The main sources of such anomalies are: 1) temperature of generated gases at open cell configuration cannot be accurately measured; 2) low pressures of open cell experiments favor vaporization of peroxide and solvent; and 3) gas dissolution issues in closed cell experiments.

Using computational quantum chemistry, transition state theory, and thermodynamic principles reaction networks for DCP and CHP decomposition were proposed. These networks are composed by a set of 12 and 18 reactions, respectively. Comparison of the products obtained by the proposed networks and their autocatalytic behavior match experimental results.

It was demonstrated that thermodynamic and kinetic principles combined with Density Functional Theory can be successfully applied to study the decomposition mechanism of runaway systems and to get insight of solvent role. The same approach could be used to understand the role of other factors such as impurities.

7.2 Future Work

Both experimental and computational findings of this research can be validated by performing experimental tests at higher concentrations (*e.g.*, 50%w/w-80%w/w) in different solvents and coupling calorimetric techniques with analytical ones. Because of the severity of the runaway, mainly fast pressure rise and fast temperature increase during CHP and DCP decompositions; obtaining meaningful adiabatic experimental data

at higher concentrations without damaging the equipment, is not possible. Therefore the recommended testing is to be done in equipment different than the ones used during this research, for example in a differential scanning calorimeter (DSC) or in a micro-calorimeter.

Coupling calorimetric studies, as the ones used in this research, with analytical techniques such as Gas Chromatography (GC), Mass Spectrometry (MS) and/or High-performance liquid chromatography (HPLC) will allow to perform a product distribution analysis and also to verify the main findings obtained in the theoretical part of this thesis. If the aforementioned theoretical findings are validated, the approach used in this study could be used to evaluate chemical reactivity and runaway behavior of different reactive chemical systems. This would avoid the need for experimental testing which can be not only costly but also hazardous when highly reactive chemicals are tested.

Due to the limitations of the current state-of-the-art equipment, temperature behavior of the gas system at open cell testing is not fully understood. In this research, open cell gas generation rate was estimated by following these three different approaches: 1) assuming gas temperature equal than liquid temperature, 2) assuming the ambient temperature, and 3) taking the average between the previous two temperatures. A modification of the Phi-TEC II (or equivalent equipment) would allow to obtain a better assessment of the gas generation rate. This modification can be done by adding thermocouples in different places of the head space of the equipment. Consequently a better estimation of the gas generation rate would be obtained. This data would further

result in accurate vent sizing calculations and in gaining better understanding of the behavior of untempered systems during runaway conditions.

In this dissertation, the theoretical observations of DFT calculations results were qualitative in nature. In order to validate these observations a kinetic modeling of the proposed CHP and DCP decomposition networks can be performed. A material balance for each of the species participating in the network with an energy balance equation can predict the experimental findings. Later equation will be dependent of the experimental mode, *i.e.*, adiabatic, scanning or isothermal.

The performed theoretical work can be complemented by performing further molecular simulations, using different solvents. This will allow getting a better understanding of the role of different solvents in the thermodynamic and kinetic behavior of the decomposition of untempered peroxide systems under runaway conditions. The solvents used should be testable to experimentally corroborate theoretical findings.

In relation to the phi factor correction several issues are still to be solved. In this study it was shown that assumptions of ideal gas and n^{th} order kinetics utilized to correct temperature behavior during runaway experiments lead to inconsistencies in systems with fast temperature rises. Moreover, pressure or time corrections were not considered in this research either. Open cell data was not correct by the phi factor, because the fluid dynamics of the systems under runaway was not fully understood. In future work, equipment can be modified so that it is possible to determine: mass transfer between solution in the cell and its surroundings and factors affecting the level swell during

experiments. Linking the fluid dynamics with the thermodynamics and kinetics of the system would allow a better scale up of the runway behavior of untempered systems.

REFERENCES

[1] US Chemical Safety and Hazard Investigation Board CSB, Improving Reactive Hazard Management, 2002. http://www.csb.gov/assets/1/19/ReactiveHazardInvestigationReport.pdf.

[2] French Ministry of Ecology Energy Sustainable Development, French ARIA Data Bank, (2001). http://www.aria.developpement-durable.gouv.fr/ (accessed April 1, 2015).

[3] P.F. Nolan, J.A. Barton, Some lessons from thermal-runaway incidents, J. Hazard. Mater. 14 (1987) 233–239. doi:10.1016/0304-3894(87)87015-2.

[4] D.A. Crowl, J.F. Louvar, Chemical Process Safety: Fundamentals with Applications, Third Edit, 2011.

[5] H.G. Fisher, H.S. Forrest, S.S. Grossel, J.E. Huff, A.R. Muller, J.A. Noronha, et al., Emergency Relief System Design Using DIERS Technology: The Design Institute for Emergency Relief Systems (DIERS) Project Manual, Design Institute for Physical Property Data/AIChE, 1992.

[6] L. Véchot, J. Kay, D. Carson, J.P. Bigot, Round robin vent sizing excercise on a gassy system: 40% dicumyl peroxide in butyrate solvent, in: HAZARDS XXII, 2011: pp. 156, 278–286.

[7] J. Barton, R. Rogers, Chemical Reaction Hazards: A Guide to Safety, Gulf Publishing Company, 1997.

[8] N.N. Semenov, Some Problems of Chemical Kinetics and Reactivity, Vol 2, Pergamon Press, London, 1959. http://www.sciencedirect.com/science/book/9780080091976.

[9] P. A Bertazzi, Long-term effects of chemical disasters. Lessons and results from Seveso, Sci. Total Environ. 106 (1991) 5–20.

[10] M.S. Mannan, H.H. West, K. Krishna, A. Aldeeb, N. Keren, S.R. Saraf, Y. Liu,

and M. Gentile, The legacy of Bhopal: The impact over the last 20 years and future direction, J. Loss Prev. Process Ind. 18 (2005) 218–224. doi:10.1016/j.jlp.2005.06.037.

[11] H.K. Fauske, J.C. Leung, C.F. Askonas, T.. Fitzsimons, Z. Wang, Runaway Characterization and Vent Sizing based on DIERS Methodology, in: Proc. Int. Symp. Run. React. Press. Reli. Deisgn, Boston Massachusetts, 1987: pp. 186–199.

[12] S.R. Graham, R. Hodgson, L. Vechot, M. Iqbal Essa, Calorimetric studies on the thermal stability of methyl ethyl ketone peroxide (MEKP) formulations, Process Saf. Environ. Prot. 89 (2011) 424–433. doi:10.1016/j.psep.2011.08.005.

[13] Y.W. Wang, C.M. Shu, Y.S. Duh, C.S. Kao, Thermal Runaway Hazards of Cumene Hydroperoxide with Contaminants, Ind. Eng. Chem. Res. 40 (2001) 1125–1132. doi:10.1021/ie990900s.

[14] K.W. Wu, H.Y. Hou, C.M. Shu, Thermal phenomena studies for dicumyl peroxide at various concentrations by DSC, J. Therm. Anal. Calorim. 83 (2006) 41–44. doi:10.1007/s10973-005-6983-2.

[15] J.C. Leung, H.K. Fauske, Runaway system characterization and vent sizing based on diers methodology, Plant/Operations Prog. 6 (1987) 77–83. doi:10.1002/prsb.720060208.

[16] G.W. Höhne, W. Hemminger, H.J. Flammersheim, Differential Scanning Calorimetry, Springer-Verlag, Heidelberg, 2003.

[17] C. Wei, Thermal runaway reaction hazard and decomposition mechanism of the hydroxylamine system, PhD Dissertation, Texas A&M University, 2006. http://pscfiles.tamu.edu/library/center-publications/theses-and-dissertations/chunyangwei.pdf

[18] HarsNet, Safety Engineering in Practice Vol. 6: HarsBook, A technical guide for the assessment of highly reactive chemical systems., Dechema e.V, Frankfurt, 2002.

[19] R.J. Kersten, M.N. Boers, M.M. Stork, C. Visser, Results of a Round-Robin with

di-tertiary-butyl peroxide in Various Adiabatic Equipment for Assessment of Runaway Reaction Hazards, J. Loss Prev. Process Ind. 18 (2005) 145–151.

[20] L.O. Cisneros, W.J. Rogers, M.S. Mannan, Effect of air in the thermal decomposition of 50 mass% hydroxylamine/water., J. Hazard. Mater. 95 (2002) 13–25. http://www.ncbi.nlm.nih.gov/pubmed/12409236.

[21] J. Schoppelrei, M. Kieke, T. Brill, Spectroscopy of Hydrothermal Reactions. 2. Reactions and kinetic parameters of NO3 and equilibria of (NH4) 2CO3 determined with a flow cell and FT Raman spectroscopy, J. Phys. Chem. 100 (1996) 7463–7470. http://pubs.acs.org/doi/abs/10.1021/jp950966a (accessed January 1, 2013).

[22] H. Lee, T. a Litzinger, Chemical kinetic study of HAN decomposition, Combust. Flame. 135 (2003) 151–169. doi:10.1016/S0010-2180(03)00157-3.

[23] F. Jensen, Introduction to Computational Chemistry, 2nd ed., Wiley, 2006.

[24] D.B. Cook, Handbook of Computational Quantum Chemistry, First, Courier Corporation, 2005.

[25] H.P. Hratchian, H.B. Schlegel, Theory and Applications of Computational Chemistry, Elsevier, 2005. doi:10.1016/B978-044451719-7/50053-6.

[26] C.J. Craner, Essentials of Computational Chemistry: Theories and Models, Second, Wiley, 2004.

[27] R.G. Parr, Density functional theory, Annu. Rev. Phys. Chem. 34 (1983) 631–656.

[28] D. Cremer, The Chemistry of Peroxides, Wiley, Chichester, 1983.

[29] M.P. Melrose, R.G. Parr, Some integral Hellmann-Feynman calculations on hydrogen peroxide and ammonia, Theor. Chim. Acta. 8 (1967) 150–156.

[30] P.A. Christiansen, W.E. Palke, A study of the ethane internal rotation barrier,

Chem. Phys. Lett. 31 (1975) 462–466. doi:10.1016/0009-2614(75)85064-0.

[31] Z. Rappoport, ed., The Chemistry of Peroxides, Volume 2, Part 1, Wiley, West Sussex, 2006.

[32] M.R. Blomberg, P.E. Siegbahn, Quantum chemistry as a tool in bioenergetics., Biochim. Biophys. Acta. 1797 (2010) 129–42. doi:10.1016/j.bbabio.2009.10.004.

[33] R. Bach, General and Theoretical Aspects of the Peroxide Group, Patai's Chemistry of Functional Groups, 2009. doi:10.1002/9780470682531.pat0347.

[34] A. Bell, M. Head-Gordon, Quantum Mechanical Modeling of Catalytic Processes, Annu. Rev. Chem. Biomol. Eng. (2011) 453–477.

[35] N. Turra, Peroxide-Mediated Oxidations, ETH Zurich University, 2013. http://e-collection.library.ethz.ch/eserv/eth:7098/eth-7098-02.pdf.

[36] A. Aldeeb, Systematic Approach For Chemical Reactivity Evaluation, PhD Dissertation, Texas A&M University, 2003. http://repository.tamu.edu/handle/1969.1/159.

[37] S.M. Rowe, Thermal Stability : A Review of Methods and Interpretation of Data, Org. Process Res. Dev. 6 (2002) 877–883.

[38] E. Marco, S. Cuartielles, J. Pena, J. Santamaria, Simulation of the decomposition of di-cumyl peroxide in an ARSST unit, Thermochim. Acta. 362 (2000) 49–58.

[39] Y. Iizuka, M. Surianarayanan, Comprehensive Kinetic Model for Adiabatic Decomposition of Di-tert-butyl Peroxide Using BatchCAD, Ind. Eng. Chem. Res. 42 (2003) 2987–2995. doi:10.1021/ie020687r.

[40] M.E. Levin, N.O. Gonzales, L.W. Zimmerman, J. Yang, Kinetics of acid-catalyzed cleavage of cumene hydroperoxide., J. Hazard. Mater. 130 (2006) 88–106. doi:10.1016/j.jhazmat.2005.07.068.

[41] I. Di Somma, R. Marotta, R. Andreozzi, V. Caprio, I. Chimica, N. Federico, et al.,

Dicumyl Peroxide Thermal Decomposition in Cumene : Development of a Kinetic Model, Ind. Eng. Chem. Res. 51 (2011) 7493–7499.

[42] J.M. Tseng, T.F. Hsieh, Y.M. Chang, Y.C. Yang, L.Y. Chen, C.P. Lin, Prediction of thermal hazard of liquid organic peroxides by non-isothermal and isothermal kinetic model of DSC tests, J. Therm. Anal. Calorim. 109 (2011) 1095–1103. doi:10.1007/s10973-011-2125-1.

[43] G. Maschio, D.G. Lister, V. Casson, Use of screening analysis calorimetry in the study of peroxides decomposition, in: Chem. Eng. Trans., 2010: pp. 347–352. doi:10.3303/CET1019057.

[44] V. Casson, G. Maschio, Screening Analysis for Hazard Assessment of Peroxides Decomposition, Ind. Eng. Chem. Res. (2011) 7526–7535.

[45] L.C. Tsai, Y.T. Tsai, C.P. Lin, S.H. Liu, T.C. Wu, C.M. Shu, Isothermal versus non-isothermal calorimetric technique to evaluate thermokinetic parameters and thermal hazard of tert-butyl peroxy-2-ethyl hexanoate, J. Therm. Anal. Calorim. 109 (2012) 1291–1296. doi:10.1007/s10973-012-2519-8.

[46] L.C. Tsai, J.W. Chen, H.Y. Hou, S.H. Liu, C.M. Shu, Exothermic behaviors in decomposition of three solid organic peroxides by DSC and VSP2, J. Therm. Anal. Calorim. 109 (2012) 1303–1309. doi:10.1007/s10973-012-2520-2.

[47] K.Y. Chen, S.H. Wu, Y.W. Wang, C.M. Shu, Runaway reaction and thermal hazards simulation of cumene hydroperoxide by DSC, J. Loss Prev. Process Ind. 21 (2008) 101–109. doi:10.1016/j.jlp.2007.09.002.

[48] Y. Lu, D. Ng, L. Miao, M.S. Mannan, Key observations of cumene hydroperoxide concentration on runaway reaction parameters, Thermochim. Acta. 501 (2010) 65–71. doi:10.1016/j.tca.2010.01.011.

[49] S.H. Wu, Thermal hazard investigation of cumene hydroperoxide in the first oxidation tower, J. Therm. Anal. Calorim. 109 (2011) 921–926. doi:10.1007/s10973-011-1821-1.

[50] H.Y. Hou, C.M. Shu, Y.S. Duh, Exothermic decomposition of cumene

hydroperoxide at low temperature conditions, AIChE J. 47 (2001) 1893–1896. doi:10.1002/aic.690470819.

[51] S.H. Wu, Y.-W. Wang, T.C. Wu, W.N. Hu, C.M. Shu, Evaluation of thermal hazards for dicumyl peroxide by DSC and VSP2, J. Therm. Anal. Calorim. 93 (2008) 189–194. doi:10.1007/s10973-007-8874-1.

[52] Y.W. Wang, Y.S. Duh, C.M. Shu, Evaluation of adiabatic runaway reaction and vent sizing for emergency relief from DSC, J. Therm. Anal. Calorim. 85 (2006) 225–234. doi:10.1007/s10973-005-7361-9.

[53] Y. Duh, C. Kao, H. Hwang, W. Lee, Thermal decomposition kinetics of cumene hydroperoxide, Process Saf. Environ. Prot. 76 (1998).

[54] I. Di Somma, R. Andreozzi, M. Canterino, V. Caprio, F. Ii, V. Tecchio, Thermal Decomposition of Cumene Hydroperoxide : Chemical and Kinetic Characterization, AIChE J. 54 (2008) 1579–1584. doi:10.1002/aic.

[55] A. Miyake, Y. O'hama, Thermal hazard analysis of cumene hydroperoxide using calorimetry and spectroscopy, J. Therm. Anal. Calorim. 93 (2008) 53–57. doi:10.1007/s10973-007-8799-8.

[56] I. Ben Talouba, L. Balland, N. Mouhab, M. a. Abdelghani-Idrissi, Kinetic parameter estimation for decomposition of organic peroxides by means of DSC measurements, J. Loss Prev. Process Ind. 24 (2011) 391–396. doi:10.1016/j.jlp.2011.02.001.

[57] K.T. Lu, Y.C. Chu, T.C. Chen, K.H. Hu, Investigation of the decomposition reaction and dust explosion characteristics of crystalline dicumyl peroxide, Process Saf. Environ. Prot. 88 (2010) 356–365. doi:10.1016/j.psep.2010.06.003.

[58] I. Di Somma, R. Andreozzi, M. Canterino, V. Caprio, Thermal Decomposition of dicumylperoxide Chemical and Kinetic Characterization, AIChE Annu. Meet. 54 (2008) 1579–1584. doi:10.1002/aic.

[59] I. Di Somma, R. Marotta, R. Andreozzi, V. Caprio, Kinetic and chemical characterization of thermal decomposition of dicumylperoxide in cumene., J.

Hazard. Mater. 187 (2011) 157–63. doi:10.1016/j.jhazmat.2011.01.023.

[60] I. Di Somma, R. Marotta, R. Andreozzi, V. Caprio, Detailed thermal and kinetic modeling of cumene hydroperoxide decomposition in cumene, Process Saf. Environ. Prot. (2012) 1–7. doi:10.1016/j.psep.2012.07.001.

[61] N. Sebbar, J. Bozzelli, H. Bockhorn, Kinetic Study of Di-Tert-Butyl Peroside: Thermal Decomposition and Product Reaction Pathways, Wiley Online Libr. (2005). doi:10.1002/kin.20899.

[62] C. Bruneton, C. Hoff, P.I. Barton, Computer aided identification of chemical reaction hazards, Comput. Chem. Eng. 21 (1997) S311–S317. doi:10.1016/S0098-1354(97)87520-5.

[63] A. Aldeeb, W. Rogers, M. Mannan, Theoretical and experimental methods for the evaluation of reactive chemical hazards, Process Saf. Environ. Prot. 80 (2002) 141–149. http://www.sciencedirect.com/science/article/pii/S0957582002710215.

[64] Q. Wang, C. Wei, L. Pérez, W. Rogers, M. Hall, S. Mannan, Thermal Decomposition Pathways of Hydroxylamine: Theoretical Investigation on the Initial Steps, J. Phys. Chem. 114 (2010) 9262–9269. doi:10.1021/jp104144x.

[65] J. Huang, C. He, C. Liu, H. Tong, L. Wu, S. Wu, A computational study on thermal decomposition mechanism of β-1 linkage lignin dimer, Comput. Theor. Chem. 1054 (2015) 80–87. doi:10.1016/j.comptc.2014.12.007.

[66] H. Kung, A. Teplyakov, Selectivity and Mechanism of Thermal Decomposition of β-diketones on ZnO Powder., J. Catal. 330 (2015) 145–153. doi:10.1016/j.jcat.2015.07.021.

[67] N. Shopova, S. Ivanov, Thermal decomposition of cy -tetralyl hydroperoxide under non-isothermal conditions , without solvents, 231 (1994) 193–202.

[68] H.Y. Hou, T.S. Liao, Y.S. Duh, C.M. Shu, Thermal hazard studies for dicumyl peroxide by DSC and TAM, J. Therm. Anal. Calorim. 83 (2006) 167–171. doi:10.1007/s10973-005-7054-4.

[69] HEL GROUP, Adiabatic Calorimetry, (2014). http://www.hazards.co/calorimeters/adiabatic-calorimetry/.

[70] HEL, PHI-TEC Operating Manual Volume 3: Verification of Equipment Performance And Examples of Data, 3 (2004) 1–15.

[71] S.H. Gove, Emergency Pressure Relief for Intermediate Bulk Containers Contining Dicumyl Peroxide, in: DIERS User Gr. Meing, 1996.

[72] T. Amy, B. James, A. Charles, Safely Scale-up Processes and Acommodate Recipe Changes, Process Saf. Prog. 25 (2006) 326–330. doi:10.1002/prs.

[73] L. Véchot, J. Kay, J. Wilday, Round robin vent sizing exercise on a gassy system: 40% dicumyl peroxide in butyrate solvent, in: Proceeding Hazards XXII Conf. IChemE Symp. Ser. 156, Institution of Chemical Engineers, 2011: pp. 278–286. http://hal.archives-ouvertes.fr/emse-00598618/ (accessed November 20, 2014).

[74] S.H. Wu, M.L. Shyu, Y.P. I, J.H. Chi, C.M. Shu, Evaluation of Runaway Reaction for dicumyl peroxide in a Batch Reactor by DSC and VSP2, J. Loss Prev. Process Ind. 22 (2009) 721–727. doi:10.1016/j.jlp.2008.08.004.

[75] Z. Na, Thermal Stability Analysis of Dicumyl Peroxide, in: Adv. Control Commun., 2012: pp. 279–286.

[76] D.I. Townsend, J.C. Tou, Thermal hazard evaluation by an accelerating rate calorimeter, Thermochim. Acta. 37 (1980) 1–30. doi:http://dx.doi.org/10.1016/0040-6031(80)85001-5.

[77] J. Etchells, J. Wilday, Workbook for Chemical Reactor Relief System Sizing, HSE,Health & Safety Executive, 1998. http://www.hse.gov.uk/research/crr_htm/1998/crr98136.htm.

[78] LUPEROX, Diakyl Peroxides. https://intranet.ssp.ulaval.ca/cgpc/fsss/fichiers/LUPEROX 101XL45_dialkyl-peroxides tech.pdf.

[79] J.P. Burelbach, Quick Hazard Screening by closed cell ARSST using standard

ARC bombs, (1989) 1–4. https://www.fauske.com/sites/default/files/QuickHazardScreeningbyClosedCellARSSTUsingStandardARCTMBombs.pdf.

[80] O. Reyes-Valdes, V. Casson-Moreno, S. Mannan, L. Véchot, Evaluation of the Thermal Runaway Decomposition of Cumene Hydroperoxide by Adiabatic Calorimetry, Chem. Eng. Trans. 43 (2015).

[81] E. Wilcock, D.Wiesbaden, A review of the phi factor during runaway conditions, J. Loss Prev. Process Ind. I (1997) 289–302.

[82] S. Mannan, A. Chowdhury, O. Reyes-Valdes, A portrait of process safety: From its start to present day, Hydrocarb. Process. 91 (2012) 55–62. http://www.hydrocarbonprocessing.com/Article/3050913/A-portrait-of-process-safety-From-its-start-to-present-day.html.

[83] R. Saada, D. Patel, B. Saha, Causes and consequences of thermal runaway incidents—Will they ever be avoided?, Process Saf. Environ. Prot. 97 (2015) 109–115. doi:10.1016/j.psep.2015.02.005.

[84] O.J. Reyes-Valdes, V. Casson Moreno, S.P. Waldram, L.N. Véchot, M.S. Mannan, Experimental sensitivity analysis of the runaway severity of Dicumyl peroxide decomposition using adiabatic calorimetry, Thermochim. Acta. 617 (2015) 28–37. doi:10.1016/j.tca.2015.07.016.

[85] J.M. Hsu, M.S. Su, C.Y. Huang, Y.S. Duh, Calorimetric studies and lessons on fires and explosions of a chemical plant producing CHP and DCPO, J. Hazard. Mater. 217-218 (2012) 19–28. doi:10.1016/j.jhazmat.2011.12.064.

[86] Center for Chemical Process Safety (CCPS), Guidelines for Pressure Relief and Effluent Handling Systems, John Wiley & Sons, 1998.

[87] F. Stoessel, Planning protection measures against runaway reactions using criticality classes, Process Saf. Environ. Prot. 87 (2009) 105–112. doi:10.1016/j.psep.2008.08.003.

[88] Center for Chemical Process Safety (CCPS), Layer of Protection Analysis:

Simplified Process Risk Assessment, annotated, John Wiley & Sons, 2011.

[89] H. Pasman, W. Rogers, Bayesian networks make LOPA more effective, QRA more transparent and flexible, and thus safety more definable!, J. Loss Prev. Process Ind. 26 (2013) 434–442. doi:10.1016/j.jlp.2012.07.016.

[90] L. Véchot, J.-P. Bigot, D. Testa, M. Kazmierczak, P. Vicot, Runaway reaction of non-tempered chemical systems: Development of a similarity vent-sizing tool at laboratory scale, J. Loss Prev. Process Ind. 21 (2008) 359–366. doi:10.1016/j.jlp.2008.01.005.

[91] J. Singh, Reliable scale-up of thermal hazards data using the PHI-TEC II calorimeter ', Thermochim. Acta. 226 (1993) 211–220.

[92] HEL GROUP, PHI-TEC Operating Manual Volume 2 WinISO Data Acquisition and Control Software, 2 (2002).

[93] U. Setzmann, W. Wagner, A New Equation of State and Tables of Thermodynamic Properties for Methane Covering the Range from the Melting Line to 625 K at Pressures up to 1000 MPa, J. Phys. Chem. Ref. Data. 20 (1991) 1061. doi:10.1063/1.555898.

[94] V. Casson Moreno, R. Kanes, J. Wilday, L. Véchot, Modeling of the venting of an untempered system under runaway conditions, J. Loss Prev. Process Ind. (2015). doi:10.1016/j.jlp.2015.04.016.

[95] S.K. Upadhyay, ed., Chemical Kinetics and Reaction Dynamics, Springer Science & Business Media, 2007.

[96] National Fire Protection Association, NFPA 704: Standard System for the Identification of the Hazards of Materials for Emergency Response, 2012th ed., 2012.

[97] V. Casson, E. Battaglia, G. Maschio, Hydrogen Peroxide Decomposition Analysis by Screening Calorimetry Technique, Chem. Eng. Trans. 26 (2012) 27–32.

[98] S.H. Wu, Runaway reaction and thermal explosion evaluation of cumene

hydroperoxide (CHP) in the oxidation process, Thermochim. Acta. 559 (2013) 92–97. doi:10.1016/j.tca.2013.02.028.

[99] J.E. Huff, Pressure Relief System Flow: Results of the DIERS Phase II Projects, in: Emerg. Reli. Syst. Des. Using DIERS Technol. Des. Inst. Emerg. Reli. Syst. Proj. Man., n.d. doi:10.1002/9780470938317.ch2.

[100] G. Zhao, Beyond the Phi Factor: Correction of Experimental Data for Vaporization in Tempered Reactions for Pressure-Relief Systems, Process Saf. Prog. 34 (2015) 1547–5913. doi:10.1002/prs.

[101] Y. Duh, C. Kao, C. Lee, S.W. Yu, Runaway hazard assesment of cumene hydroperoxide from cumene oxidation process, Process Saf. Environ. Prot. 75 (1997) 73–80.

[102] A. Miyake, M. Sumino, Y. Oka, T. Ogawa, Y. Iizuka, Prediction and evaluation of the reactivity of self-reactive substances using microcalorimetries, Thermochim. Acta. 352-353 (2000) 181–188. doi:10.1016/S0040-6031(99)00465-7.

[103] J.R. Chen, S.Y. Cheng, M.H. Yuan, A. Kossoy,C.M. Shu, Hierarchical kinetic simulation for autocatalytic decomposition of cumene hydroperoxide at low temperatures, J. Therm. Anal. Calorim. 96 (2009) 751–758. doi:10.1007/s10973-009-0023-6.

[104] M.J. Frisch, G.W. Trucks, H.B. Schlegel, G.E. Scuseria, M.A. Robb, J.R. Cheeseman, et al., Gaussian 09, Revision H.13, (2009).

[105] J.M. Goodman, M. a Silva, QRC: a rapid method for connecting transition structures to reactants in the computational analysis of organic reactivity, Tetrahedron Lett. 44 (2003) 8233–8236. doi:10.1016/j.tetlet.2003.09.074.

[106] V. Risorgimento, C. Generale, P. Area, W. Avenue, N. Haven, Polarizable Continuum Model (PCM) Calculations of Solvent Effects on Optical Rotations of Chiral Molecules, J. Phys. Chem. (2002) 6102–6113.

[107] C. Legault, CYLview, version 1.0.561 BETA.

[108] S. a. Zygmunt, L. a. Curtiss, Quantum-chemical studies of molecular reactivity in nanoporous materials, Comput. Mater. Chem. Methods Appl. (2005) 191–245. doi:10.1007/1-4020-2117-8_5.

[109] R.D. Bach, P.Y. Ayala, H.B. Schlegel, A Reassessment of the Bond Dissociation Energies of Peroxides. An ab Initio Study, J. Am. Chem. Soc. 118 (1996) 12758–12765.

[110] J. Lv, L. Chen, W. Chen, H. Gao, M. Peng, L. Jiayu, et al., Kinetic Analysis and Self-Accelerating Decomposition Temperature (SADT) of Dicumyl Peroxide, Thermochim. Acta . 571 (2013) 60–63. doi:10.1016/j.tca.2013.08.029.

[111] D. Swern, Organic Peroxides, Wiley - Interscience, New York, 1970.

APPENDIX A

NOMENCLATURE

A: Frequency factor

$C_{P\,cell}$: Heat capacity of the cell and magnetic stirrer [kJ kg^{-1} °C^{-1}]

$C_{P\,sample}$: Heat capacity of peroxide solutions in DIB and CUM [kJ kg^{-1} °C^{-1}]

$\left(\frac{dG}{dt}\right)_{max,\varphi>1}$: Experimental maximum gas generation rate [mol min^{-1} kg^{-1}]

$\left(\frac{dnG}{dt}\right)_{max,\varphi=1}$: Maximum gas generation rate corrected by the phi factor [mol min^{-1} kg^{-1}]

dP/dt_{max}: Maximum pressurization rate [bar min^{-1}]

dT/dt_{max}: Maximum self-heating rate [°C min^{-1}]

$\left(\frac{dT}{dt}\right)_{\varphi>1}$: Experimental temperature rise [°C min^{-1}]

$\left(\frac{dT}{dt}\right)_{\varphi=1}$: Adiabatic temperature rise (corrected by the phi factor) [°C min^{-1}]

dX/dt: Rate of reaction [mol s^{-1}]

E_a: Activation energy [kJ/mol]

E_{TS}^{gas}: Gas phase potential energy of transition state [kJ/mol]

E_{TS}^{sln}: Solution phase potential energy of transition state [kJ/mol]

ΔG_r: Gibbs energy of reaction [kJ/mol]

G_{TS}^{gas}: Gas phase Gibbs energy of transition state [kJ/mol]

G_{TS}^{sln}: Solution phase Gibbs energy of transition state [kJ/mol]

ΔG_r: Gibbs free energy of reaction [kJ/mol]

ΔG^{+}_{gas}: Gibbs free energy of activation gas phase [kJ/mol]

ΔG^{+}_{sln}: Gibbs free energy of activation solution phase [kJ/mol]

ΔH_r: Enthalpy of reaction

k: Kinetic constant [dependent of reaction order]

m: Mass [kg]

m_{cell}: Mass of cell (including magnetic stirrer) [kg]

m_s: Mass of solution [kg]

m_0: Mass of the solution before starting the experiment

Δm: Difference between initial mass of solution and final mass of solution

n: Order of the reaction

n_g: Moles of non-condensable gases [mol]

Δn: Moles of non-condensable gases formed [mol]

n_{final}: Final moles of non-condensable gases after cooling down [mol]

$n_{initial}$: Initial moles of gases inside the cell (air gas) [mol]

P: Pressure [bar]

$P_{c:}$ Methane critical pressure [4.6 MPa]

$P_{initial}$: Initial Pressure before starting the experiment [bar]

P_{final}: Pressure inside the test cell after cooling down [bar]

P_{max}: Maximum Pressure [bar]

ΔP_{max}: Pressure build-up [bar]

R: Universal gas constant [J K^{-1} mol^{-1}]

T_o: Onset temperature [[°C]

$(T_o)_{\varphi=1}$: Adiabatic onset temperature after phi factor correction [°C]

$(T)_{\varphi=1}$: Adiabatic temperature after phi factor correction [°C]

T_{max}: Maximum temperature [°C]

T_r: Ratio between temperature after cooling to critical temperature

TMR: Experimental time to maximum rate [min]

ΔT_{ad}: Adiabatic temperature rise [°C]

X: conversion

φ: Phi factor or thermal inertia factor

ρ: Density [g ml^{-1}]

ω: Acentric factor methane [0.01141]